ASSESSING TARGET CENTRING ALGORITHMS FOR USE IN NEAR-REAL-TIME-PHOTOGRAMMETRY

Michael Rubinstein, B.Sc (Eng), Cape Town

October 1990

Submitted to the University of Cape Town
in partial fulfilment for the degree of
Master of Science in Engineering.

I, Michael Rubinstein, submit this thesis in partial fulfilment of the requirements for the degree of Master of Science in Engineering. I affirm that this is my original work and that it has not been submitted in this or a similar form for a degree at any University.

ABSTRACT

Target Centring Algorithms were investigated for use in the Near-Real-Time-Photogrammetry NRTP system: PHOENICS. PHOENICS, a Photogrammetric Engineering and Industrial digital Camera System, has been developed over the past three years in the Surveying Department of UCT to provide a semi-automatic system to determine three dimensional co-ordinates of surfaces and objects using a photogrammetric method.

Targets are attached to an object in order to facilitate measurement of the shape, size and orientation of the object. The centre of the target uniquely defines the target co-ordinate. Target centres (from images of the same object) are used in photogrammetric models to locate the three dimensional (3-D) co-ordinates of the target. The accuracy of the target 3-D location is dependent on the accuracy of the target centring algorithm.

A series of sub-algorithms were employed to arrive at a single target centring algorithm. Various combinations of these sub-algorithms were compared in order to obtain the optimal target centring algorithm.

Three images were used to test various aspects of the target centring algorithms:

- their potential accuracy was tested on an image having symmetric synthetic targets
- their robustness was tested on an image having targets with artificial blemishes
- their performance in a real (noisy) environment was tested on an image with real targets on a control frame, captured by PHOENICS.

When the target centring algorithms were run on the three images, target location with an accuracy of from 1/10 of a pixel for real images, to 1/1000 of a pixel for ideal synthetic targets was obtained.

ACKNOWLEDGEMENTS

The author would like to gratefully acknowledge the contributions of the following:

My supervisor, Assoc. Prof. Heinz Rüther, for his inspiration, guidance and willingness to give of his time.

Assoc. Prof. Heinz Rüther for the use of his computer programs.

The staff of the Surveying Department.

Ms Jo Caesar, for her sprightly typing and the endurance with which she deciphered my handwriting.

My Father, Mother, sister, brothers and Arnold Rubinsztein for their continual support.

and Olivia McAdie for her warm and sometimes heated encouragement.

CONTENTS

APPENDICES

FIGURES

TABLES

CHAPTER 1

1.0 INTRODUCTION

A project to investigate aspects of Near-Real-Time-Photogrammetric (NRTP) systems has been initiated in the Surveying Department at the University of Cape Town, Rüther and Parkyn (1990). The project, which started in 1987, is ongoing and has involved the development of a Photogrammetric Engineering and Industrial digital Camera System (PHOENICS), a low cost PC-based Near-Real-Time-Photogrammetric system. PHOENICS provides a semi-automatic system to determine three dimensional co-ordinates of surfaces and objects using a photogrammetric method.

Central to the real time photogrammetric determination of object points is the determination of target centres. The objective of this thesis is to investigate this aspect of PHOENICS, namely to develop and compare the precision of a number of alternate algorithms, which calculate the centre of circular targets within a NRTP system.

The process of algorithms calculating target centres in NRTP systems can be compared with that of an archer finding the centre of a target.

In the same manner as an archer tries to shoot an arrow at the centre of a target, where the closeness of the arrow to the centre of the target is indicative of the accuracy of the shot, target centring algorithms within a photogrammetric digital image processing system are used to determine, as accurately as possible, the centre co-ordinates of targets as viewed by the imaging system, see Figure 1.1 .

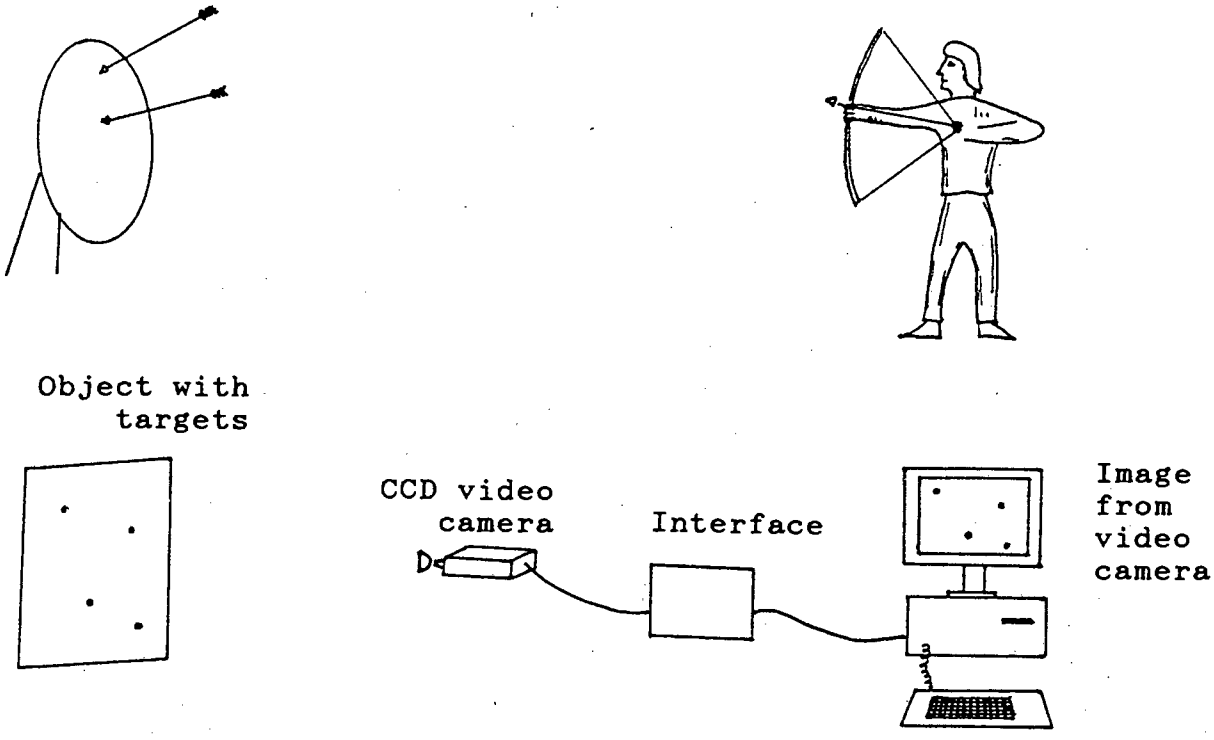

Figure 1.1 Archer and photogrammetric system

Table 1.1 Similarities between an archer and a NRTP system

PROCESS	FACTORS AFFECTING ARCHER	FACTORS AFFECTING NRTP SYSTEM
1 Environmental factors	- Contrast between target & background, is a function of: o texture, o ability to reflect incident light - Lighting intensity & direction - Focus	- Contrast between target & object or background, a function of: o texture, o ability to reflect incident light - Lighting intensity & direction - Focus

2 Image acquisition	- Eye and brain	- CCD camera and frame grabber
3 Preprocessing	- Account for wind and distance	- Account for lens distortion - Threshold level to find target
4 Recognition	- Search field for target - Determine centre of target - Aim and release	- Search image for target - Use algorithm to determine centre
5 Positioning	- A measure of how close the arrow landed to target centre	- A measure of the algorithm's centre relative to the known target centre

More formally, a general overview of the tasks involved with digital photogrammetry include , Gruen (1987) :

i) Preparation of environmental factors. This involves the light source and the target reflecting the light. The 'background' object should be considered when evaluating the surface of the target being used, to ensure good contrast.

ii) Image acquisition. A two dimensional representation of the target is formed and stored as a matrix of grey values. The hardware includes the lens, video camera and 'frame grabber' to acquire the image and store it in memory.

iii) Preprocessing. This may involve enhancing the image by removing noise or a step to support the recognition of targets. Target recognition is achieved by selecting a threshold level, determined interactively. A binary image of the targets is formed at this threshold level, with targets at one level and background represented by another level. Incorrectly identified targets may be eliminated at this stage.

iv) Recognition of the targets. This may be achieved by finding the extent of connected points (constituting a target) on a digital binary image. A window surrounding the target perimeter is determined and the target window is transferred to an algorithm to find the centre of the target.

v) Positioning. This usually involves determining the three dimensional locations of targets in space using photogrammetric methods on corresponding (conjugate) target locations from two images of the same object taken from different positions.

Note For this thesis, step (iv) involves determining each target centre using an assortment of algorithms and step (v) evaluates the accuracies of all the (target centring) algorithms by relating the location of the target in the object space to the expected target centre location determined previously using non-photogrammetric survey methods. The Photogrammetric Restitution Program (PREP) (Rüther) , provides a calibration routine, based on control frame points with known 3-D co-ordinates. The variance σ_o^2, derived as part of this process, provides a measure of the overall accuracy of the image point position.

Traditionally, photogrammetry involves manually measuring conjugate identifiable features of an object from two photographs (a stereo-pair) of the object taken from different positions, in order to determine the third dimension of the feature. A grid of the object obtained in this manner maps and defines the contours of the object in three dimensions. In NRTP, features of an object in space are often automatically identified by attaching thereto a number of clearly recognisable/ contrasting circular flat disks (referred to as targets) , and measuring the resulting location of the target in the image taken by the video camera.

Since the image is digitised for evaluation by the computer, the target is represented by a spatially uniform array of weighted points (pixels), see Figure 1.2 . The centre of the target defines the target co-ordinate uniquely. The precision of the evaluation of the third dimension of the object target is related to the precision of locating the target centre.

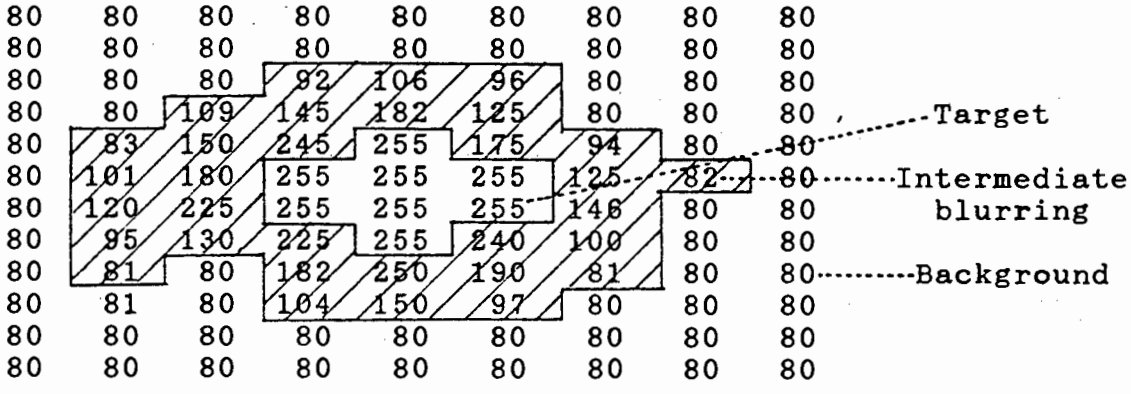

where - '255' defines the target
- '80' defines the background level
- all other values indicate the blurring between target and background level

Figure 1.2 Illustrating a target within a digital image

Existing algorithms have been implemented, adapted and investigated to compare their ability to accurately locate target centres in a digital image.

CHAPTER 2

2.0 OVERVIEW

32 target centring techniques, consisting of combinations of ten algorithms, are implemented for evaluation. Three types of images are formed to test various aspects of the algorithms. The images are:

Image #	Description of Targets	Reason for Image
Image 1	Perfect Symmetrical Synthetic Target	Evaluate Potential Accuracy of Algorithm
Image 2	Synthetic Target with an Artificial Blemish	Observe Effect of Partial Occlusion on the Algorithm
Image 3	(Real) Image Captured by PHOENICS	Test Accuracy of Algorithms on Real Image

The thesis can be subdivided into four parts illustrated by overlays 1..4 (These are further translated into the following chapters):

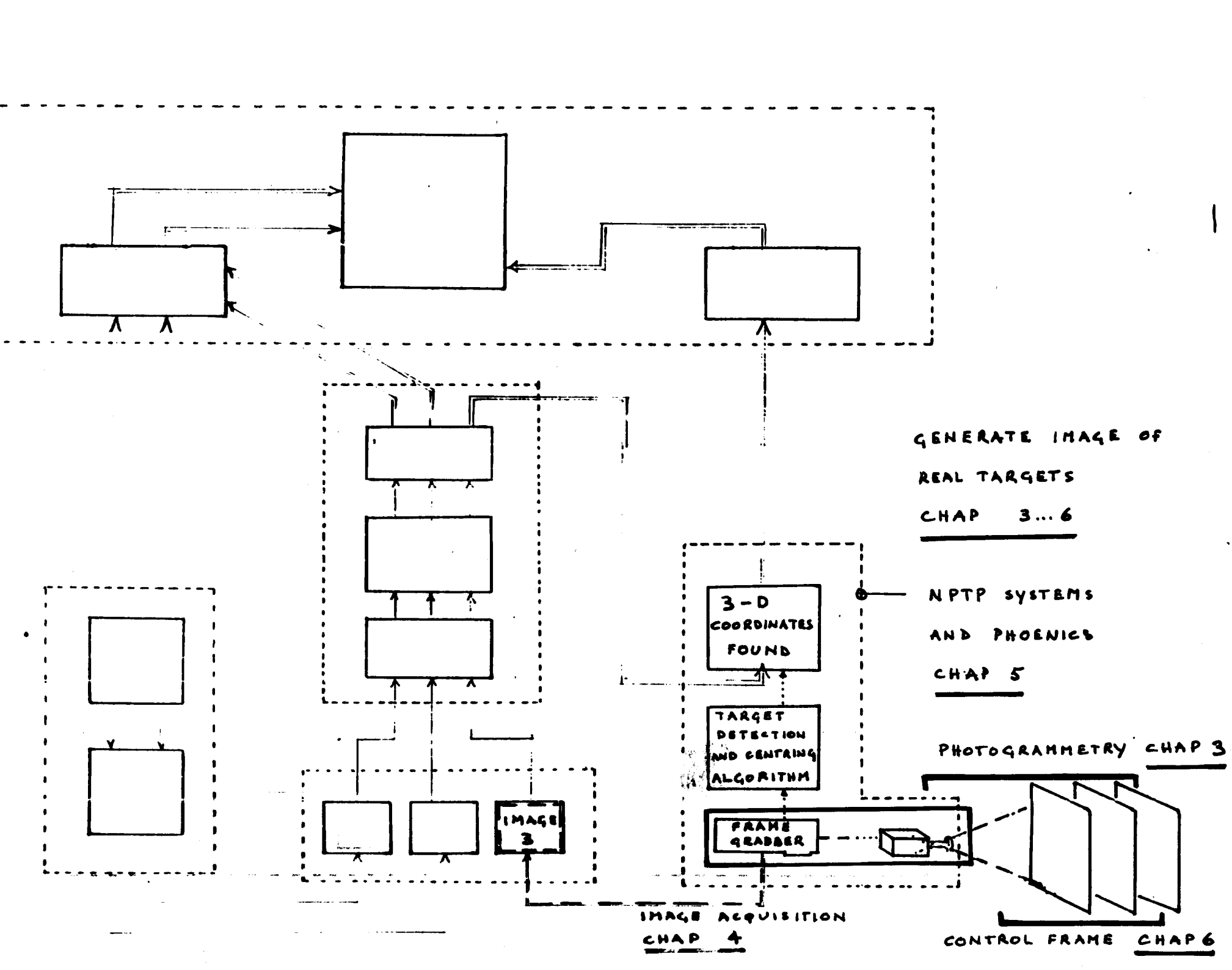
GENERATE IMAGE OF
REAL TARGETS
CHAP 3...6
3-D
COORDINATES
FOUND
NPTP SYSTEMS
AND PHOENICS
CHAP 5
TARGET
DETECTION
AND CENTRING
ALGORITHM
PHOTOGRAMMETRY CHAP 3
IMAGE
3
FRAME
GRABBER
IMAGE ACQUISITION
CHAP 4
CONTROL FRAME CHAP 6

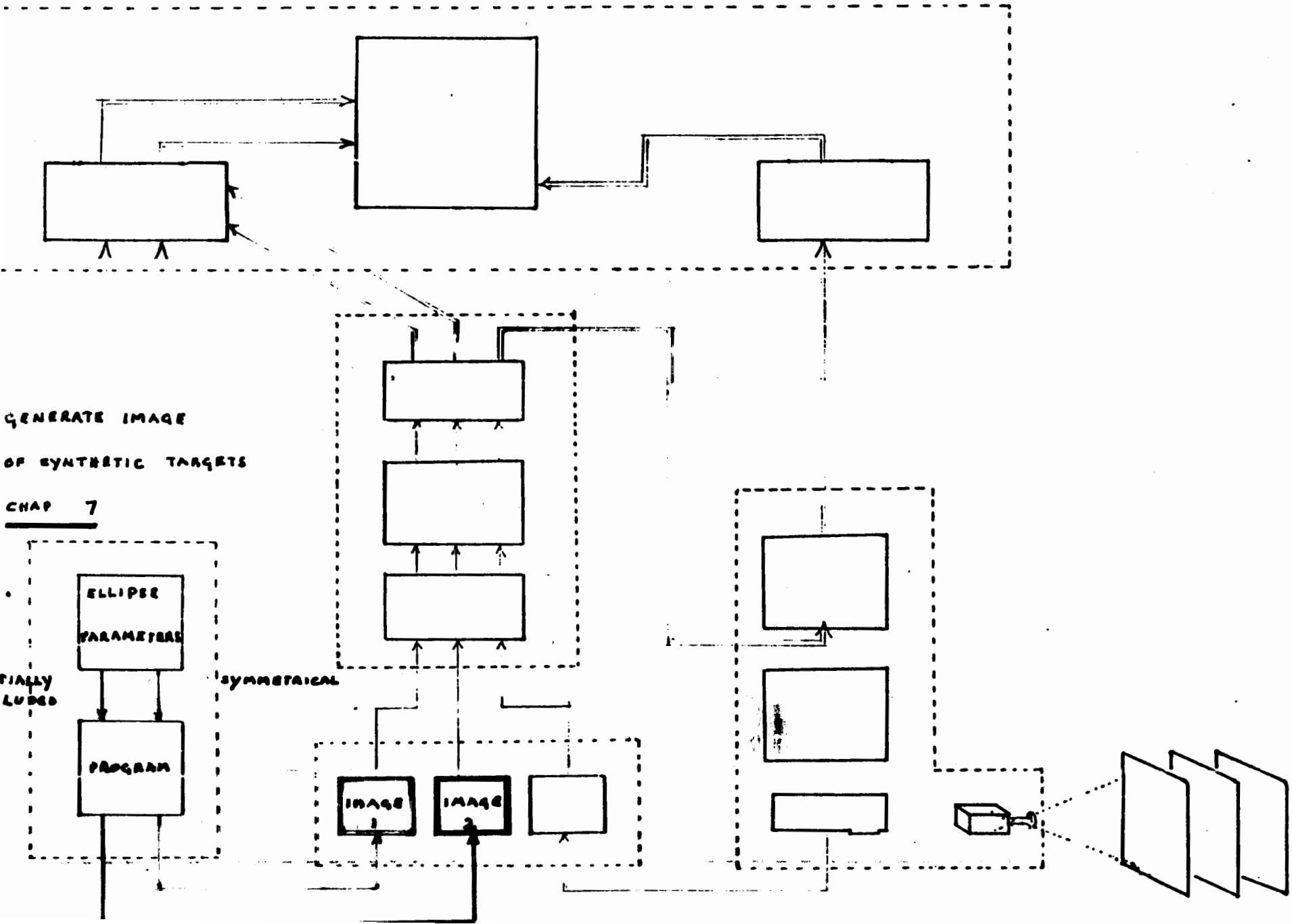
GENERATE IMAGE
OF SYNTHETIC TARGETS
CHAP 7
ELLIPSE
PARAMETERS
PROGRAM
IMAGE
IMAGE
SYMMETRICAL

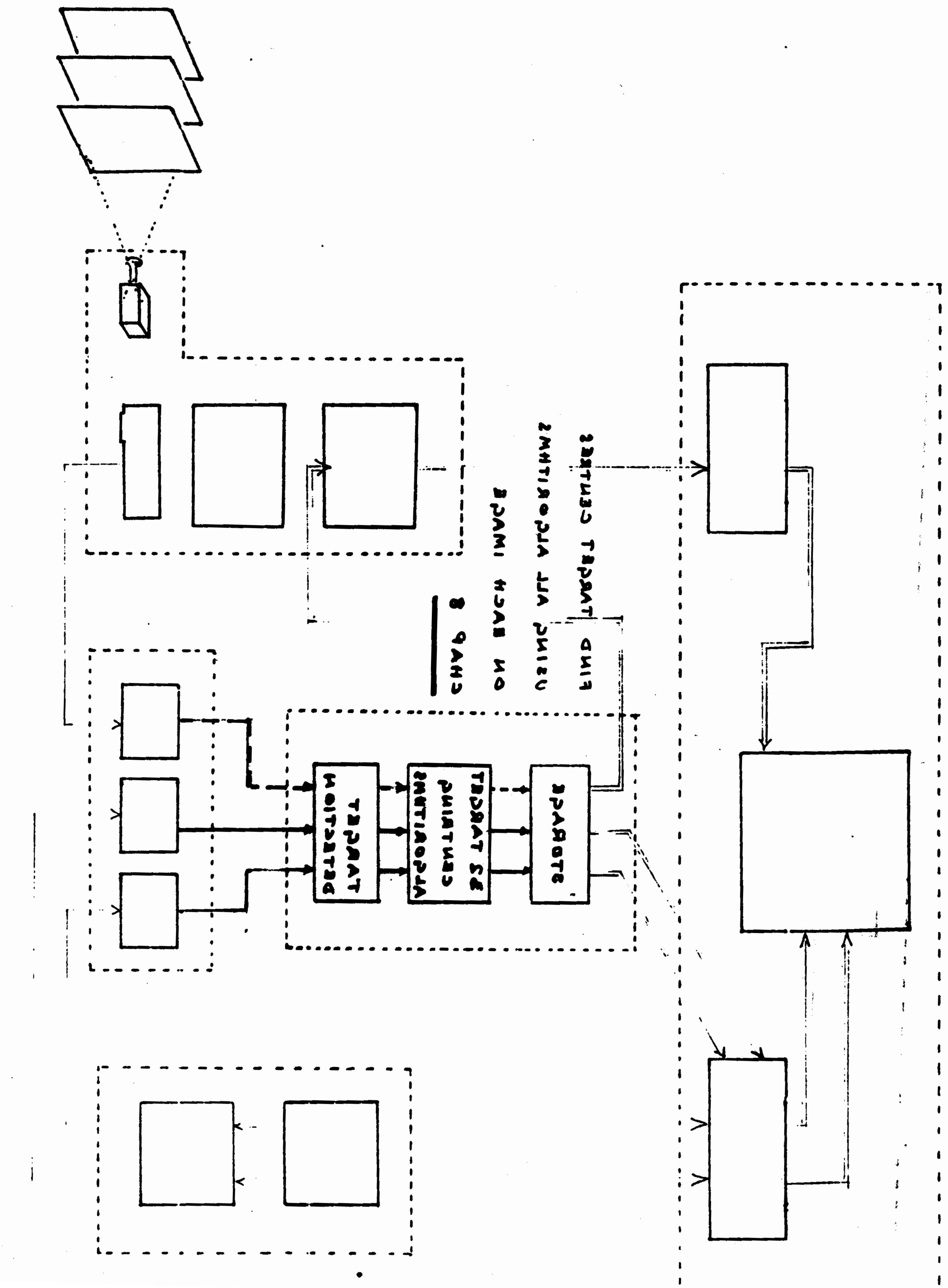
FIND TARGET CENTRES
USING ALL ALGORITHMS
ON EACH IMAGE
CHAP 8
TARGET DETECTION
3E TARGET CENTRING ALGORITHMS
STORAGE

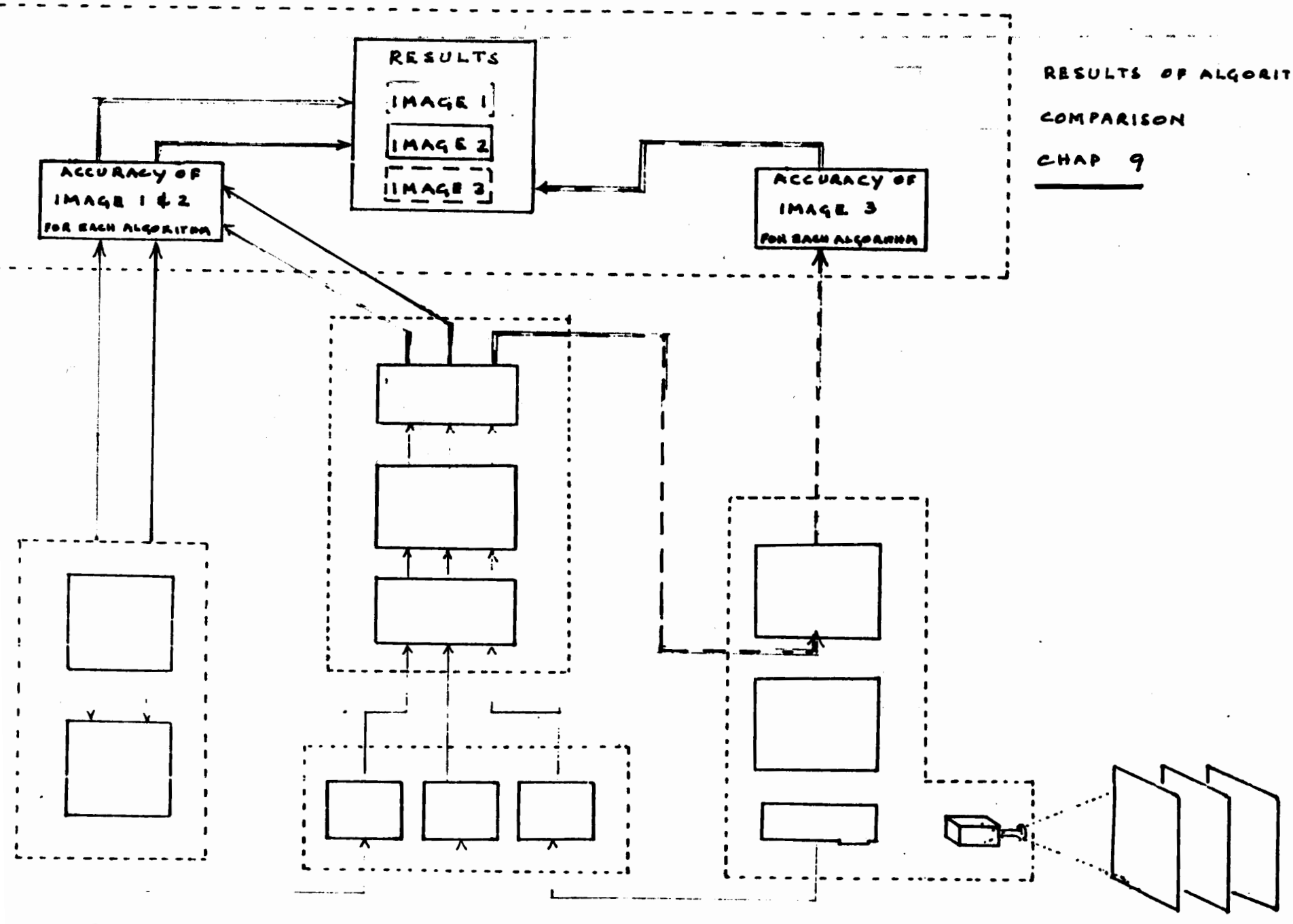

RESULTS OF ALGORITHM COMPARISON

CHAP 9

OVERLAY

Overlay 1 : Overview of necessary steps to capture and interpret a digital image of a control frame, using a video camera interfaced to a computer.

Chapter 3 introduces the terms and approach to solve the photogrammetric problem for engineers with no surveying background.

Chapter 4 presents an explanation of the process of capturing a digital image and includes a description of the video camera and frame-grabber (interface) to the computer.

Chapter 5 deals with a description of Near-Real-Time-Photogrammetric systems, and in particular PHOENICS

Chapter 6 embodies the fabrication and surveying of a control frame, followed by capturing a digital image of it. The image is stored for further processing.

Overlay 2

Chapter 7 deals with the generation of two digital images, each containing a number of synthetic targets. One image contains symmetric-synthetic targets and the other contains targets with an artificially introduced blemish. The two images are stored for further processing.

Overlay 3

Chapter 8 describes the target detection program followed by an explanation of the target centring algorithms which are implemented. The three images (1 image from overlay #1 and 2 images from overlay #2) are viewed by the program to locate the centres of each target. For each image, all the algorithms are tested and the target centres for each algorithm are stored for further processing.

Overlay 4

Chapter 9 determines the accuracies of the target centring algorithms:

- For images 1 and 2 a comparison is made between the target centres obtained by using each algorithm and the expected target centres in the parameter listing.
- For image 3 the target centres are fed back into the photogrammetric component of PHOENICS (PREP) and correlated with the three dimensional control frame co-ordinates to obtain a measure of fit by each algorithm.

For each image, a graph and an analysis compare the accuracy of each algorithm.

Chapter 10 concludes the thesis with recommendations regarding the implementation of target centring algorithms.

Superimposing all the overlays illustrates the fact that the target detection and centring algorithm (SEARCH), used by the PHOENICS system, is by-passed and the detection and centring algorithms program developed in this thesis is used in its place.

CHAPTER 3

3.0 PHOTOGRAMMETRY

3.1 DEFINITION AND DISCUSSION OF PHOTOGRAMMETRIC TERMS

The word photogrammetry is derived from the Greek: 'photo' = light, 'gramma' = something drawn or written, and 'metron' = measurement. Thus the task described by photogrammetry is 'measuring graphically using light'. The American Society for Photogrammetry's (1980) definition of photogrammetry is :

> "Photogrammetry is the art, science and technology of obtaining reliable quantitative information about physical objects and the environment through the process of recording, measuring and interpreting photographic images and patterns of radiant imagery derived from sensor systems."

Since its inception, over a century ago, the primary use for photogrammetry has been the compilation of topographic maps. The art of photogrammetry has developed over the years to become an efficient, economical and convenient mapping tool, giving precise and reliable measurements of the earth's surface. Applications outside the ambit of topographic mapping are encompassed by the term non-topographic or close range photogrammetry. In close range photogrammetry, the object to be measured is limited to a maximum size of 300m.

3.2 DISCUSSION OF PHOTOGRAMMETRIC TERMS

3.2.1 Metric and Non-Metric Cameras

Traditionally cameras used in the photogrammetric process are specially designed for this purpose. These cameras are known as metric cameras, because the photographs produced with them can serve to derive quantitative (metric) information. Metric cameras are characterised by their high mechanical stability. They are calibrated by the manufacturer and the principal point position and principal distances are known accurately to within a few micrometres and generally remain unchanged unless exposed to extreme conditions. Metric cameras are equipped with high quality lenses designed to minimise lens distortion.

Non-metric cameras used in photogrammetric applications are typically high quality amateur cameras with preference given to large format cameras. With few exceptions, non-metric cameras lack the mechanical stability of metric cameras. As a rule one can not rely on the calibration values for principal distance or principal point to remain constant for any length of time, therefore the cameras are often calibrated 'on the job'. Non-metric cameras are notorious for their large lens distortions.

The use of non-metric cameras in close range photogrammetry has increased substantially in recent years as a result of the development of special photogrammetric algorithms and powerful computing facilities at PC level.

CCD cameras belong with few exceptions, to the family of lower quality non-metric cameras. It appears that video camera lenses have not yet attained the quality of top-of-the-range conventional cameras.

3.2.2 Object Space and Image Space

The space in front of the lens (outside the camera) contains the object to be measured and is known as 'object space'. The area inside the camera contains the image and is referred to as 'image space'.

3.2.3 Principal Point

The principal point (PP) is the point where a ray entering the lens system through the centre of the external (entrance) pupil at a right angle to the image plane intersects this plane. This point is the reference point for image co-ordinates, i.e. the origin of the image co-ordinate system, see Figure 3.1 .

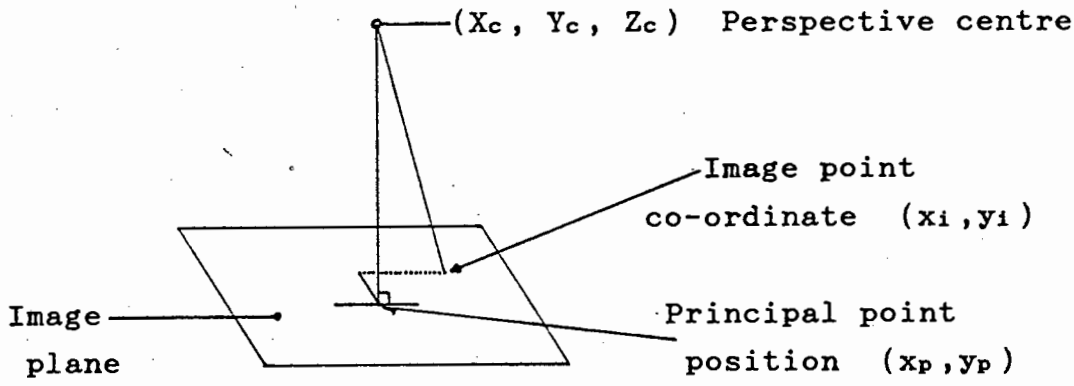

Figure 3.1 Defining an image point in the image plane

3.2.4 Perspective Centre

The perspective centre, or the centre of projection, is the point in space where all connecting lines between object points and associated image point intersect. When transferring this concept to the reality of the lens system of a camera, this definition no longer holds. Here the perspective centre is represented by two points, the internal

and external node of the lens system. The perspective centre position as used in photogrammetric models is the position of the external node in terms of object space co-ordinates (X_c, Y_c, Z_c) .

3.2.5 Image Co-ordinate System and Image Co-ordinates

Points on the image are measured in image co-ordinates (x_i, y_i), counted from the principal point as the co-ordinate origin. The positive x axis extends from the principal point to the right (as seen on the positive image) and the positive y axis to the top. The direction of the x axis is approximately parallel to the horizontal image frame borders and the y axis is at a right angle to the x axis.
All measured image co-ordinates must be expressed in this co-ordinate system in order to satisfy the standard mathematical formulations of photogrammetric problems.

> [Image co-ordinates are measured by means of a comparator, or in the case of CCD cameras, by software on the 'pseudo chip' image of a frame grabber.]

3.2.6 Control and Object Points

Control points are points in object space for which 3-dimensional co-ordinates in the object space co-ordinate system are known.

Object points are points on the imaged object for which no co-ordinates are known in object space. It is normally the objective of photogrammetric procedures to determine these co-ordinates.

3.2.7 Pseudo-chip and Pseudo-pixel

The video signal output from a CCD camera represents a video image of l lines and c columns generated by the camera's CCD chip. This signal is analog. In order to process the image in a PC it is necessary to convert the signal into digital form, capture it and store it. This can be done by means of a so-called frame grabber card which can be slotted into a PC type computer. In the PHOENICS system this card is a MATROX PIP 512 image processing board with a 512 by 512 pixel format. The format of the camera chip will generally differ from that of the frame grabber board in which case a one to one chip-to-board pixel transformation can not be achieved. The analog image coming from the camera chip must be resampled and subdivided into new pixel units before it can be captured on the frame grabber. (Part of the image is lost if the camera chip has more pixel rows than the frame grabber.) Once captured, the image no longer exists in terms of chip-pixels. It is now fully converted into the frame grabber format, which can be seen as a 'pseudo-chip' of 512 by 512 'pseudo-pixels'. All measurements on the image are therefore in units of 'pseudo-pixels'.

3.3 THE CONCEPT OF ORIENTATION IN PHOTOGRAMMETRY

To describe the characteristics of a camera and the position of a camera arrangement in space, the following concepts are used in photogrammetry :

- Interior or inner orientation
- Relative and absolute orientation

3.3.1 Interior Orientation

Interior orientation defines the geometric characteristics of a camera. The three elements of interior orientation are:

- Principal distance (in equations this is represented by the symbol f)
- Principal point position (two co-ordinate values: x_p , y_p)

3.3.2 Relative and Absolute Orientation.

The elements of absolute orientation serve to position and orient a camera in space. They are :

- Position of perspective centre in object space (X_c , Y_c , Z_c)
- Rotation angles between the camera axes and the axes of the object space co-ordinate system. Rotations are defined as Omega, Phi and Kappa for the x, y and z axes respectively.

The elements of absolute orientation form part of the set of unknowns evaluated in the camera calibration method used here.

The differences between the absolute orientation parameters of two cameras are known as 'relative orientation'.

3.4 MATHEMATICAL MODELS IN CLOSE RANGE PHOTOGRAMMETRY

Photogrammetry makes it possible to determine three-dimensional co-ordinates of points on an object by means of photographic images of the object taken from a number of camera stations distributed in space around the object.

This problem can be seen as consisting of two stages

- the restitution of the position and orientation of the cameras in space (relative and absolute orientation)

- the determination of points on the object.

If non-metric cameras are used then a third stage must precede these photogrammetric procedures

- the determination of principal point position, principal distance and (often) lens distortion parameters (interior orientation).

In modern photogrammetry these three stages are often combined into a single mathematical model.

The most frequently used models for the analytical solution of the photogrammetric problem in close range applications of non-metric cameras are

- Direct Linear Transformation (DLT) or 11-Parameter Transformation

- Modified 11-Parameter Transformation

- Bundle Solution

Nomenclature

The following nomenclature is used in the equations formulating these models :

X_i , Y_i , Z_i = object space co-ordinates of object or control point P_i

X_c , Y_c , Z_c = object space co-ordinates of perspective centre (position of external pupil in camera lens)

x_i , y_i = image co-ordinates corresponding to object space point P_i (observations a priori)

x_p , y_p = principal point position

$x_i - x_p$, $y_i - y_p$ = image co-ordinates x_i , y_i transformed to the principal point

f = principal distance (calibrated focal length)

$b_{11}..b_{33}$ = parameters of the 11-parameter transformation

$m_{11}..m_{33}$ = elements of a rotation matrix R

3.4.1 Bundle Solution

The bundle solution is derived in Appendix A using the 'collinearity' condition. The solution is:

$$(x_i - x_p) = f \frac{m_{11}(X_i - X_c) + m_{12}(Y_i - Y_c) + m_{13}(Z_i - Z_c)}{m_{31}(X_i - X_c) + m_{32}(Y_i - Y_c) + m_{33}(Z_i - Z_c)}$$

$$(y_i - y_p) = f \frac{m_{21}(X_i - X_c) + m_{22}(Y_i - Y_c) + m_{23}(Z_i - Z_c)}{m_{31}(X_i - X_c) + m_{32}(Y_i - Y_c) + m_{33}(Z_i - Z_c)}$$

This formulation directly links image point x_i, y_i and object point X_i, Y_i, Z_i.

In order to account for imperfections in the lens system, additional parameters (APs) are used to describe lens distortion correction and other imperfections.

To compensate for incorrect image point locations, due to imperfect target centring algorithms or noise in the images (after taking into account the lens distortion), a least squares solution is executed which adds residual corrections v_{xi}, v_{yi} to the image points, giving:

$$(x_i - x_p) + v_{xi} + dx = f \frac{m_{11}(X_i - X_c) + m_{12}(Y_i - Y_c) + m_{13}(Z_i - Z_c)}{m_{31}(X_i - X_c) + m_{32}(Y_i - Y_c) + m_{33}(Z_i - Z_c)}$$

$$(y_i - y_p) + v_{yi} + dy = f \frac{m_{21}(X_i - X_c) + m_{22}(Y_i - Y_c) + m_{23}(Z_i - Z_c)}{m_{31}(X_i - X_c) + m_{32}(Y_i - Y_c) + m_{33}(Z_i - Z_c)}$$

where:

dx,dy lens distortion effects

v_{xi}, v_{yi} residuals. These are corrections required to allow the image ray to pass through the object point, perspective centre and image point.

σ_o^2 variance from the least squares solution where:

$$\sigma_o^2 = \frac{y^T P y}{n-m}$$

may be derived. This value is a measure of the variations of all image points.

3.4.2 DLT or 11-Parameter Transformation

Given the collinearity condition equations: multiplying out the parenthesis and defining new constants, enables the Bundle solution to be rewritten as the DLT or 11-Parameter transformation :

$$(x_i - x_p) + v_{xi} + dx = \frac{b_{11} X_i + b_{12} Y_i + b_{13} Z_i + b_{14}}{b_{31} X_i + b_{32} Y_i + b_{33} Z_i + 1}$$

$$(y_i - y_p) + v_{yi} + dy = \frac{b_{21} X_i + b_{22} Y_i + b_{23} Z_i + b_{24}}{b_{31} X_i + b_{32} Y_i + b_{33} Z_i + 1}$$

3.4.3 Modified 11-Parameter Transformation or Projective Transformation.

Of the eleven unknowns in this solution only nine are independent. Relationships between the nine independent and

the two dependent parameters can be introduced as restraints into the adjustment. The standard adjustment case of the so-called 'parametric adjustment' must then be modified to include the condition equations between the parameters. The modified 11-parameter solution is an approximation of the mathematically rigorous approach. This method is sometimes referred to as the projective transformation.

3.5 LENS DISTORTION

Lens distortion has been the object of numerous scientific publications. The most widely used model is the **D. Brown formulation** in the form :

$$dx_i = (x_i - x_p)(k_1 r^2 + k_2 r^4 + k_3 r^6 + ..) + p_1 (r^2 + 2(x_i - x_p)^2) + 2p_2 (x_i - x_p)(y_i - y_p)$$

$$dy_i = (y_i - y_p)(k_1 r^2 + k_2 r^4 + k_3 r^6 + ..) + 2p_1 (x_i - x_p)(y_i - y_p) + p_2 (r^2 + 2(y_i - y_p)^2)$$

The polynomial terms k_i model the radial lens distortion while the p_i-terms describe the decentring distortion. Decentring is caused by inaccuracies in the mechanical alignment of the lenses which make up the camera's lens system.

It has been shown that in close range applications the higher order polynomial terms k_2, k_3 etc. contribute little to the distortion model and evaluations are often restricted to k_1, p_1 and p_2.

In our application, only the first polynomial term k_1 is used to model radial distortion.

3.6 SUMMARY

In this chapter a photogrammetric solution to the task of correlating object target co-ordinates with image target centre co-ordinates has been discussed. The Brown model has been added to compensate for radial lens distortion.

In the case of a real image, the evaluation of the photogrammetric model includes a measure of accuracy for the target centring algorithm, namely the residuals v_{xi} and v_{yi} (to correct for the image target centre location: x_i, y_i). The variance σ_o^2, derived from the residuals, is a means to compare the precision of one algorithm with another.

CHAPTER 4

4.0 IMAGE ACQUISITION

Cameras form the principal tool of any photogrammetric measurement. Photographic film is not used in modern NRTP systems because of the time taken to process the film and difficulties involved with digitising the film for interpretation. Instead, solid state digital video cameras are normally used to capture an image and an interface (frame grabber) board is used to transfer the image from the camera to the computer for analysis.

To correctly interpret the image, it is essential to understand the primary components in, and the process of, image acquisition.

4.1 SOLID STATE SENSORS

Solid state sensors use semiconductors to transform incident light into an electrical signal. The popularity of the charge coupled device as an imaging array, has led to the terms 'CCD' and 'solid state camera' being synonymous. The CCD camera is, however, only one class of the solid state sensors.

The three main types of solid state sensors are :

- Photodiode
- Charge Injection Device (CID)
- Charge Coupled Device (CCD) - with interline transfer
  - with frame transfer

4.1.1 The Photodiode

The photodiode was the first of the solid state sensors to be developed. It was developed two decades ago in response to aerospace requirements. They are typically addressed with a MOSFET (Metal Oxide Silicon Field Effect Transistor) gate connected at each crossing point.

4.1.2 The Charge Injection Device

The charge injection device (CID) has 'nearly' continuous photo sites in both directions and has been used extensively in astronomy. The advantage of the system is the inherent noise reduction capability, since the signal can be transferred to the read capacitor and back to the integrating element without affecting the integration. This non-destructive read is unique to the CID, where the charge is injected into the substrate after each integration period, Real (1986).

4.1.3 The Charge Coupled Device

The charge coupled device (CCD) belongs to a more general class of charge transferring sampled analogue devices. Its most promising use has been in imaging systems. The photodetectors of the CCD imaging chip have a MOS (Metal Oxide Semiconductor) structure. They consist of a 'doped' semiconductor, an insulator (glass) and a metal electrode. A large number of photodetectors are arranged next to one another to form a sensor row.

Applying a positive charge to the metal electrode will lead to a negative charge build up on the other side of the insulator. The extent of the charge build up is dependent on the incident light on the detector. The more light, the more free electrons there are, the larger the charge.

The accumulated charges of the complete row of adjacent sensors are moved along the row with little loss, driven by an appropriately phased sequence of potential shifts from the clocking system.

A number of sensor rows placed next to one another make up a sensor array.

Interline and Frame Transfer

The CCD sensors can be categorised according to the distribution of active cells and passive storage cells. The two methods in which this is achieved are by interline transfer or frame transfer.

4.1.3.1 Interline Transfer

The image area of the interline design consists of alternate columns of photosensitive sensors and opaque drift registers, see Figure 4.1 .

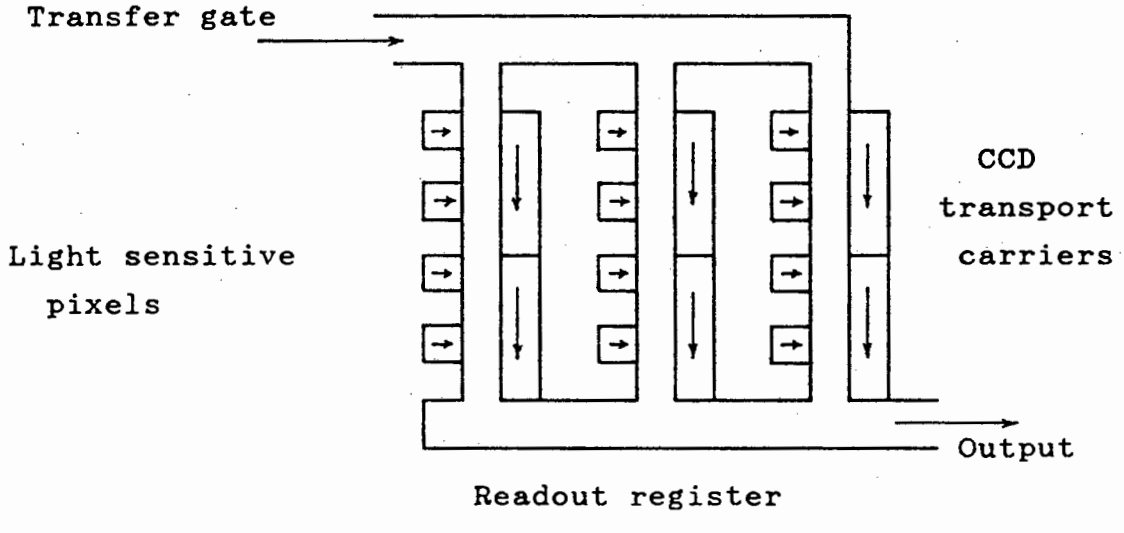

Figure 4.1 Interline charge transfer

During the integration time, charge is accumulated at the photosensors and passed to the shift registers for storage. The charges are shifted vertically down the register to the horizontal readout register during the following integration time. In this manner, an image in the form of a string of pixel grey values is transferred out of the CCD chip to be processed further by the camera, to give an output compatible with the CCIR (European black and white video standard) format. Since every second column in the CCD chip is a shielded readout register, only half of the chip area is photosensitive.

4.1.3.2 Frame Transfer

The rows of light sensitive cells are placed next to one another, in frame transfer CCD sensors, making a continuous imaging plane, see Figure 4.2 .

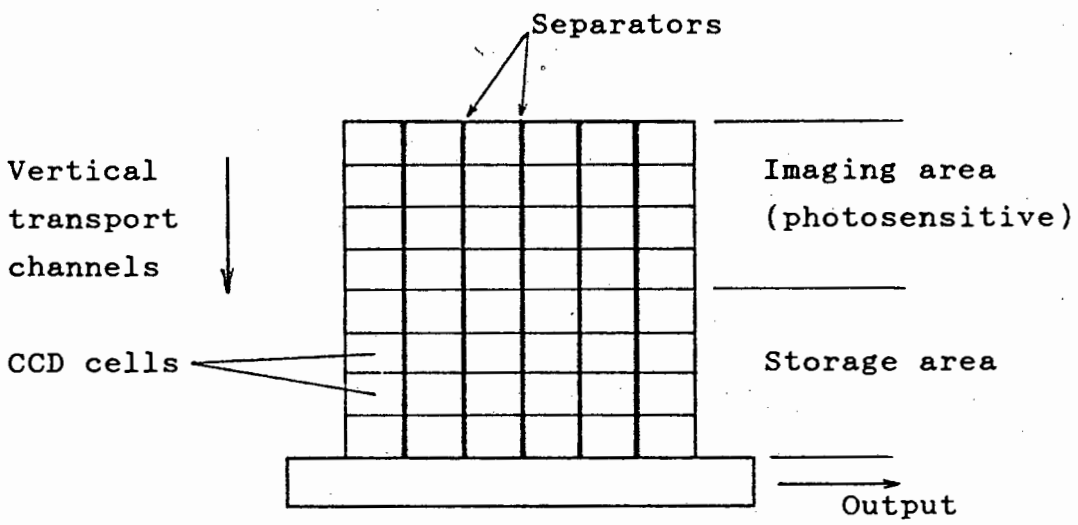

Figure 4.2 Frame transfer

Half of the chip area is optically sensitive, accumulating a charge during the integration time. From here, the charges are transferred to the opaque region of the CCD surface where they are stored and read out with a horizontal shift register in the following integration period.

4.1.4 Sources of Inaccuracies on the CCD Chip

Errors inherent in the silicon structure of the CCD solid state sensor include the following:

- Blooming: The solid state sensor may find stray paths for charges due to excess light in a particular sensor cell. The excess charges may migrate into neighbouring cells. With additional structures, the additional charges can be drained off, Flory (1985).

- Transfer smearing: In frame transfer devices, the illumination during transfer time between the imaging and storage sections results in vertical streaks for very bright objects. One way around this problem is by removing illumination with a shutter during transfer time, with little effect on the sensitivity.

- Reflections: These occur on the surface of the sensor as well as on boundaries between different materials due to the different refractive indices of silicon dioxide and silicon, thus reducing the pixel grey value.

- Absorption: Absorption of charges by gates made of aluminium or polycrystalline silicon degrades the sensitivity of the sensor cells.

- Change in grey value: The charges acquired from the readout register of the sensor are amplified and used to form a time discrete analogue signal. The slew rate of the amplifier (limiting the rate at which the output of an amplifier can vary) results in a change in the grey values.

Some systematic errors relating to the position of the imaging plane to the optical axis have been modelled by photogrammetrists for calibration and correction of the resulting image. These include, Gruen and Beyer (1987):

- The sensor is mounted on a ceramic carrier and protected by a glass plate. The parallel aligning of the glass plate with the sensor is a source of errors.

- The sensor assembly is mounted in the camera housing by soldering it in place or by pressing the housing on a special surface of the camera body. The sensor is thus not necessarily orthogonal with the optical axis.

The CCD camera with frame transfer readout is currently the most promising imaging device for real time photogrammetry. The primary features of the CCD camera include the high geometric accuracy of the sensors, the stability over time of the geometry and the sensors' sensitivity, surpassing the characteristics of other video cameras available.

4.2 THE FRAME GRABBER BOARD

The output of the CCD camera is a dampened composite synchronous video signal. The video signal is converted to a discrete digital signal, which can be interpreted and manipulated by a computer, using a frame grabber (interface) card. One significant source of errors is the conversion of the discrete pixel values to a video signal and reconverting the video signal to an array of grey values on the frame grabber board.

The European video standards (PAL for colour and CCIR for black and white) define images of 625 lines at 25 Hz. The

images are made up of two sub-images, consisting of alternate lines scanned at 50 Hz, which are interleaved to form the complete image. Only 575 lines are displayed, since a number of lines are required for the vertical retrace at the end of each line. Thus for 25 complete frames of 625 lines per second, with a theoretical 625 picture elements (pixels) per line, there are $625 \times 625 \times 25 = 9.77 \times 10^6$ pixels per second,which requires a bandwidth of half of this, namely 4.88 MHz.

> [The image width to image height ratio is approximately 4:3 , increasing the resolution of the image by a factor $^4/_3$. The increase is, however, almost cancelled out by the 'Kerr factor' where the scanning pattern, that has a slight downward slope, does not align perfectly with a 'checker-board' pattern, therefore reducing the resolution by a factor of 0.7], Lathi (1983).

The image from the CCD sensors is transferred on the video signal, limiting the array size of the CCD to a maximum of 575 rows. The number of columns of the CCD chip are apparently unlimited because the row information in a video signal is a sampled data continuous analogue signal, allowing all the pixels in a row of a CCD chip to be transferred using one row of a video signal. Slewing will however limit the resolution of the CCD rows. The frame grabbing board interprets the data from the video signal using a sample and hold device followed by an analogue to digital (A/D) converter. If the pixel rate of the frame grabber differs from that of the CCD camera, a scaling error in the image pixel is introduced. This is proportional to the ratio of the two pixel rates. The number of lines read in from the video image is limited to the size of the frame grabber's image buffer which, in current systems, is often 512x512 pixels.

The use of television signals can be the source of many errors. One solution is to convert the data from analogue to digital directly after it is read from the sensor and to use a data bus to transfer the digital image directly to an image processing system. The implementation of this solution would be limited by the data transfer rates required for real time image acquisition.

4.3 INTERPRETING A DIGITAL IMAGE

All imaging systems have a limited resolution. The resolution is a measure of the 'granularity' or 'continuity' of a curve. In photographic systems, resolution is measured as the number of discrete lines distinguishable (on the medium) per millimetre e.g. for slides, the resolution is approximately 100 lines per mm.

The resolution of a digital imaging system is limited by the number of rows and columns of the combined video camera and frame grabber system.

The output of the frame grabber, which limits the final system resolution, is an array of 512x512 picture elements (pixels). Each pixel has a grey scale range of eight bits, equivalent to 256 levels of grey, from black (with a grey level of '0'), to white (with a grey level of '255'), see Figure 4.3a .

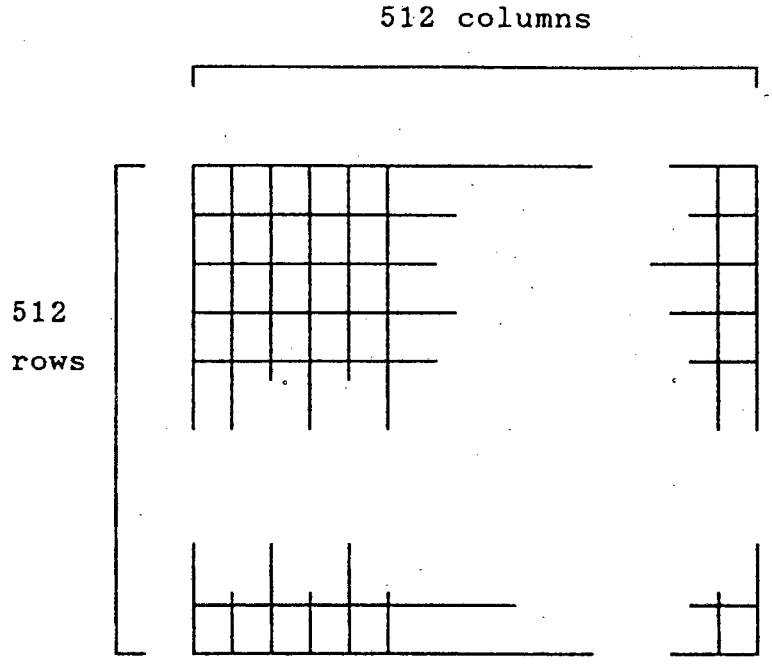

Figure 4.3a Discrete rows and columns in a digital image

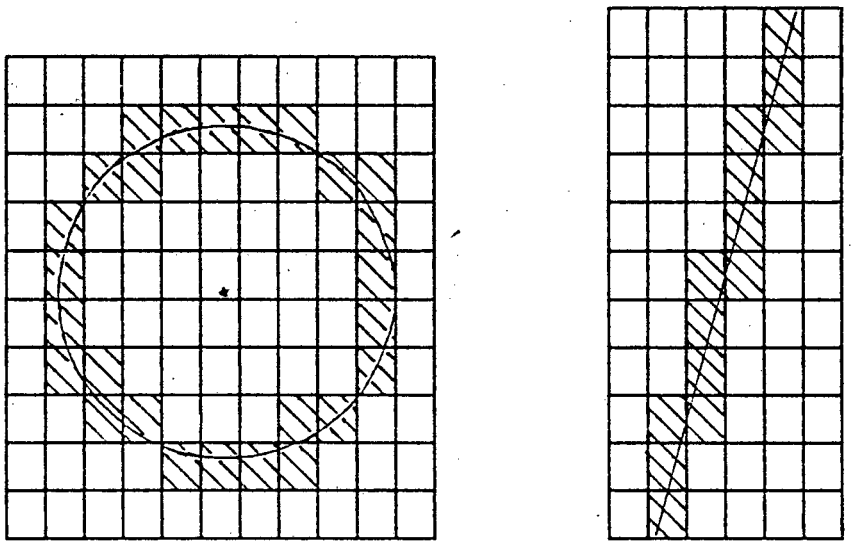

Figure 4.3b Finite pixel effect on a circle and straight line

Figure 4.3 The effect of forming a discrete digital image

The effect of the limited resolution of the imaging system causes continuous lines to have jagged edges as illustrated in Figure 4.3b. The distortion of the image is particularly noticeable on smaller objects, such as the targets used in this thesis, which form an average image size of 10x10 pixels.

The initial target centring algorithms which were used for photogrammetric purposes in digital systems, evaluated target centres to the nearest pixel precision. With improved target centring algorithms, target co-ordinates are being evaluated to sub-pixel accuracies.

CHAPTER 5

5.0 THE DEVELOPMENT OF A NRTP SYSTEM: PHOENICS

PHOENICS (Photogrammetric Engineering and Industrial digital Camera System) has been designed as a low cost, PC based, NRTP system, Rüther and Parkyn (1990). The system is operational but is still at prototype level.

It is currently being applied to test object surface measurements and algorithms such as:

- target detection
- target centre location.

Those algorithms which are found to improve the characteristics of PHOENICS are implemented to further enhance the system. The system has been used to generate contours of sculptured surfaces and to measure a number of control frames.

The present hardware configuration of PHOENICS, see Figure 5.1 , comprises:

- a personal computer, the IBM PS/2 model 30
- two video frame grabber boards, the Matrox PIP-512 and PIP-1024
- two Siemens K211 CCD cameras
- two external monitors, Phillips R6BCM 8833 and
- one Parallon 8088 compatible parallel processor.

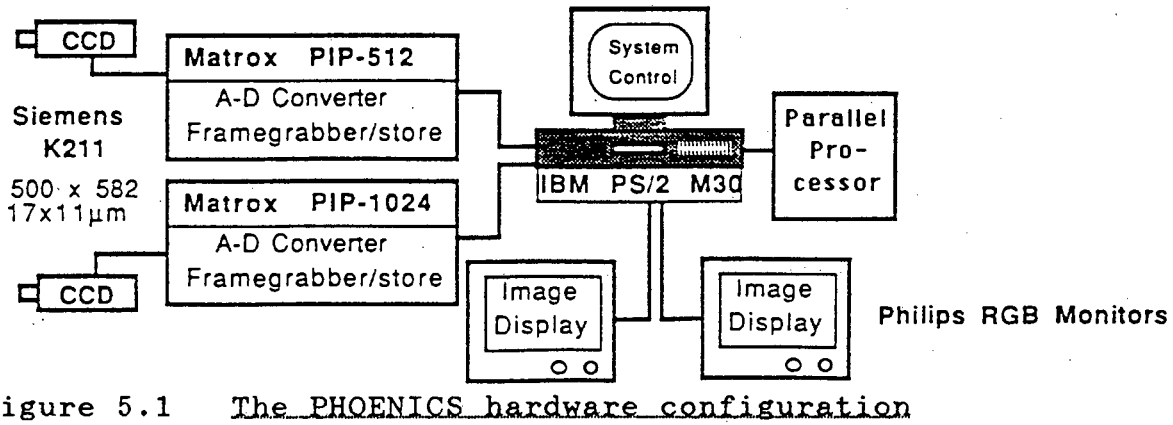

Figure 5.1 The PHOENICS hardware configuration

5.1 THE HARDWARE COMPONENTS OF THE SYSTEM

The system specification has been centred around low cost and flexibility, with a tradeoff of slow processing time. The objective of PHOENICS is to provide a platform for photogrammetric three dimensional co-ordinate location. With higher efficiency algorithms, image correlation algorithms and the incorporation of the parallel processing card, PHOENICS will be upgraded from an experimental digital photogrammetric workstation to a NRTP system. A more detailed description of the hardware components follow:

5.1.1 The Cameras

The cameras used in the system are two solid state Siemens K211 cameras with the Sony XC-57 CE solid state CCD chip. The cameras have the European black and white CCIR video standard of 625 lines at a frequency of 25 Hz.

The dimension of the CCD chip measures 8.8mm x 6.6mm (horizontally and vertically respectively) with a sensor resolution of 500 x 582 pixels. The resulting pixel size of each sensor element is 17μm x 11μm. However, only 468 x 568 pixels of the sensor array are active.

5.1.2. The Video Digitiser

A Matrox PIP-1024 board is the primary image acquisition and processing card, used by PHOENICS. It provides for simultaneous stereo imaging and storage facilities in quick succession. Images of size 512 x 512 (rows and columns) with 8 bits (256 levels of grey), are acquired from each camera, providing a different format image to that obtained from the CCD camera. The pixel size on the Matrox card of an image obtained using a Siemens K211 CCD camera (with an active pixel array size of 468 x 568 pixels) is 15mm to 11mm, as

compared to the camera pixel size of 17μm x 11μm. Approximately 15% of the camera image is lost due to the lower line count of the Matrox card in relation to that of the camera.

Simple image processing tasks can be accomplished on board the Matrox card using a combination of inbuilt hardwired operations and a macro command based software package called PIP. A further level of sophistication is achieved by the capability of standard programming languages, such as 'Microsoft C' and 'True Basic', manipulating data on the Matrox card using a macro command set.

The Matrox PIP board allows for transfer of the image array in memory resident on the Matrox card to the system's memory, via direct memory access (DMA). The transfer of the image or image segments to the system's memory becomes necessary for complex image algorithm execution.

5.1.3. The Host Computer

The criteria for the choice of a computer were : (Rüther et al. (1990))

- low cost, off the shelf
- high resolution graphics allowing a large range of grey scales to be displayed
- compatibility with parallel processing hardware and frame grabber boards
- system portability.

The IBM PS/2 Model 30 with a high resolution monochrome screen satisfies the above criteria. The model 30 is equipped with an Intel 8086 microprocessor running at 8 MHz, a 16 bit internal bus and a 8087 maths co-processor. It is the only model in the PS/2 range which accepts standard PC cards.

5.2 SOFTWARE DEVELOPMENT FOR PHOENICS

The process of obtaining three dimensional co-ordinates of a target, or the evaluation of lens distortion characteristics for a digital image in relation to a precalibrated control frame, is achieved in a two stage process:

5.2.1 Using the Target Detecting and Centring Program: SEARCH

The function of this program is to search a digital image to locate targets and find their centres. Before the program is run, a number of preliminary steps must be carried out to ensure that the targets are easily recognisable on the image.

- Targets of suitable contrast to the object being measured are placed on the object.
- The lighting is set so as to highlight the target while ensuring minimal reflection from the object.
- An image is snapped with the image processing card. The threshold level that highlights targets is found interactively.
- A binary image is formed where all objects below the threshold level (background) are eliminated i.e. their pixel values are set to zero, and the pixel values of all objects above the threshold (targets) are set to 255.
- Both the binary and the full grey level image are stored.

Firstly a program to determine the centre location of all targets on an image is run. The thresholded image is used to determine all target windows by finding the extent of all connected pixels with a grey level 255. A number is given to

each target corresponding to the order in which the target is located. A target centring routine using the 'weighted centre of gravity' is used to determine each target's centre, using the full grey level image.

Next, the full grey image is formed and displayed on an RGB (colour) monitor. On this image, the targets found are indicated by circles with their corresponding associated number. The image is viewed and all partially obscured targets or incorrectly identified targets, such as bright areas, are eliminated from the target list.

The target co-ordinates of control and object points are manually matched and then used in the PREP program to determine their object space co-ordinates.

5.2.2 Using the PREP Program

The software package has been developed for use in close range photogrammetry applications, Rüther (1989). It gives a choice of two well established photogrammetric models:

- 11-parameter
- bundle adjustment

The acronym DLT (Direct Linear Transformation) is a widely used technique in close range photogrammetry. The method was developed by Abdel-Aziz and Karam in 1971. The solution is based on the concept of a direct transformation from comparator co-ordinates into object space co-ordinates, eliminating the traditional intermediate step of transforming image co-ordinates from a comparator system to a photo co-ordinate system. Therefore the system makes no use of fiducial marks. Further enhancements of DLT have allowed for lens distortion using various models. DLT has the advantage of not requiring initial approximations for the unknowns, Rüther and Adams (1984).

The input data that is required by the program is :

- Object Space Co-ordinates of Control Points
  The X,Y,Z co-ordinates of a number of the surveyed positions of targets are read into the program from a file.

  At least six control points are required with the condition that the points may be neither coplanar nor near coplanar.

- Image Points
  The image co-ordinates of control and object points are required for the determination of 3-D co-ordinates of object points.

The PHOENICS system achieves precise 3-D co-ordinate determination. It lacks the speed and automation necessary to be classed as a NRTP system, but provides a feasible testbed for the development of NRTP algorithms. The two procedures that are necessary to convert the system to a near automatic 3-D co-ordinate detector are to fully automatically detect targets and to correlate the targets obtained from one image with corresponding targets of a stereo image.

Fully automated target detection on individual images can be simply implemented under laboratory conditions, where the lighting level can be controlled and a consistent threshold level can be preset for the centring procedure. This eliminates the need for targets to be manually thresholded.

Automatic target correlation or identification can be achieved by placing a unique code next to each target, Wong et al. (1988). In a simple application, a priori knowledge of approximately where the targets on the image are to be

found, can be used to identify the precise location of a known target.

PHOENICS is used to snap digital images of the control frame containing an array of accurately surveyed targets. The fabrication of the control frame is described in chapter 6. The image target centre co-ordinates are evaluated using a number of different target centring algorithms. The accuracies of each algorithm are given by the variance σ_o^2, obtained by correlating all image target co-ordinates of the algorithm with the control frame target co-ordinates, using PREP. The variance of each algorithm is used to compare the accuracy of all the target centring algorithms.

CHAPTER 6

6.0 CONTROL FRAME

Control frames consist of a distribution of targets. They are used to calibrate camera stations.

The 3-D co-ordinates of control frame targets may be obtained using accurate traditional surveying methods, such as a theodolite. In NRTP systems, a digital image of the control frame is snapped and the image point co-ordinates are evaluated using one of a number of target centring algorithms. The control frame image and object co-ordinates are run through one of the photogrammetric models in the PHOENICS:PREP system to evaluate the camera station characteristics including camera orientation, lens distortion and a measure of the accuracy of the target centring algorithms.

This chapter describes the design criteria involved in constructing two control frames and briefly describes the surveying accuracies and capturing an image of the control frame.

6.1 DESIGN CONSIDERATIONS FOR THE FIRST CONTROL FRAME

6.1.1 Shape and Size of the Frame

The control frame is designed to have a distribution of targets in three planes at distances of 0.70m, 0.85m and 1.00m from the camera. It is tested using an 8mm focal length video camera. The field of view of the video camera is illustrated in Figure 6.1 .

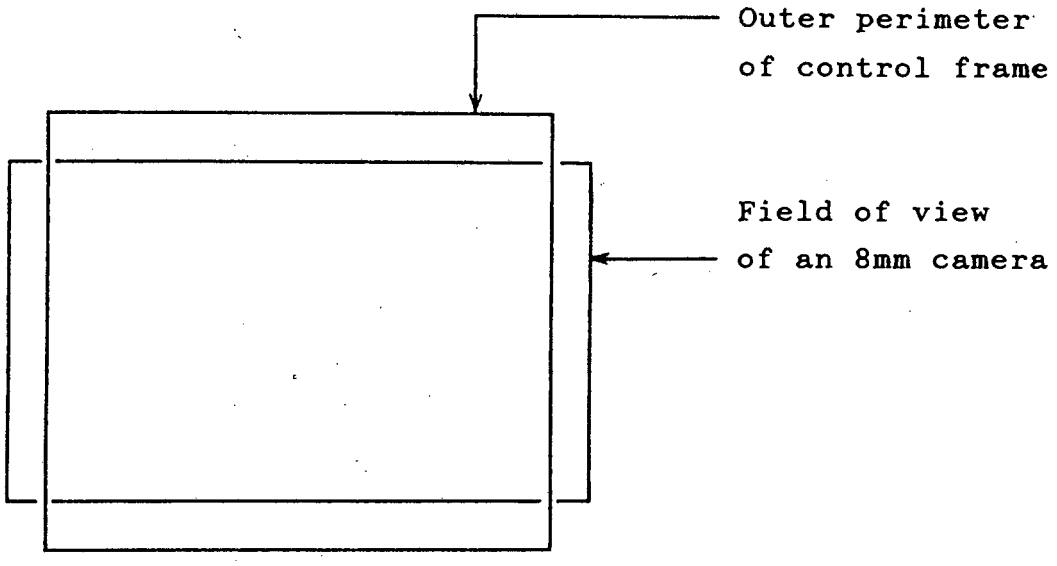

Figure 6.1 Field of view of the control frame by the camera with an 8mm focal length lens

The majority of the control frame is visible in the video camera image.

Targets are positioned on the three planes of the control frame to evenly cover the image plane.

6.1.2 Target Considerations

6.1.2.1 Targets used in Different NRTP Systems

Different shaped targets have been fabricated for various algorithms and applications in NRTP systems.

Some of the different means to find 3-D co-ordinates of locations on an object include:

- projecting a grid onto an object and locating intersections, Wildschek (1989)
- locating a small black disk surrounded by a white ring, surrounded by another black ring attached to the object, Gruen (1987).

Targets may be of:

- an active nature, i.e. light-emitting-diodes, which can be viewed in a dark environment, Bayer (1988)
- a passive nature as in the case of disks pasted onto the object. The targets may be
  - o a white disk
  - o a black disk, El-Hakim (1986), Wong (1986)
  - o a black hole target, Rüther and Parkyn (1990).

An illustration of the different target shapes are given in Figure 6.2 together with examples of profiles through two targets.

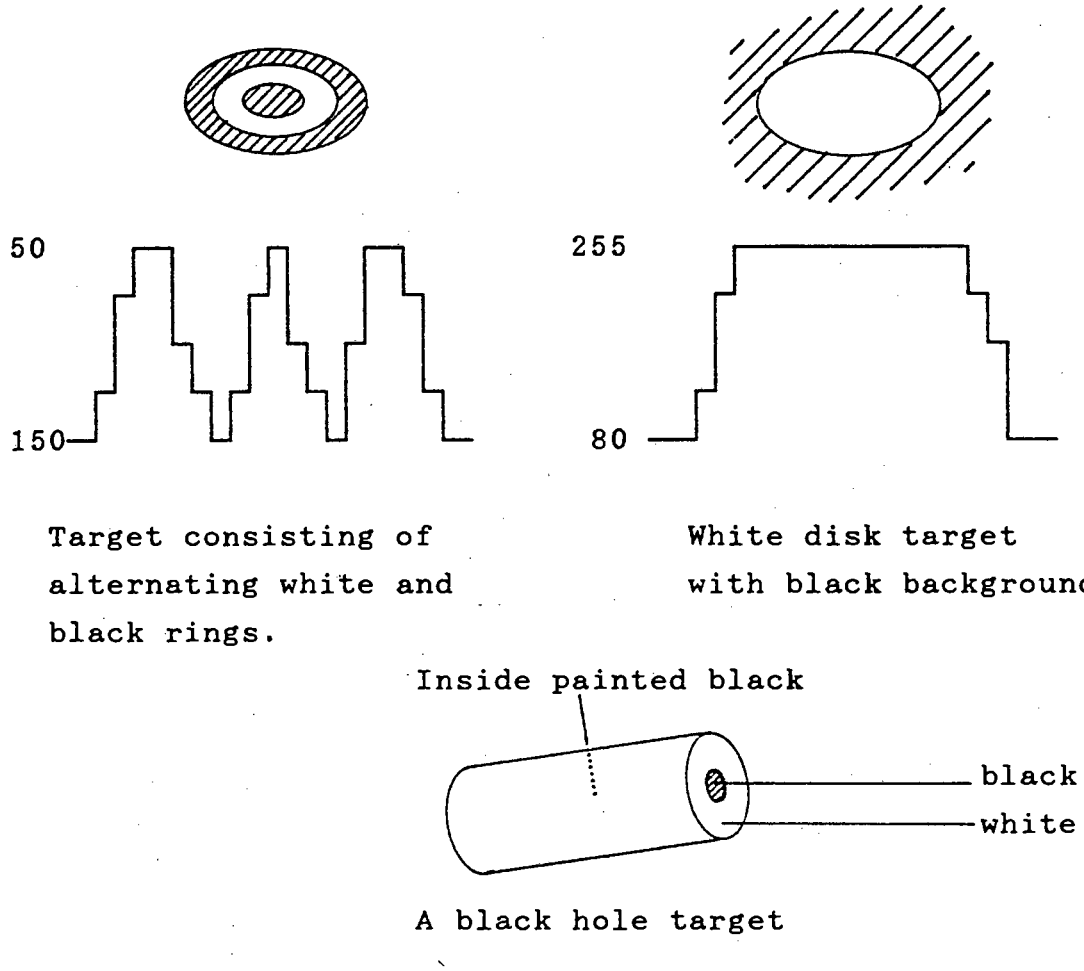

Figure 6.2 Target shapes implemented in different systems

In this thesis a solid white circular (disk) target was chosen to test the assorted algorithms.

6.1.2.2 Target Material and Colour

Black painted targets were found to be unsuitable since no paint or material could be found to be light absorbing enough to provide a contrast to ensure reliable thresholding. A *black hole* target consisting of a hollow closed cylinder, painted black inside, with a lid coloured white having a hole punched through it, was fabricated to overcome this problem, Rüther and Parkyn (1990). Although this form of target provides a good contrast, it is difficult to attach this target to the object.

The targets investigated for photogrammetric applications are fabricated in a variety of ways including targets punched from white paper, low-grade retro-reflective material and higher grade retro-reflective material, all pasted on a contrasting dark background. The targets are mounted on a control frame and viewed by video cameras to determine their contrast with the background object.

For the PHOENICS system, the aperture and lighting of the system are set to drive the targets towards saturation level (white). Targets close to saturation level are desirable because this allows for the greatest contrast between the target and its background. A further advantage is that the targets can be reliably and quickly found using thresholding. White paper and retro-reflective targets with black backgrounds both gave grey scale (target) levels of '255' (corresponding to white saturation), after selecting an appropriate aperture setting to drive the target into saturation.

6.1.2.3 Size of Targets and Pixels

The targets are designed to give an equal image size of approximately 8 pixels on the pseudo chip for all three planes (at 0.7m, 0.85m and 1.0m from the centre). The target size on the image is controlled by the physical size of the target and the distance of the target from the lens.

To design the physical size of the targets to an 8 pixel image size specification, it is necessary to evaluate the area in an object space which is covered by a single pixel at the three distances. The previously mentioned complication of line loss and image distortion due to the transfer of the image from the chip to the pseudo chip (section 4.2) becomes relevant in this context. Unless detailed information on the chip design, i.e. the area of the chip that is usable for imaging is available, a simplified geometric consideration is acceptable to determine approximate pseudo pixel sizes and suitable target sizes.

One approach to estimate the pixel size is:

> An image of a rectangular area with well defined black borders is taken. This area must be located perpendicular to the optical axis of the camera. The dimensions of the area are measured in units of pixels on the frame grabber image, i.e. the pseudo chip. The pixel counts (h_p and v_p for horizontal and vertical object dimensions respectively) are then related through the principal distance (f) and the distance of the lens-to-object (d) to the actual size of the object horizontally (t_h) and vertically (t_v), see Figure 6.3 .

- horizontal pixel length : $p_h = f \cdot t_h / (d \cdot h_p)$
- vertical pixel length : $p_v = f \cdot t_v / (d \cdot v_p)$

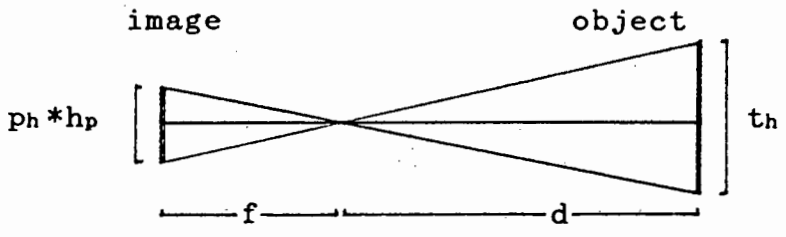

Figure 6.3 The distances and measurements in image and object space

The chip and pseudo chip are related to each other by assumptions concerning the chip design that estimates the active imaging area. In the horizontal direction only a few pixels are lost. It can be assumed that 500 pseudo pixels are equivalent to approximately 8.6mm. In the vertical direction, a number of chip rows are lost (approximately 20%) due to the transfer from the 640 line camera to the 512 line pseudo chip and some 500 pixels are equivalent to 5.6mm. From this, values of 17 and 11 micrometres can be estimated for pixel width (p_h) and pixel height (p_v) respectively.

This in turn leads to the following horizontal and vertical target sizes (t_h and t_v) for 8 pixel target images and 8mm focal length cameras:

$$t_h = 8x0.017xd/f$$

$$t_v = 8x0.011xd/f$$

Target sizes for the various planes are listed in table 6.1

target size	distance 'd' between camera and plane		
	1m	0.85m	0.7m
t_h	17 mm	14.5 mm	12 mm
t_v	11 mm	9.5 mm	8 mm

Table 6.1 Theoretical target sizes for the various planes resulting in a target image of 8 pixels

It was found that these theoretical values did not lead to the required 8 pixel target sizes due to the difficulty in controlling the light source, chip sensitivity and target reflectivity.

A pragmatic approach of imaging targets of different sizes under close to ideal conditions and selecting the most suitable one on the image, proved more efficient.

The three materials investigated as targets were white paper, high intensity and engineering grade retro-reflective tapes. It was found that the higher grade tapes were highly reflective in all directions and only the engineering grade material appeared to be retro-reflective. Engineering grade tape is not sufficiently retro-reflective at low angles of incident light and the periphery targets do not reflect sufficient light back into the camera to generate good images. Image target quality degenerates with distance from the image centre.

The best targets for the control frame applications were found to be white circular disks punched from cardboard. These targets produce a better and more uniform target image than the retro-reflective targets. In practical tests it was found that due to the strong lighting and revolving

spread of light off the targets (Gaussian spread function) a circular target with diameter 12mm, 8mm and 6mm for the frames at distances of 1m, 0.85m and 0.7m respectively (from the camera) would give the image target sizes of approximately 8 pixels. The practical targets implemented were thus smaller than anticipated in theory.

6.1.3 Fabrication of the Control Frame

The outer frames (supporting the target arrays) at 1m, 0.85m and 0.7m from the camera frame, together with the extension to hold the camera and frame stiffeners are made of hollow, square, cross-sectional tubing. For purposes of transportability they are bolted together.

The targets on the back frame are evenly distributed in a row/column configuration. They are attached to intersecting horizontal and vertical fine wires secured to the tubing frame. The innermost square of targets is mounted on a square sheet of board fixed to the wire mesh.

The outer targets in the middle frame are supported by a similar wire mesh and the two inner target squares are made of a thicker gauge wire which support the targets.

The targets in the frame closest to the camera are all fixed to thicker gauge wire. All wires and frames are painted black and a black backdrop is added to contrast with the targets, see Figure 6.4.

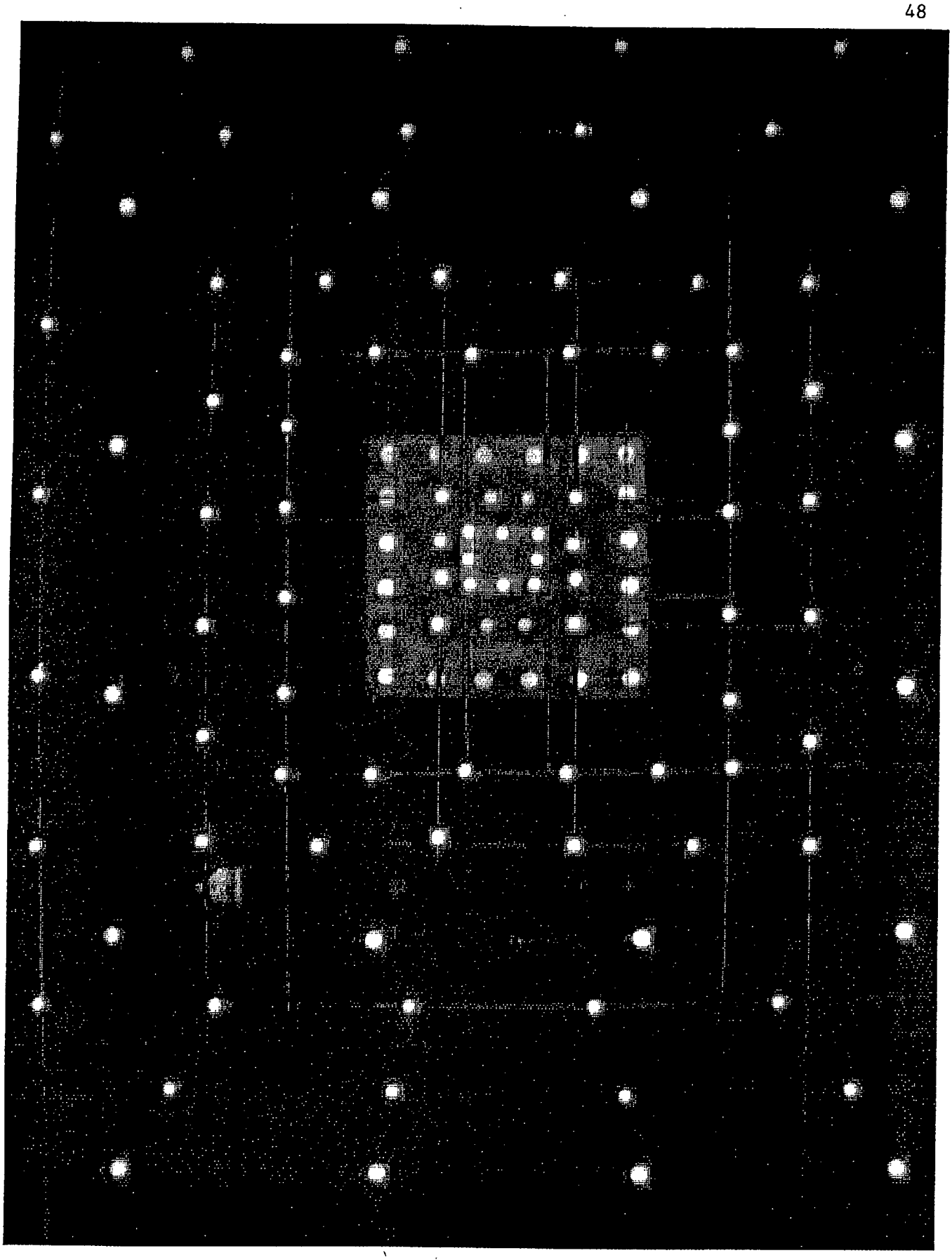

Figure 6.4 The ccd camera's view of the First Control Frame

6.1.4 Surveying the Control Frame

The frame is surveyed using a stereo pair of photographs taken by two Zeiss UMK10 Jena precision cameras. The 3-D co-ordinates of the targets are obtained using the Zeiss (AUSJENA) Jena stereo comparator.

The target locations are determined to a precision of 0.3mm. This relates to an image target of positional accuracy of approximately $^1/_3$ of a pixel.

Difficulties experienced with this control frame includes:

i) Fine wires supporting the targets in the front and the middle rows bisected targets in the image, leading to double targets being detected in the searched image.

ii) Insufficient contrast between targets and background make it occasionally difficult to automatically distinguish between them.

iii) Light reflection off parts of the black wires simulates targets.

iv) Targets having a finite (approximately 0.5mm) thickness appear distorted when viewed as perimeter targets. The edge of the target appears as part of the circular shape and target centres are displaced towards the image centre, see Figure 6.5 .

v) Inaccuracy in fabricating the targets by punching out cardboard targets result in slightly asymmetrical targets.

vi) The tube/wire construction proved unstable.

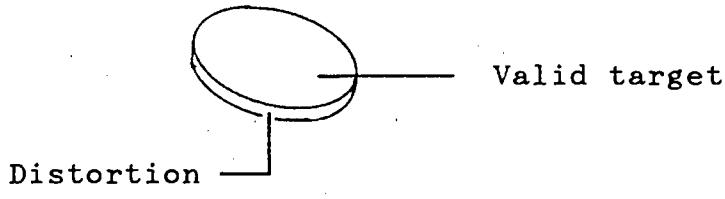

Figure 6.5 Thick target's distortion on image

Since the algorithms were designed to find centres to a sub-pixel accuracy, the control frame fabrication was found to be not rigid enough for the level of precision required.

6.2 THE SECOND CONTROL FRAME

A second control frame was designed to overcome some of the drawbacks of the first design with a particular view to producing a highly rigid frame with targets of constant relative positions. Target design considerations had a major role in this second frame design. These priorities were defined after it was established in working with the first frame that the determination of target positions on the frame by survey techniques was cost- and time intensive.

6.2.1 Design of the Second Frame

The control frame consists of three grids placed at 0.7m, 0.85m and 1.0m from the camera. Each grid consists of three square frames, placed one within the other. The sequence of frames as viewed by the video camera is:

Starting from the middle of the grid and moving out to the grid perimeter: front- mid- back- front- mid- back- front- mid- back- plane, beginning with the central front plane and ending with the outermost back plane, Figure 6.6a and Figure 6.6b. These figures show the distribution of the square frames:

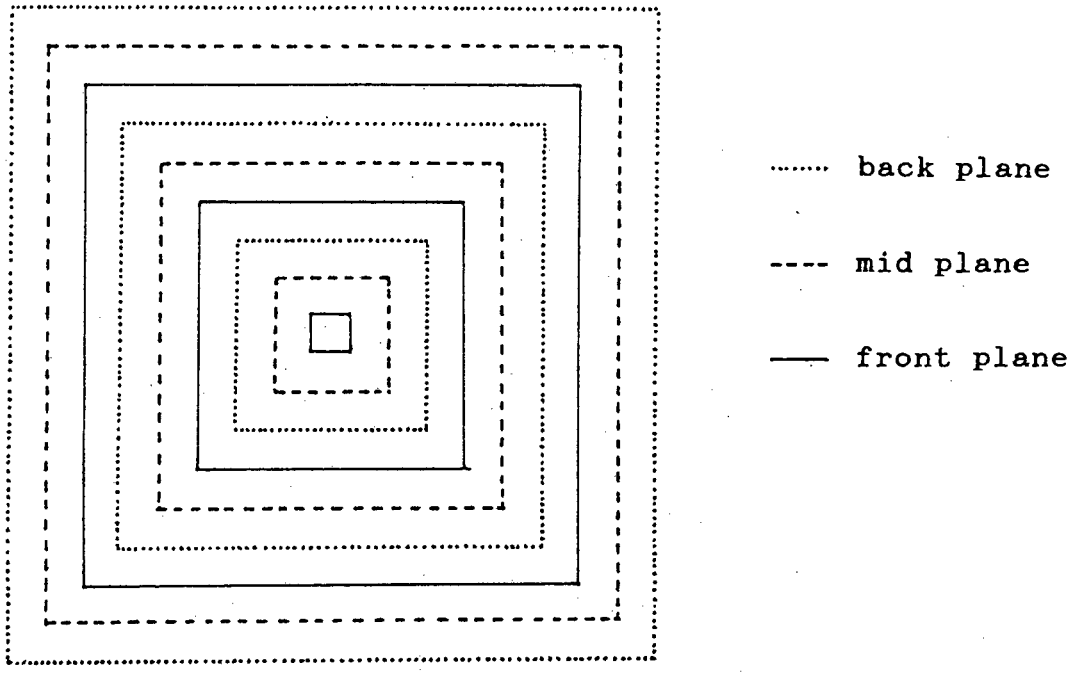

Figure 6.6a Looking at the frames from the camera position

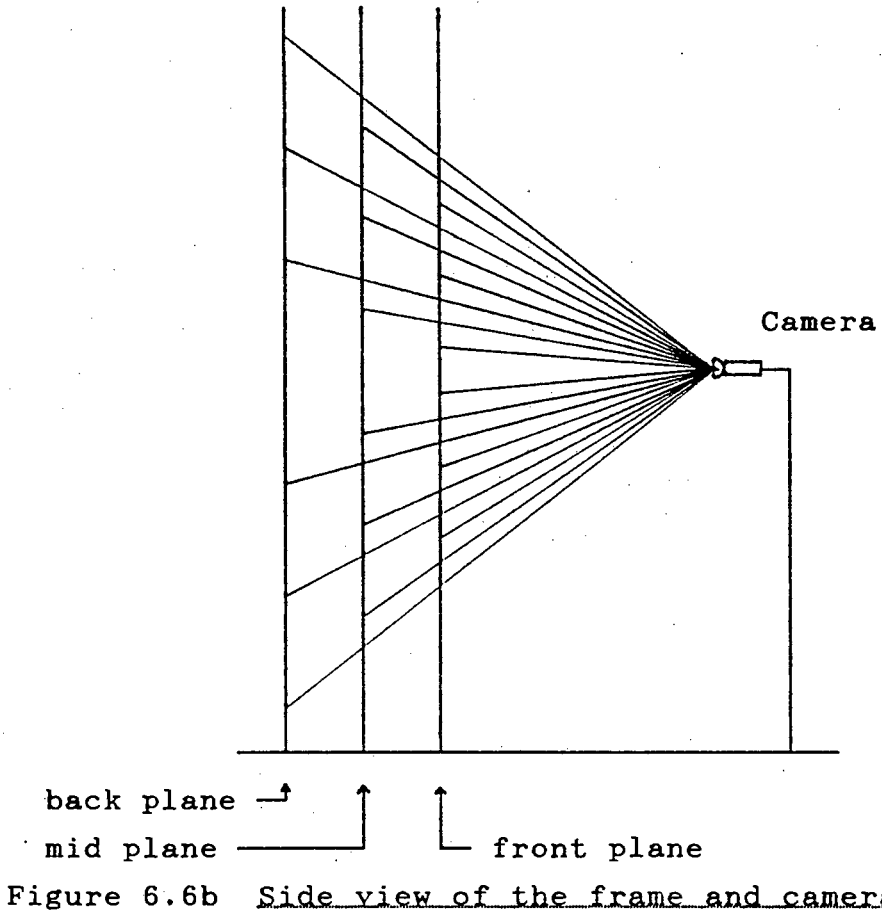

Figure 6.6b Side view of the frame and camera unit

The dimensions of each square frame can be calculated from the geometry of the above diagram. They are tabulated in Table 6.2 below:

	front plane	mid plane	back plane
outer square	.544 m	.755 m	1.000 m
mid square	.310 m	.471 m	.666 m
inner square	.077 m	.188 m	.332 m

Table 6.2 Frame lengths for the three planes

The entire control frame is built from angle-iron, with the squares of each plane attached to an outer square support frame with radially placed supports. The planes are connected to one another with eight short lengths, two on each side and one through the centre of each frame. This structure proved to be rigid.

The camera mount was attached to the frame with a removable extension to facilitate portability.

6.2.2 Design of the Targets

Accurate targets were designed using a photographic process to print a high resolution plot of the target on an aluminium surface. The targets are in the natural aluminium and the background is anodised matt black. At the centre of each target is a point of 0.5mm diameter to facilitate accurate and simple sighting of the target when surveying it with a theodolite. The points were kept to a minimum size, i.e. just visible in the theodolite, in order not to disturb

the homogeneous appearance of the target for the automatic target search. Targets were produced to specifications which required the target diameter to be consistent to 0.1mm, and having a centre point accuracy, with respect to circumference, of the same magnitude.

Based on the experiments with target sizes in the previous trials, described in [6.2], the sizes of the targets chosen were:

back plane (1m)	mid plane (.85m)	front plane (.7m)
12mm	10mm	8mm

Table 6.3 Target sizes on each plane

There are twenty targets on each square except for the central front square, which is limited to sixteen targets because of space constraints. The distribution of the targets are illustrated in Figure 6.7.

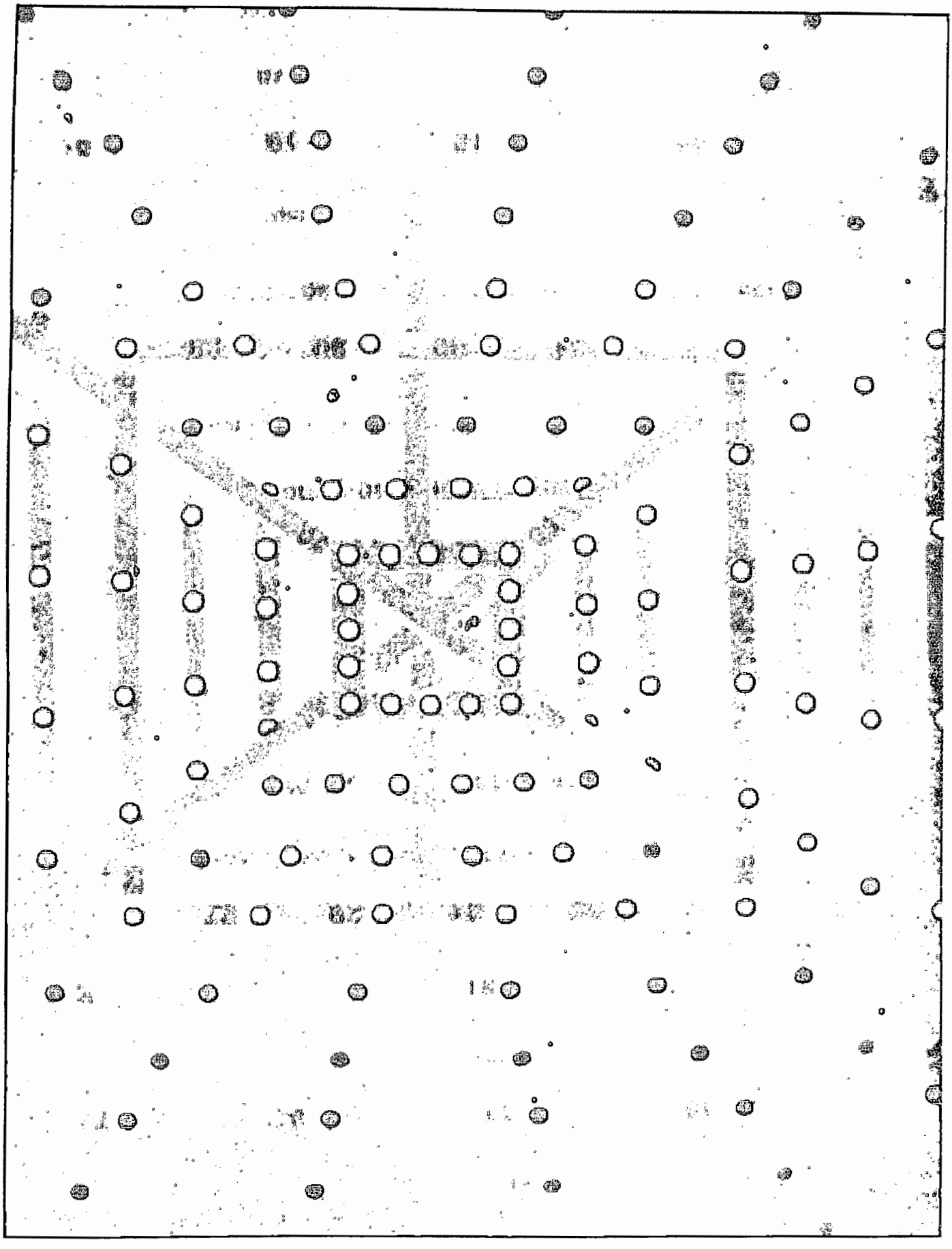

Figure 6.7 Distribution of targets on the Second Control Frame

Target numbers with a reflective value lower than that of the targets are added to facilitate target identification. (These numbers can be thresholded out of the image when searching for the targets.)

It was found that this target design:

- satisfies the requirements for accurate surveying
- avoids 'thickness of target' distortion
- satisfies the requirements of high target symmetry for automatic target centre detection

6.3 SURVEYING THE CONTROL FRAME

The control frame was measured using a theodolite in order to achieve a higher accuracy than was obtained using a photogrammetric approach.

The initial precision of the 3-D target location, using all the target co-ordinates surveyed with the PHOENICS:PREP program (using the bundle adjustment method), was approximately 0.5mm. A subset of the poorly surveyed targets were removed from the target list and only the accurately surveyed targets were used in the bundle adjustment to obtain their 3-D target co-ordinates. The precision of these accurately surveyed targets was approximately .2mm. The 3-D co-ordinates of the balance of the targets were then evaluated. The resulting target co-ordinate accuracy (not including the front central targets) is:

The precision of the 3-D target co-ordinate location is ± .2mm on the control frame, converting to an accuracy of 1/10th of a pixel accuracy on the frame grabber image.

6.4 USING THE CONTROL FRAME

Lighting of the frame proved to be of great importance in achieving an even and clean set of imaged targets. The best results were achieved using strip neon lights. To capture an image, the frame was placed on its back on the floor directly 3.5m below a single standard light source consisting of 3 neon tubes attached to the ceiling. Thus the steps involved in using the control frame to determine the precision with which target centres are located using a NRTP system can be summarised as:

- fabricate a control frame with targets
- survey the control frame
- arrange lighting
- capture an image of the control frame

(Chapter 6)

- locate target centres in the image using each of the target centring algorithms

(Chapter 8)

- Evaluate the variance for each algorithm by correlating the algorithm's target centres with the 3-D surveyed target co-ordinates, using least squares to evaluate one of the photogrammetric models
- Compare the target centring algorithm performances by plotting a graph of the variances of each algorithm

(Chapter 9)

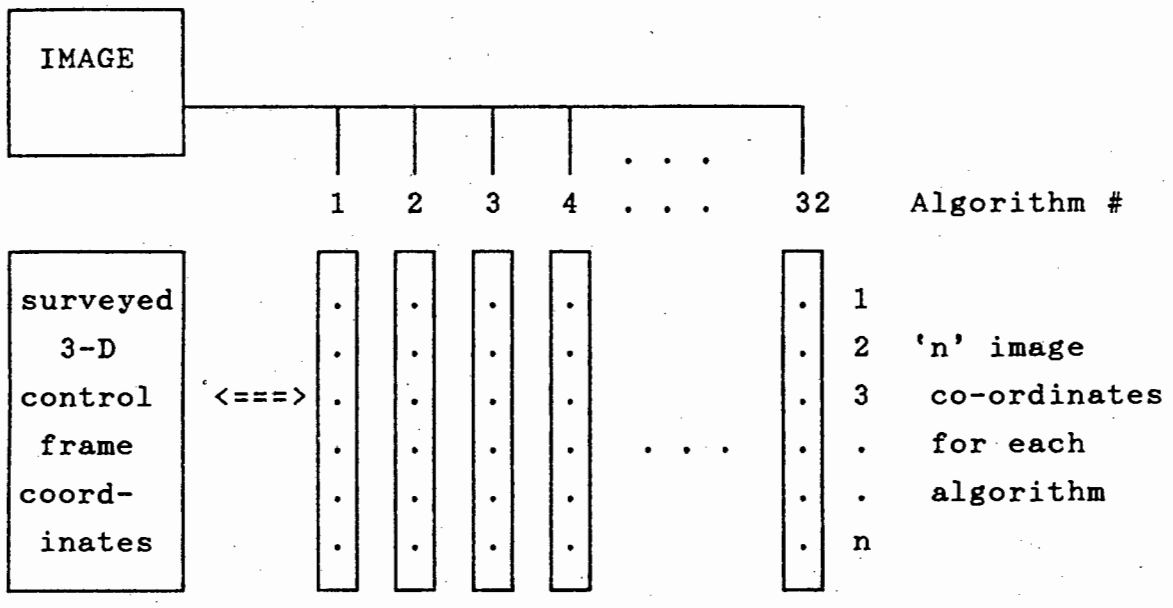

variance: σ_o^2 [1 , 2 , 3 , 4 , ... , 32]
corresponding with the algorithm.

Figure 6.8 Steps to evaluate the accuracy of target centring algorithms on images of real targets

The procedure to use the control frame is outlined in Appendix G. An example to determine the centring accuracy for one algorithm on an image of the control frame is outlined in Appendix C. The method outlined is used with all the algorithms. The Brown model, as provided in the PHOENICS:PREP software, is used to correct radial lens distortion.

CHAPTER 7

7.0 GENERATING SYNTHETIC ELLIPSES

The accuracy of target centring algorithms may be evaluated on an image consisting of ideal synthetically fabricated targets. Synthetic targets are modelled to resemble real targets.

Images consisting of synthetic targets are used to test target centring algorithm sensitivities, Trinder (1989), Zhou (1986), but to the author's knowledge, no complete description of the automatic fabrication of elliptical targets is available.

A program was written to generate synthetic elliptical targets in a digital image. Elliptical targets were chosen since although circular targets are used on the control frame, the projection of a circular target which is not on axis with the camera, is an ellipse. The inputs required by the program are: the number of ellipses per image, the parameters appropriate to each ellipse including ellipse size, ellipse centre co-ordinates and the 'falloff' function.

The 'falloff' is the smoothing function from the ellipse plateau to the background level, see Figure 7.1. The falloff functions which have been implemented and will be described later are:

- Direct falloff
- Gaussian-Convolved-with-a-Wall falloff
- Gaussian falloff

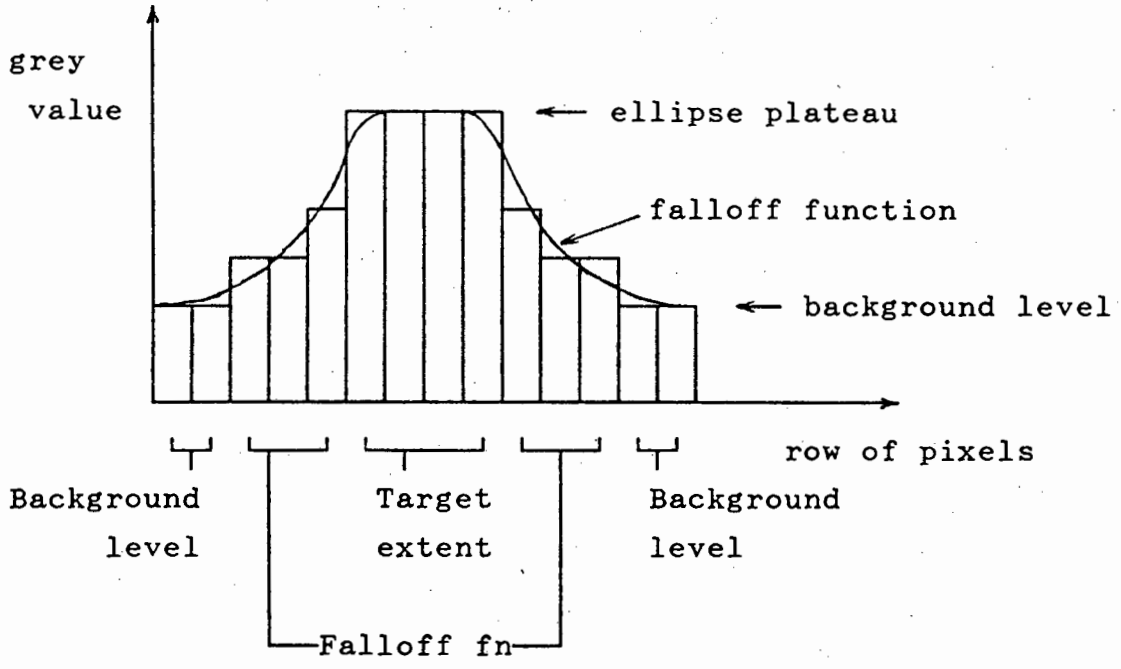

Figure 7.1 Profile through an ellipse illustrating the falloff function

Two digital images consisting of synthetic elliptical targets were generated to test target centring algorithms. The one image consists of synthetic (symmetrical) ellipses with a 'Gaussian-convolved-with-wall' falloff (see section 7.2.3.2). The second image was formed using the same ellipses with simulated partial occlusion (where a blemish was added to the perimeter of each of the targets to represent obscuring of the target by another target, or a shadow cast on the target), further discussed in [7.4].

The purpose of testing the target centring algorithms on the image consisting of:

- perfect synthetic symmetric targets, is to evaluate the potential accuracy of the target centring algorithms.
- synthetic targets with blemishes, is to evaluate the effect of partial occlusion on the accuracy of the target centring algorithms and therefore the algorithms robustness to flawed target images.

A description for generating ellipses follows:

7.1 MANUALLY DIGITISING AN ELLIPSE (WITH DIRECT FALLOFF)

The first method that was used to manually generate a precise ellipse was to plot an ellipse perimeter on graph paper. Each block (pixel) on the graph paper consisted of 50x50 1mm square sub-blocks. Pixel values appropriate to a digitised ellipse are evaluated by considering pixels within the perimeter of the ellipse and pixels entirely outside of the ellipse.

- Pixels entirely within the ellipse perimeter are set to a grey level of 255 equivalent to a white 'saturation' level and
- Pixels entirely outside of the ellipse perimeter are set to a grey scale of 'background'.
- Those pixels through which the perimeter passes, have a digitised grey scale value between 'background' level and a level of 255, proportional to the area covered by the ellipse within the pixel, see Figure 7.2

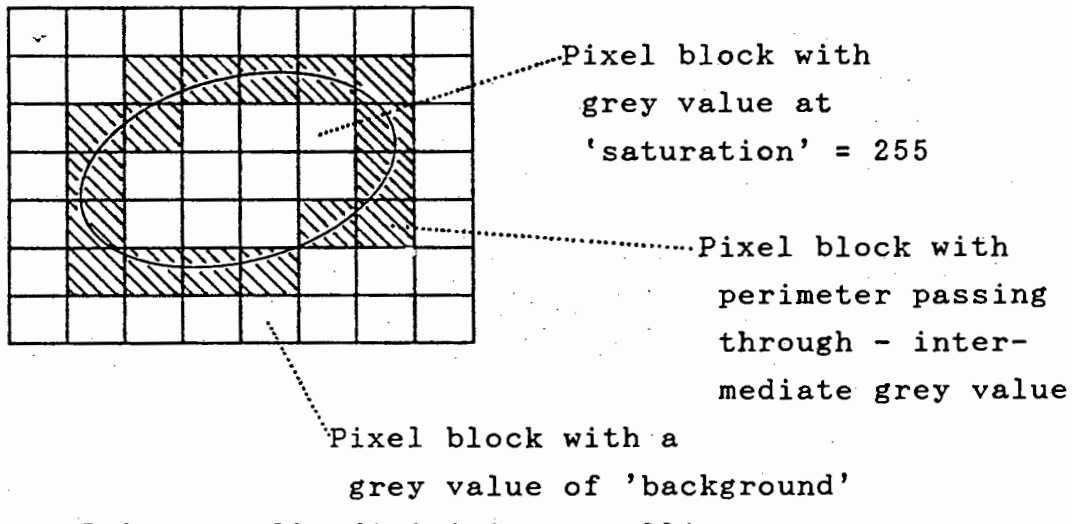

Figure 7.2 Manually digitising an ellipse

The ellipse generated using this method is considered to have *direct falloff* since the area within the ellipse perimeter is at 'saturation' level and the area beyond the

ellipse is at 'background' level. There is a direct step from saturation level to the background level at the ellipse perimeter. This target model is equivalent to that found in a digital image formed of a real target, sharply contrasting with the background.

The primary drawbacks with manually digitised ellipses are:

i) Time to evaluate ellipse pixel grey values (± 4 hours per ellipse).

ii) Inaccuracy of the digitization process which limited the centre determination to $^{1}/_{100}$ of a pixel.

iii) Each ellipse digitised with a unique size, orientation, or centre location, must be completely re-evaluated.

iv) There is no facility to automatically add a falloff function to the ellipse.

7.2 PROGRAM TO GENERATE ELLIPSES

The problems involved with manually digitising an ellipse can be avoided by automatically digitising pixel grey levels, using a program. The parameters taken into account in the program are the ellipse coefficients (including the ellipse centre co-ordinates) and the type of falloff function i.e. the function to smooth the ellipse from saturation to background levels.

7.2.1 The Ellipse Equation is:

$$\frac{(x - x_0)^2}{a^2} + \frac{(y - y_0)^2}{b^2} = 1$$

... with an angle of rotation = θ

where 'a' is the semi-major axis
'b' " semi-minor axis
'x_0' " horizontal offset of the ellipse
'y_0' " vertical offset of the ellipse
'θ' is a counter-clockwise rotation of the ellipse around its centre point (x_0, y_0)

The effect of the ellipse parameters on the shape and orientation of the ellipse are illustrated in Figure 7.3.

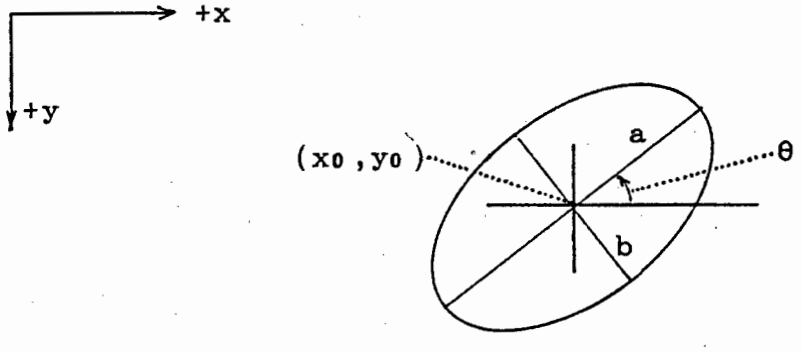

Figure 7.3 The ellipse parameters

7.2.2 Creating an Ellipse with Direct Falloff

The simplest ellipse generated was an ellipse with direct falloff, hereafter referred to as *Ellipse0* , see Figure 7.4. The domains within the window are defined as in the case of the manually digitised ellipse: the area within the ellipse perimeter is set to 'saturation' and the rest of the ellipse target window is set to 'background' level.

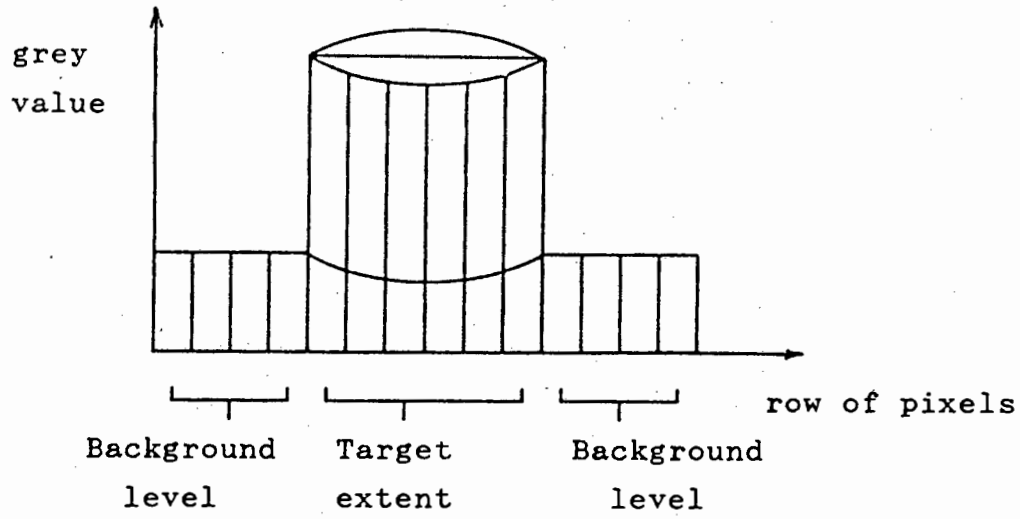

Figure 7.4 Profile through Ellipses illustrating direct falloff

Parameters are chosen for the ellipse equation and the ellipse is projected onto a pixel array within a window. Each pixel is subdivided into 'nxn' sub-pixels, where 'n' is an integer multiple of 10.

For a single pixel, the pixel grey value is determined by considering the sub-pixel grey values within the pixel:

- If the centre of the sub-pixel is within the ellipse/target perimeter, the sub-pixel value is set to the 'saturation' level (grey value = '255'),
- otherwise it is set to the 'background' level.

The sub-pixel grey values for one pixel are summed together and divided by 'nxn' (the total number of sub-pixels within a pixel), to give the grey scale for the particular pixel, see Figure 7.5 .

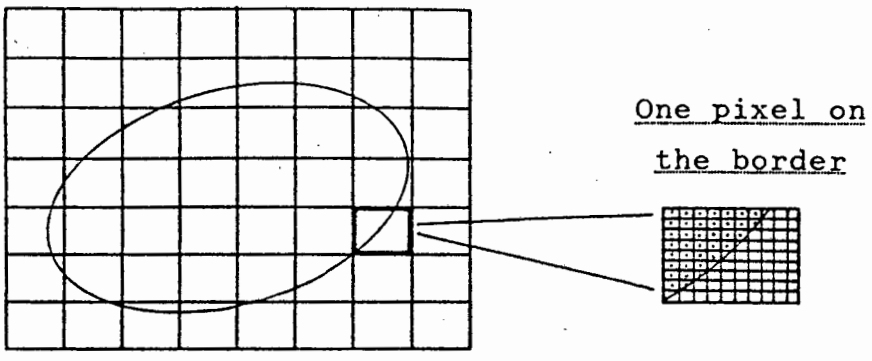

▣ sub-pixel with grey value '255' (ellipse)
□ sub-pixel with background grey value

Figure 7.5 Pixel values of an automatically generated Ellipse.

The grey values of all the pixels within the ellipse window are evaluated, starting at the top left pixel and scanning row by row ending with the bottom right pixel.

The number of sub-pixels ('nxn') within the pixel is a measure of the fineness of the digitisation which relates to the accuracy of the grey level determination.

7.2.3 Creating an Ellipse with a Falloff Function

An option to digitise an ellipse with a gradual falloff function from the ellipse perimeter to the background level is included within the program.

The falloff function models a real ellipse viewed by a camera which is not perfectly focussed or where there is an abundance of incident light on the target, resulting in an edge which appears blurred.

7.2.3.1 Methods Used by Other Authors to Define Ellipses with Falloff

The method generally used to generate falloff functions on a digital image consisting of Ellipseo targets, is to convolve the entire image with a discrete Gaussian curve (Point-spread-function or PSF) as described in Appendix D.

Trinder (1989), describes a method to create a circular target with falloff by placing a one dimensional wall symmetrically about a pixel and then convolving this wall with a continuous Gaussian curve. The resulting wall with falloff is rotated about the centrepoint. The grey value assigned to the pixel relates to the volume enclosed within the particular pixel profile under consideration, see Figure 7.6. This approach is extended and adapted to perform on elliptical targets.

Step 1: Convolving a PSF with a wall

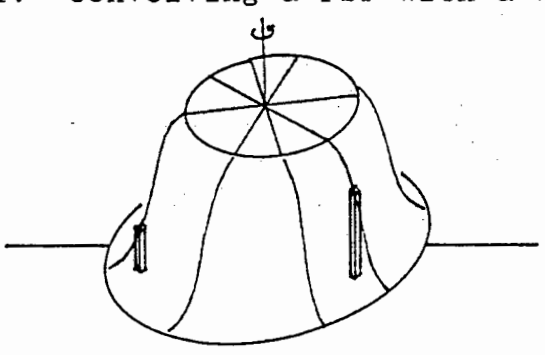

Step 2: Rotating the 'wall-convolved-with-a-PSF' and evaluating the pixel grey values.

Figure 7.6 Rotation of a wall convolved with a PSF

7.2.3.2 Modelling a Gradual Falloff Function from the Perimeter of the Ellipse

The secondary objective of the program is to generate a synthetic falloff from the ellipse. The method which was used, allows for a variety of falloff functions to be 'added' to the ellipse to model different conditions with a high level of grey scale accuracy and symmetry.

The method used to approximate the falloff function from the ellipse to background is an extension of Trinder's (1989) method of fabricating a target. Trinder's method works on the principle that a one dimension falloff function radiates out (continuously) perpendicularly to the circular target perimeter.

As in the case of Ellipse0, the sub-pixels within the ellipse perimeter are set to saturation level. The falloff principle involved is that the noise function radiates perpendicularly to the tangent on the perimeter of the ellipse, to the 'background' level at suitable distance from the ellipse perimeter, see Figure 7.7. The falloff is determined by considering the distance between a point (sub-pixel) beyond the ellipse perimeter and its closest point on the perimeter of the ellipse. The distance relates to the 'amount' of falloff from the saturation level.

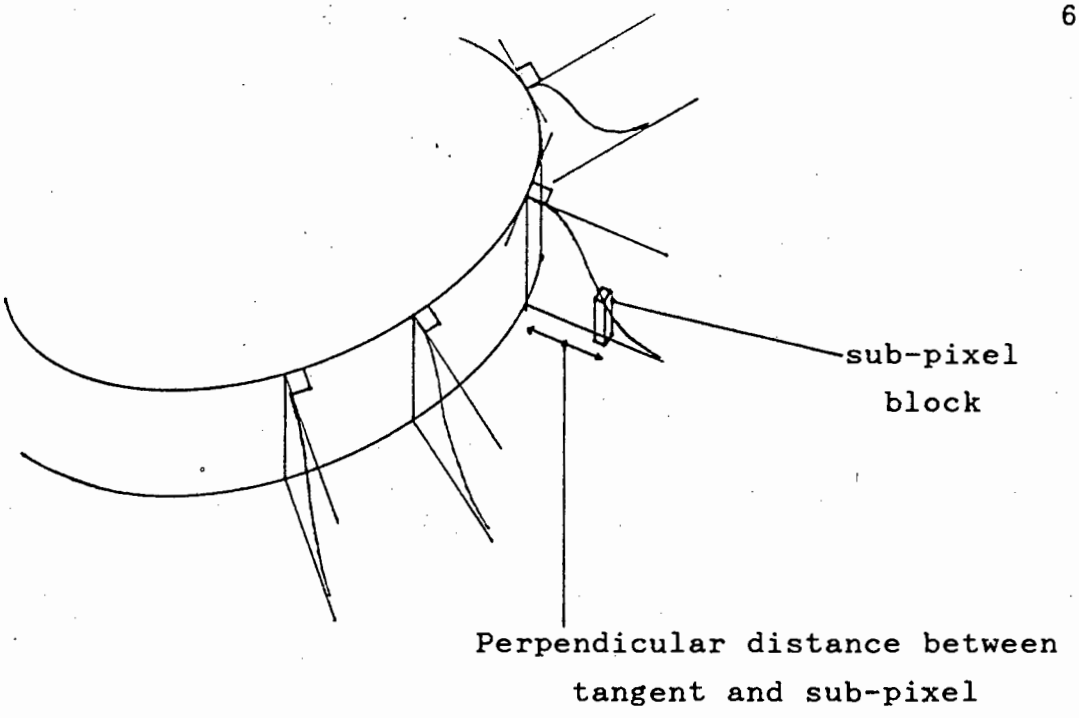

Figure 7.7 Falloff of the noise function perpendicular to the target perimeter

The method used to evaluate the perimeter point closest to the sub-pixel point under consideration is a variation of the 'hill climbing' technique:

> A point on the perimeter of the ellipse is chosen in line between the ellipse centre and the sub-pixel. It is evaluated and a new point is chosen on the perimeter at an angular distance from the original perimeter point of $+\theta$ degrees. Again the distance between the new perimeter point and sub-pixel point under consideration is evaluated. If the new distance is less than the old distance then a new perimeter point is chosen at an angle of $+\theta$ from the most recent perimeter point. If not, (if the new distance is greater than the old distance) the new point is chosen at an angle of $-\theta/2$ from the most recent perimeter location. This procedure is repeated until the difference between the new and old distances between

the sub-pixel and perimeter is considered insignificant, see Figure 7.8 .

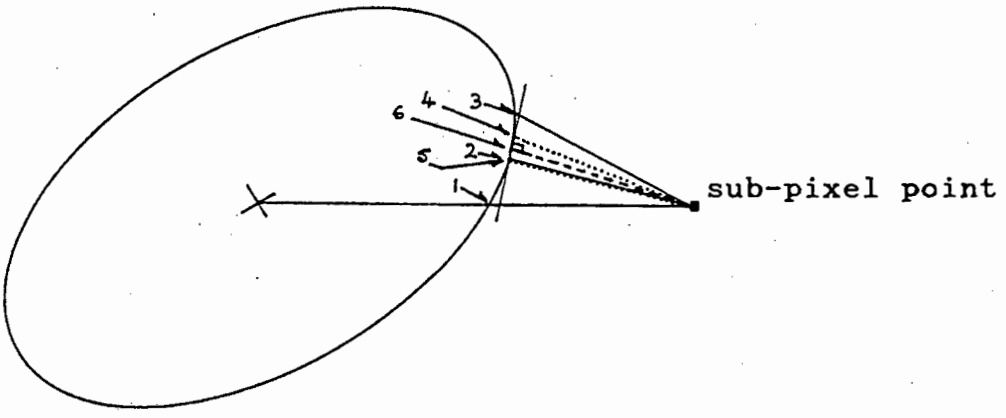

Figure 7.8 Using 'hill climbing' to determine the shortest distance between a sub-pixel point and the ellipse perimeter

Summary of falloff functions and reasons for their implementation:

i) Ellipse with direct falloff, renamed 'Ellipse$_0$', represents an ellipse with even lighting and with a clear contrast with the background grey level, viewed with a focussed camera, ensuring a sharp transition from saturation level at the perimeter of the ellipse to the background level (beyond the ellipse perimeter).

ii) Ellipse with a Gaussian-convolved-with-an-edge falloff, hereafter referred to as 'Ellipse$_1$', is suggested by the standard convolution of a wall with a PSF in one dimension. The generation of the one dimensional curve is illustrated in Appendix D. It is evaluated beforehand and stored in memory and is added onto the perimeter of the ellipse, thus adding a distortion similar to that of a traditionally convolved ellipse,

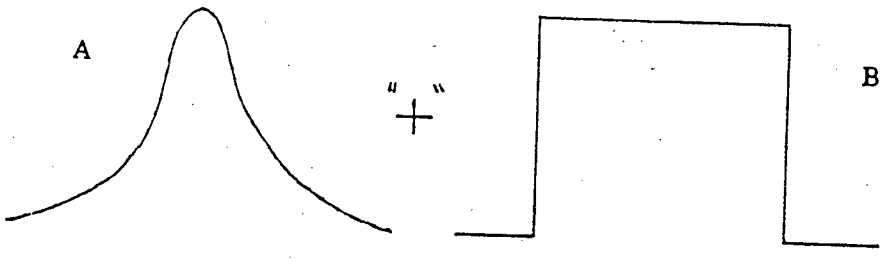

The falloff of 'A' is *added* to the wall 'B' resulting in 'C'

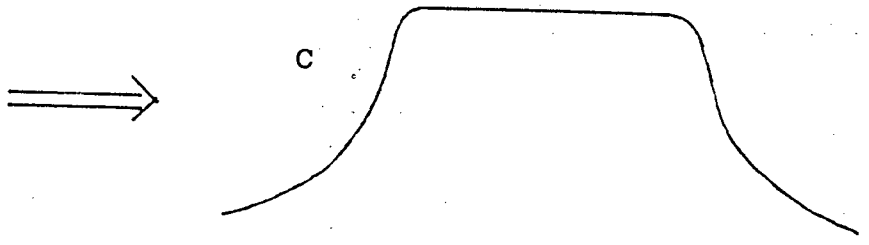

i) Ellipse profile with a PSF falloff ($Ellipse_2$)

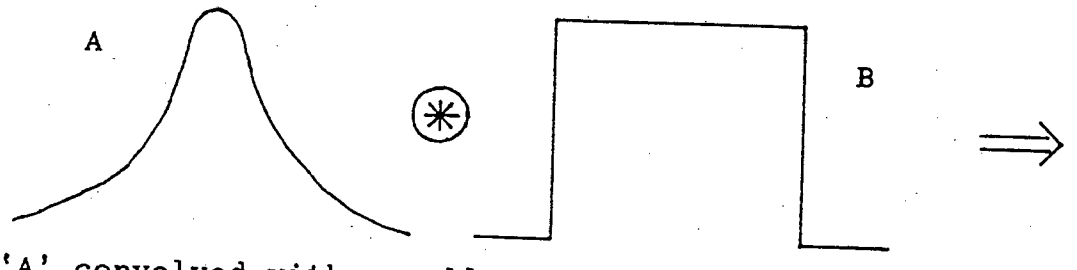

PSF 'A' convolved with a wall profile 'B' resulting in 'C'

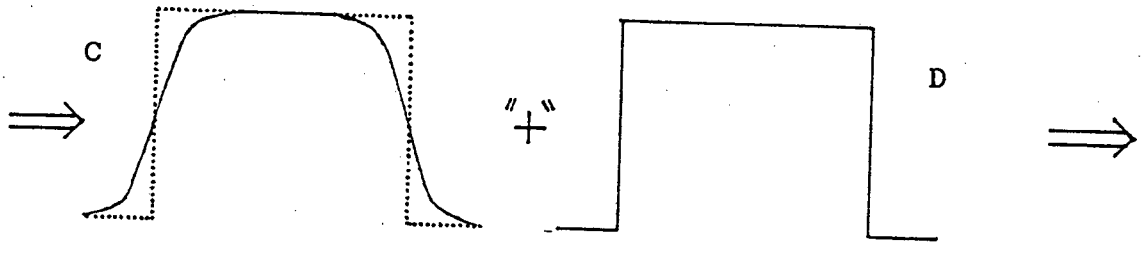

The falloff of 'C' is *added* to the wall 'D' resulting in 'E'

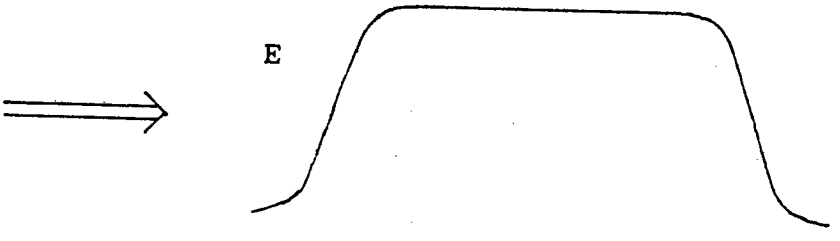

ii) Ellipse profile with PSF-convolved-with-wall falloff ($Ellipse_1$)

Figure 7.9 Adding falloff functions to a profile $Ellipse_n$

whilst maintaining symmetry about the midpoint. It represents a blurred target or a target having insufficient contrast with the background.

iii) Ellipse with Gaussian falloff, renamed 'Ellipse$_2$', which falls off from the ellipse perimeter with the Gaussian curve. This function is implemented to represent an over illuminated ellipse.

(see Figure 7.9)

The method to evaluate the sub-pixel grey value is:

The grey value (height) of each sub-pixel is determined by the value of the falloff at the centre of the sub-pixel. For a given pixel, the sub-pixel grey values are added together and divided by the number of sub-pixels per pixel to give the grey value for the pixel.

Typical profiles through a symmetrical synthetic Ellipse$_1$ together with their pixel grey values are illustrated in Figure 7.10.

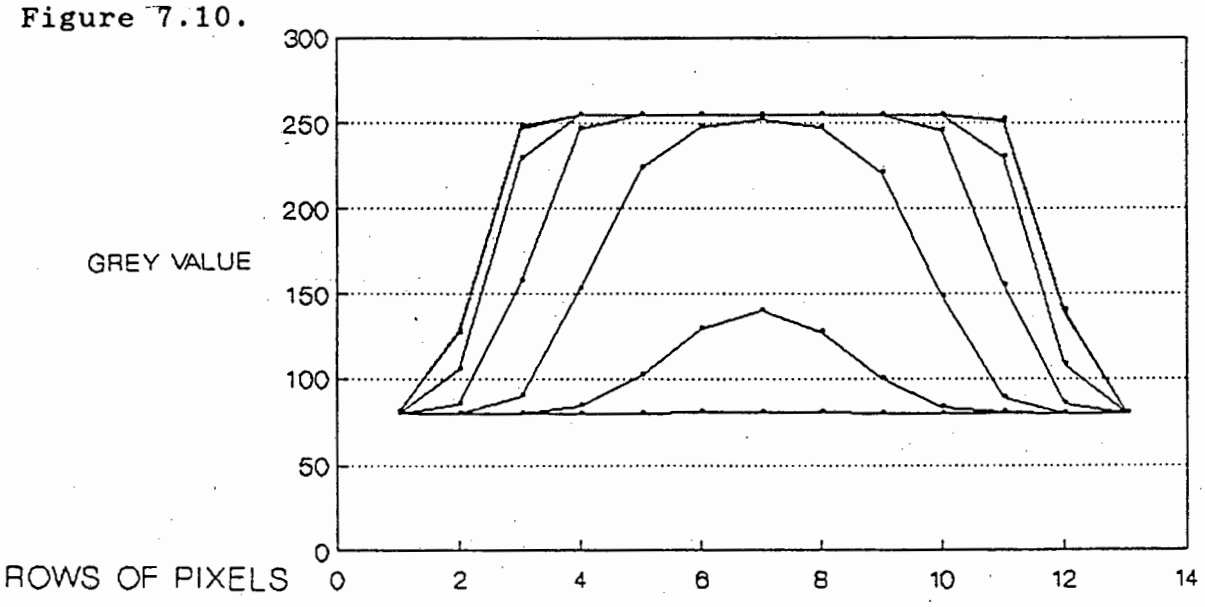

Figure 7.10a Typical profiles through symmetrical synthetic Ellipse$_1$

Example of a Synthetic Ellipse with a Falloff Function of Type Ellipse 1

	1	2	3	4	5	6	7	8	9	10	11	12	13	14	15
1	80	80	80	80	80	80	81	81	81	80	80	80	80	80	80
2	80	80	80	80	83	97	123	137	129	103	85	80	80	80	80
3	80	80	80	87	139	214	246	252	249	227	159	93	80	80	80
4	80	80	83	143	242	255	255	255	255	255	249	167	87	80	80
5	80	80	101	221	255	255	255	255	255	255	255	236	113	80	80
6	80	80	126	248	255	255	255	255	255	255	255	252	140	80	80
7	80	81	128	249	255	255	255	255	255	255	255	251	138	81	80
8	80	81	105	229	255	255	255	255	255	255	255	231	108	81	80
9	80	80	85	157	247	255	253	248	253	255	246	155	85	80	80
10	80	80	80	90	153	224	203	141	203	221	148	89	80	80	80
11	80	80	80	80	84	102	129	80	127	100	83	80	80	80	80
12	80	80	80	80	80	80	81	81	81	80	80	80	80	80	80

Figure 7.10b Pixel grey values of the symmetrical Ellipse1 corresponding to 7.10a

An image is formed consisting of 9 synthetic ellipses of type Ellipse1 and is stored as IMAGE 1 for further processing by the target centring algorithms.

7.3 TESTING THE SYNTHETIC TARGET ALGORITHM

Tests were undertaken to investigate the performance of the synthetic target algorithm.

A number of images were created with 18 consistently sized targets of type Ellipse0 (with direct falloff) having differing orientations and centre locations. For each image:

- the target sizes are either ± 8x6 pixels, 10x8 pixels or 13x10 pixels
- the sampling for each pixel is either 10x10, 20x20, 30x30 or 40x40 sub-pixel per pixel.

Two additional images with 18 targets of type Ellipse1 each are generated with a sampling of 10x10 and 20x20 sub-pixels per pixel respectively.

One of the target centring algorithms, the weighted centre of gravity algorithm (described in [8.3]) is used to evaluate the effects of increasing the size and sampling rate of the synthetic elliptical targets to ensure the correct working of the program to generate ellipses.

All the ellipse target pixel grey values are evaluated as real numbers in the range of 0 to 255. The centre of gravity algorithm is used to evaluate the error in target centre for both pixels with a real grey value and the equivalent pixels with an integer grey value. The results for all the images produced are illustrated in Table 7.1.

[Window used was 17 x 17 pixels]	Target centring accuracy as obtained using Centre of Gravity [Measured in fraction of a pixel]								
Average Target Size = 8 x 6 pixels = '100%'	n=10*10		n=20*20		n=30*30		n=40*40		Number of Sub-Pixels per Pixel
	real	int	real	int	real	int	real	int	
Scale = 100% Std Dev	1/338	1/340	1/504	1/488	1/424	1/406	1/482	1/425	Targets with Direct Falloff - Ellipse0
Scale = 130% Std Dev	1/406	1/379	1/554	1/528	n/a	n/a	1/555	1/507	
Scale = 160% Std Dev	1/485	1/466	1/791	1/778	1/921	1/843	n/a	n/a	
Targets with Gauss (PSF) convolved with wall falloff									
Scale = 100% Std Dev	1/4092	1/1317	1/4134	1/1173	n/a	n/a			Targets with Gauss (PSF) Convolved with a Wall Falloff - Ellipse1

Table 7.1 Illustrating the effect of increased target and sampling on ellipse grey value accuracy.

Table 7.1 indicates that the weighted centre of gravity algorithm is able to locate the centre of real valued targets to a higher precision than that of integer valued targets.

A trend line graph for the Ellipseo targets illustrates the effect of increasing:

i) The number of sub-pixels evaluated per pixel
ii) The size of the target
100% = normal 8x6 pixel target
130% = target magnified by 1.3x
160% = " " by 1.6x

on the accuracy of the target centre see Figure 7.11

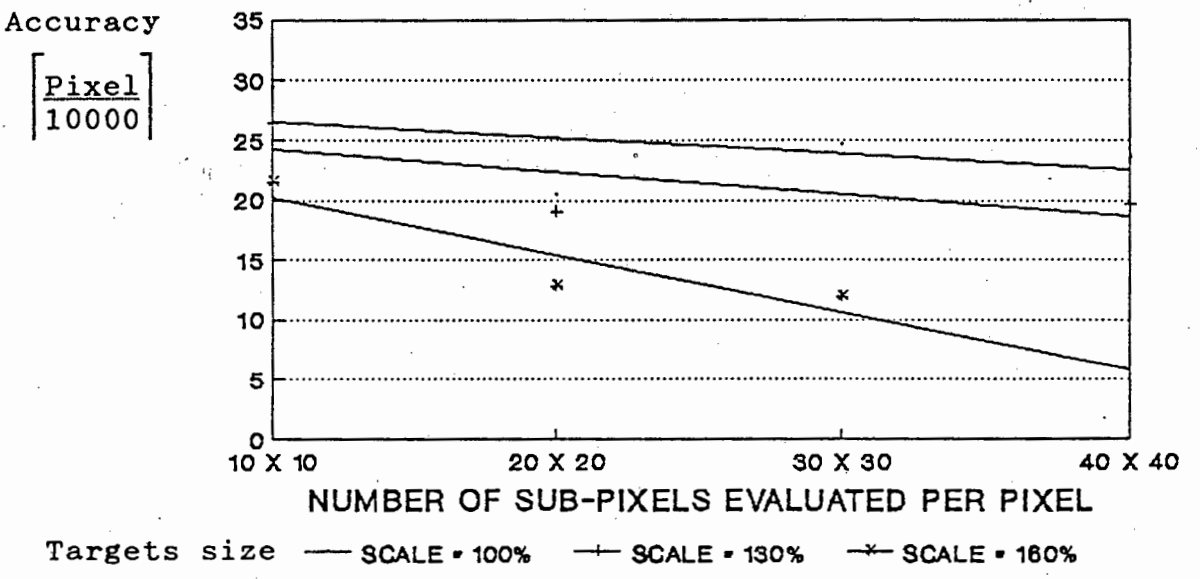

Figure 7.11 Trends of magnifying the target and evaluating increasing number of sub-pixels per pixel

The trend graphs indicate that the accuracy of the centre determination increases with:

- increasing the number of sub-pixels per pixel
- increasing the size of the ellipse targets.

The results detailed above indicate that the program works as expected when generating synthetic targets. With larger targets, the resolution improves because the target centring algorithm has a larger target array to pinpoint the centre. When using a larger number of sub-pixels, there is a finer resolution of sub-pixels to define the perimeter, for pixels with the edge passing through them.

The accuracy of all target centring algorithms is primarily a function of the number and precision of perimeter pixels (those pixels with a grey level between saturation and background).

- Increasing the target size results in more pixels (and sub-pixels) defining the target and thus a higher precision target centre is expected.

- Increasing the number of sub-pixels evaluated per pixel implies a more accurate perimeter pixel grey value from which a higher precision target centre is expected.

A second graph was plotted to indicate the accuracy of centre determination between real and integer valued $Ellipse_1$ targets. Real valued targets vs. integer valued targets have an accuracy ratio (for $Ellipse_1$ targets) of the order of 3:1 (as opposed to the accuracy ratio of 1.2:1 for real and integer valued $Ellipse_0$ targets). Thus the process to convert from real to integer grey values adds a high level of uncertainty on an otherwise accurately defined real pixel valued ellipse centre. There is no appreciable gain in accuracy for the step from 10x10 to 20x20 sub-pixels evaluated per pixel, for $Ellipse_1$.

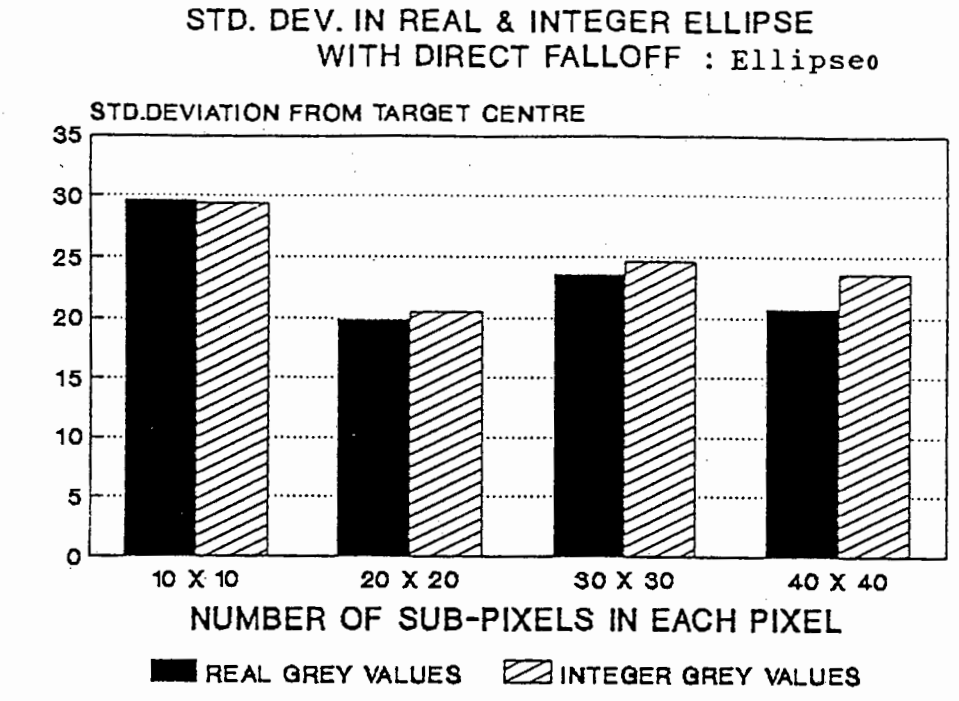

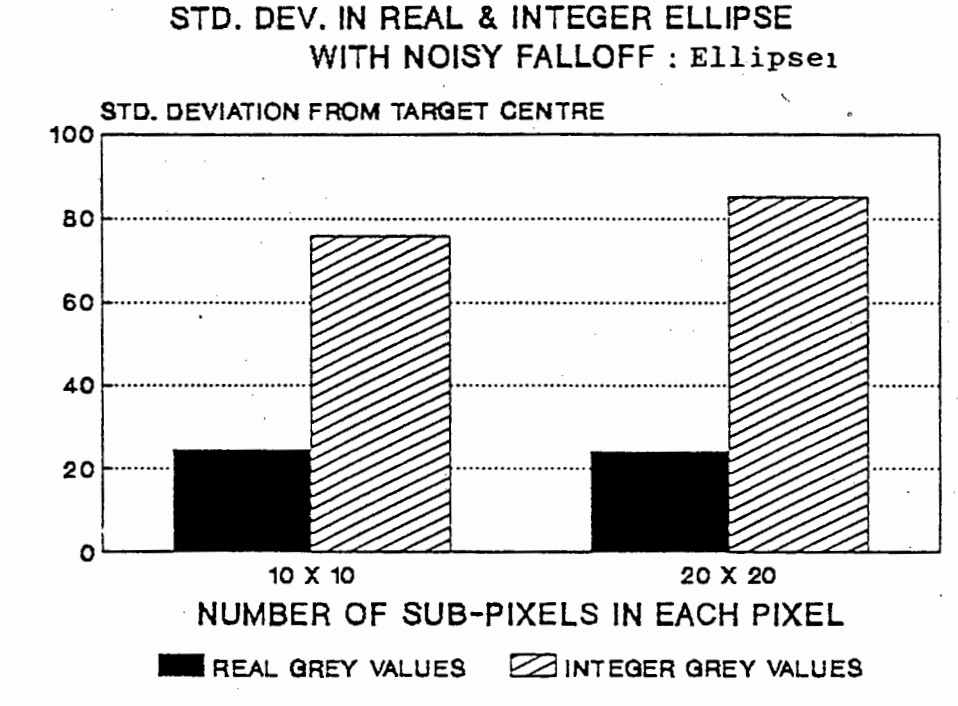

Figure 7.12 Graph of integer vs real ellipse target centring accuracy for Ellipse0 and Ellipse1 targets

To summarise:
Using the weighted centre of gravity algorithm, the centring accuracy of the ellipse targets improves with:

- increasing the number of sub-pixels evaluated per pixel
- increasing the size of the ellipse
- using real pixel grey values rather than integer valued pixels.

The algorithm appears to operate as intuitively expected.

7.4 FABRICATING SYNTHETIC TARGETS WITH BLEMISHES

An image consisting of a target with blemishes has been formed to check the robustness of the algorithms to non-symmetric targets. Obscuring of targets is typically caused by a shadow falling on the target or partial obscuring of the target by another object.

The blemish is added to the target by forming a point spread function with a falloff at the same rate as that of the target. The point spread function is to act as a shadow on the edge of the target. As a result the shadow PSF is inverted and subtracted from the pixel grey value. The concept is outlined below in Figure 7.13.

The procedure whereby the new grey values of the obscured target are calculated is:

```
If original target [i,j]  >  shadow [i,j]
     then obscured target [i,j] = shadow [i,j]     {region 1}
     else obscured target [i,j] = original target [i,j] ...
                                                   {region 2}
```

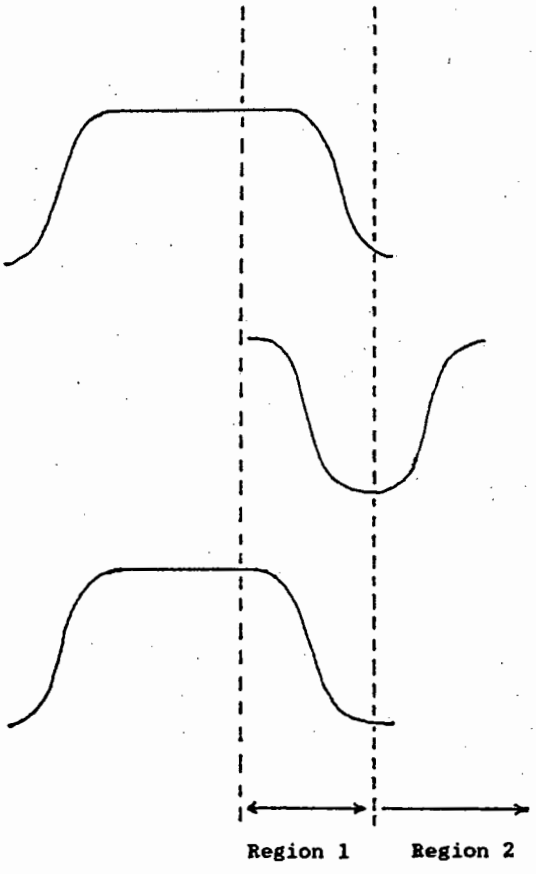

Figure 7.13 Image of the effect of a shadow on the profile of symmetrical ellipse original ellipse

The point spread function of the shadow is subtracted from different edge locations of all targets in the synthetic image. A profile through a typically obscured ellipse is illustrated below, see Figure 7.14.

Example of a Synthetic Ellipse with a Blemish Falloff function of type Ellipse 1

	1	2	3	4	5	6	7	8	9	10	11	12	13	14	15
1	80	80	80	80	80	80	81	81	81	80	80	80	80	80	80
2	80	80	80	80	83	97	123	137	129	103	85	80	80	80	80
3	80	80	80	87	139	214	246	252	249	227	159	93	80	80	80
4	80	80	83	143	242	255	255	255	255	255	249	167	87	80	80
5	80	80	101	221	255	255	255	255	255	255	255	236	113	80	80
6	80	80	126	248	255	255	255	255	255	255	255	252	140	80	80
7	80	81	128	249	255	255	255	255	255	255	255	251	138	81	80
8	80	81	105	229	255	255	255	255	255	255	255	231	108	81	80
9	80	80	85	157	247	255	255	255	255	255	246	155	85	80	80
10	80	80	80	90	153	224	248	252	248	221	148	89	80	80	80
11	80	80	80	80	84	102	129	140	127	100	83	80	80	80	80
12	80	80	80	80	80	80	81	81	81	80	80	80	80	80	80

Pixel values of an obscured ellipse

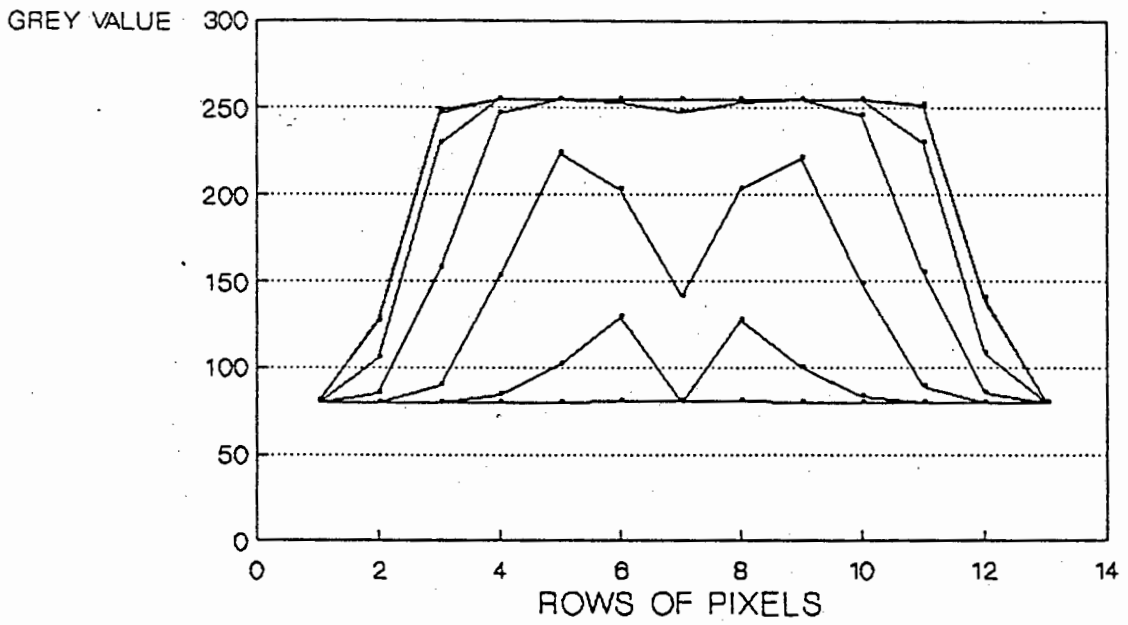

Profiles through a typically obscured ellipse

Figure 7.14 Example of a typically obscured ellipse

A second image was formed of nine synthetic ellipses of type Ellipse1 each with a blemish on its perimeter and stored as IMAGE 2 for further processing of the accuracy of target centring algorithms.

All algorithms are run on the 'partially obscured ellipse' image.

7.5 SUMMARY

A program was written to generate digital images of synthetic targets which resemble real targets. The number of ellipses and the parameters for each ellipse are entered into the program and the program then automatically generates an image containing the synthetic targets.

Two images:
- of 9 symmetric synthetic ellipses (IMAGE 1)
- of 9 synthetic ellipses with blemishes (IMAGE 2)

were formed.

The advantages of using a program to generate images consisting of synthetic ellipses are:

- the ellipse centres are known to a high precision from the parameter listing, allowing for a simple comparison of the accuracy of target co-ordinates obtained using the centring algorithms
- there is no expense involved in testing algorithm accuracies (as there is in the case of the control frame).

The only disadvantage is that the program execution time can be lengthy depending on the number of ellipses, the complexity of the falloff function and the precision to which the grey scale accuracy is required.

The steps involved in comparing target centring accuracies on images of synthetic targets are:
- enter parameters of the ellipses
- form image of synthetic ellipses
- form image of synthetic ellipses with blemishes

Chapter 7

- locate target centres in the image using the target centring algorithms — Chapter 8
- compare the target centres from each algorithm with the target centres in the program parameter listing — Chapter 9

see Figure 7.15

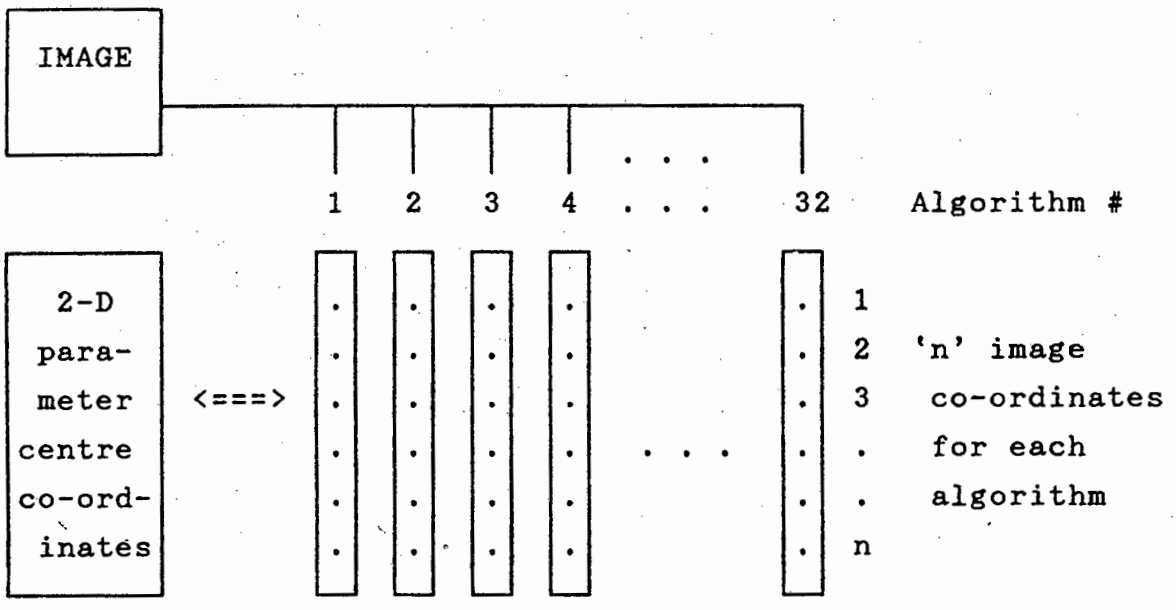

Figure 7.15 Obtaining and comparing target centring algorithms on synthetic images

CHAPTER 8

8.0 TARGET CENTRING ALGORITHMS IMPLEMENTED

8.1 OVERVIEW OF THE RUNNING OF *'TARGET CENTRING PROGRAM'*

A flow chart indicating the input options (IMAGES 1, 2 & 3) to the target centring program, in addition to the possible combinations of algorithms to form one target centring algorithm is illustrated in Figure 8.1 .

8.1.1 Images used by the Program to Test Target Centring Algorithms

Three images were formed to test aspects of the target centring algorithm:

- IMAGE 1 : of symmetric synthetic targets.
- IMAGE 2 : of synthetic targets, each with a blemish.
- IMAGE 3 : of real targets on a control frame.

Locating the targets was facilitated by forming secondary binary images of IMAGES 1,2 and 3.

8.1.1.1 Binary Image of Control Frame Targets (IMAGE 3)

Targets on an image of a control frame are identified by creating a binary image of the original, where all pixels with a grey value above an arbitrary *threshold* level (representing targets) are set to '255' and all other pixels (representing background) are set to '0'. A threshold level is interactively chosen to identify the targets optimally, with a minimum of the background object being visible.

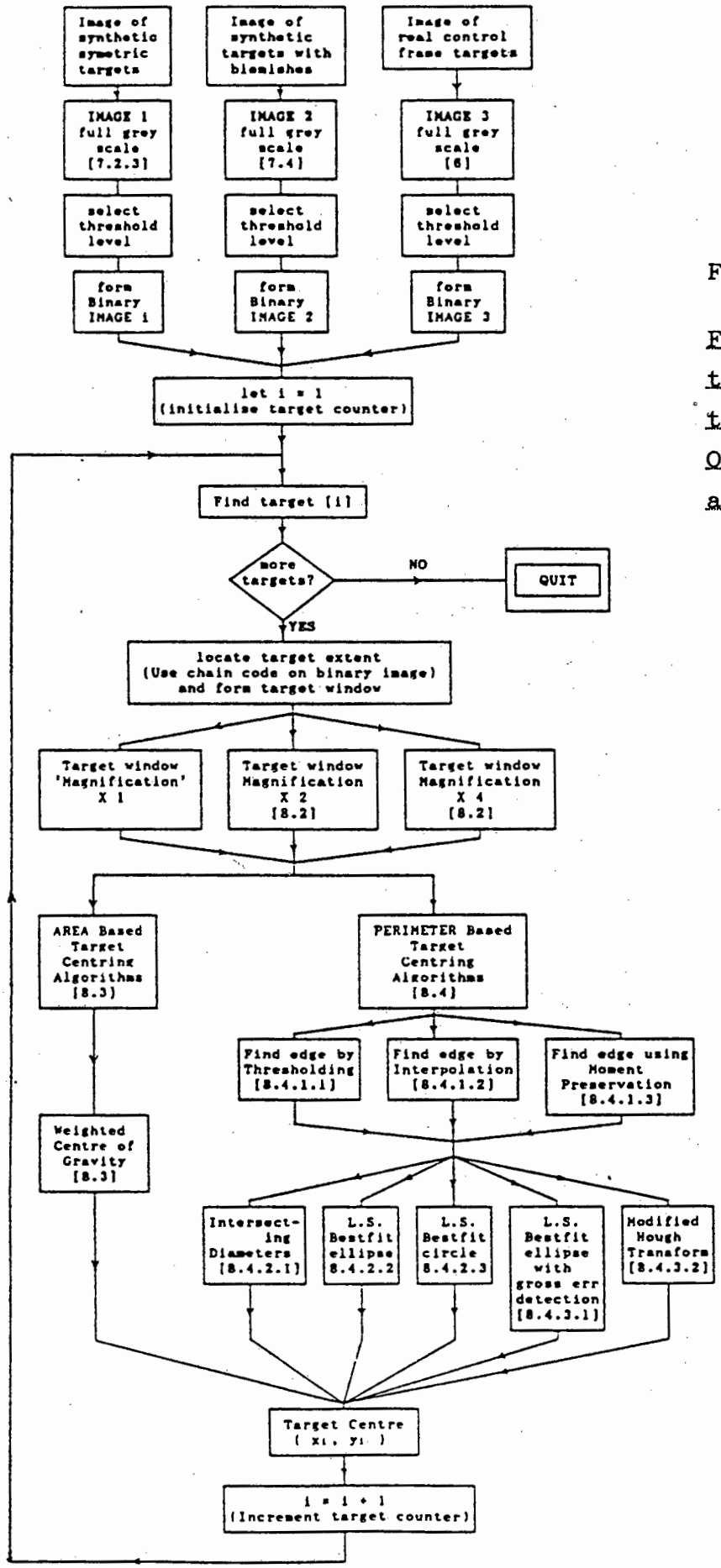

Figure 8.1

Flowchart of the images and target centring OPTIONS available

8.1.1.2 Binary Image of Synthetic Targets (IMAGES 1 & 2)

A target on a synthetically created image is located by choosing a threshold level which is higher than the background grey level selected for the image (in the synthetic ellipse program). A binary image is created of the synthetic image using the same method outlined for IMAGE 3.

8.1.2 Locating the Target and Finding the Target's Extent

8.1.2.1 Method used to Locate the Target

Targets are located on the binary image by searching the binary image row by row, for all pixels at a grey level of '255'. The first pixel which is located at the level '255', is the top left hand pixel of a target. The target extent is found [8.1.2.2] and the procedure is repeated to locate the following targets.

8.1.2.2 Method used to Find the Target's Extent: Chain Code

The target consists of a cluster of connected pixels at level '255'. In order to determine the target extent, chain coding is used. Chain coding was developed by Freeman in 1974 and described in an application by Thapa (1988) to define the edge and shape of a body. The perimeter of a connected body can be found and mapped using the chain code. The pixels surrounding the first edge pixel are searched in the sequence described by the chain code (see Figure 8.2) until the next pixel at level '255' is located. This pixel becomes the current edge pixel. The following edge pixel is located by searching all the pixels surrounding the new edge pixel, starting with the chain code direction with which the last current edge pixel was found. This ensures that the perimeter is found in a clockwise manner and the body of the target always remains to the right of the direction of the

chain of edge points. All the edge pixels are located in the same manner and the procedure ends when the first edge pixel is found again. A more complete description of the chain code algorithm is given in a flow chart form in Appendix E. The target extent is determined from the minimum and maximum 'x' and 'y' values of all the edge pixels found.

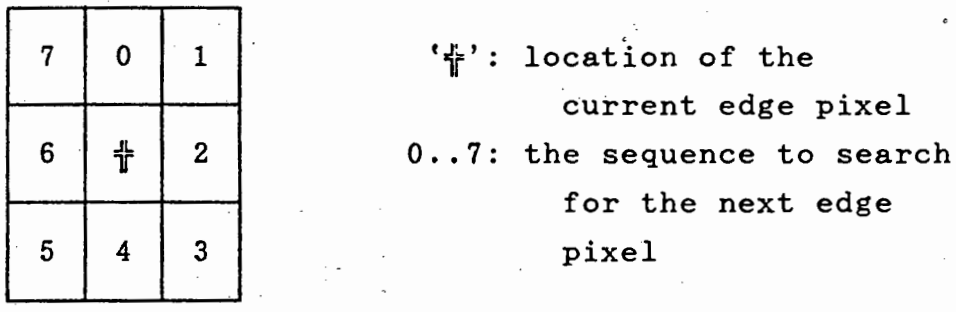

Figure 8.2 The Freeman chain code

8.1.2.3 Two Alternative Methods to Locate Targets

i) A method to locate targets and edges automatically, in an image where there is less contrast between target and object, is to 'convolve' the image with a ***mask of a high-pass filter***, locating all edges.
Convolution, described in Appendix D, may be used as a tool to locate features of an image which closely resemble the characteristics or shape of a window of pixels (mask). It is implemented by passing the mask over every location of the image, overlaying the mask on the sub-image, multiplying the corresponding mask and image pixels together, adding them together and storing the (scaled) result in a location of a second image matching the location of the convolution mask on the primary image. The second image represents the goodness of correlation (fit) of the mask with corresponding locations of the original image. Target

perimeters could be identified by searching the resulting image for pixels exceeding a preset threshold level.

ii) A method whereby targets may be almost exclusively identified within an image is to 'convolve' the image with a ***mask of a typical target*** found in the image. All objects resembling the target mask will be highlighted in the second (convolved) image.

8.1.2.4 Incorrectly Identified Targets Rejected

Incorrectly identified targets which are too large or too small to be classified as a real target are automatically rejected. False targets are often a consequence of incident light being reflected off wires, supports or the background object, or may be caused by a single target being split into two by a thin support wire obscuring the target.

8.1.3 Selecting Windows Around the Target Extent

Windows are selected about targets allowing for a border of 'n' (typically n = 2) pixels surrounding the perimeter of the target at a preset threshold level determined for the image, see Figure 8.3 below.

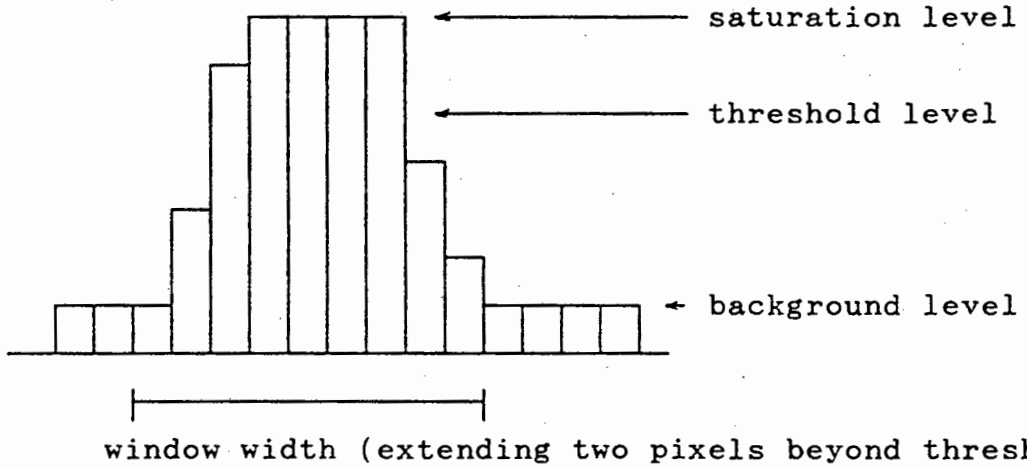

Figure 8.3a Cross section of a target

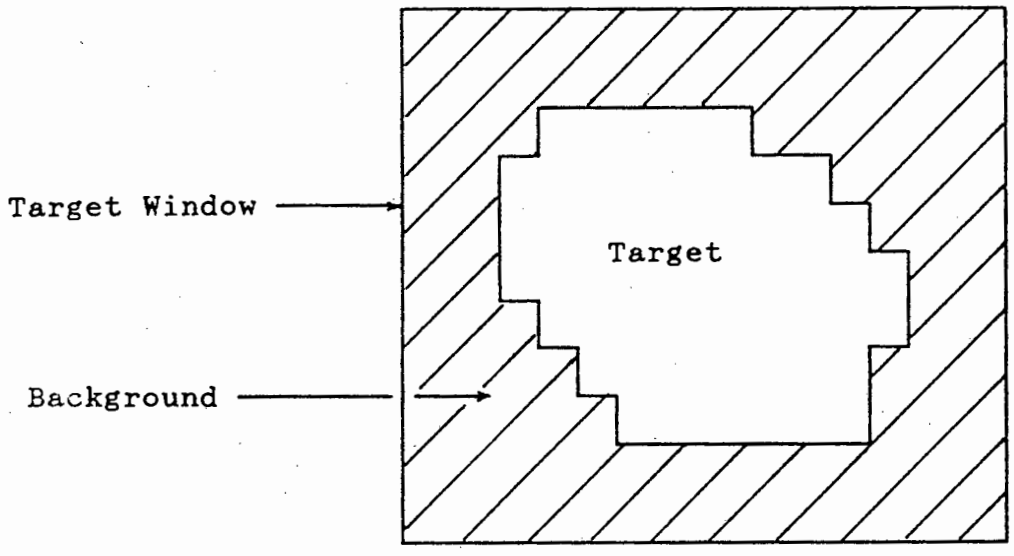

Figure 8.3b Plan view of target window with borders surrounding the target

All targets that are assessed are white in colour with a grey level above 'threshold', having a black background with grey levels below 'threshold'. For each target window located, all the centring algorithms are tested against the target and the results are stored in a file.

8.1.4 Target Centring Algorithms Implemented

The two general techniques which were used to compute target centres were based on area and edge (perimeter) evaluation. Thirty two target centring algorithms were used. Each target centring algorithm consists of a combination of sub-algorithms:

i) The target window may be magnified by either '1', 2 or 4

ii) The target window may be evaluated using area- or edge based algorithms:

AREA BASED ALGORITHM

Evaluated using the weighted centre of gravity

EDGE BASED ALGORITHM

Evaluated by firstly finding the edge using:

- Thresholding
- Interpolation
- Preservation of moments

and then using a bestfitting centring algorithm

- Intersecting diameters
- Bestfitting ellipse
- Bestfitting circle
- Bestfitting ellipse with gross error detection
- The modified Hough transform

The *bestfitting ellipse with gross error detection* and *modified Hough transform* were implemented to find target centres of partially obscured or distorted targets.

8.2 MAGNIFICATION OF THE IMAGE WINDOW

From the evaluation of synthetic targets [7.3], it was found that larger target windows led to improved target centring accuracy. The concept was extended to magnifying the target windows by interpolating between pixels in the original target window and evaluating the intermediate pixel values.

The image window may be magnified two fold or four fold. A four fold magnification of an image window of size 12x12 pixels would form a new window of size 48x48 pixels. The magnification algorithm was designed to be implemented for use by both the area and edge based algorithms.

The order of procedures is to first magnify the window containing the target. For the purpose of the comparison of

algorithms the window size was doubled. This was followed by using the centre of gravity algorithm as well as all combinations of the edge detection algorithms with bestfitting curve algorithms. For the discussion that follows, an input pixel refers to a pixel from the original target window and an output pixel refers to a sub-pixel within the magnified window.

8.2.1 Background to Magnification Algorithms Available

One method to achieve more accurate and reliable results, with the same data and algorithms, is to resample the target improving the resolution of the window. Some of the methods available include:

i) The nearest neighbour or zero order approach: this uses the grey scale value of a pixel closest to the interpolated sub-pixel. This can introduce shifts of up to $\sqrt{2}$ of a pixel in the sub area that is being analysed.

ii) Bilinear interpolation: this is where the sub-pixel takes on a grey scale of the average of its closest neighbours. This is equivalent to passing a low-pass filter over the image, resulting in a blurred image.

iii) Cubic Convolution: with an increase in computing complexity, sixteen input pixels are weighted by a function 'f' to determine the intensity of the output sub-pixel. The function f has as its primary parameter, the distance between the input and output pixels, Atkinson (1985). The algorithm was tested using synthetic targets, Saleh (1988).

iv) Multi-temporal data merging: this is where multiple images of the same object, taken at different times,

are overlaid. Some areas may occur in both images where pixels in one image are offset from those in another image by up to 1/2 of a pixel. These areas are radiometrically balanced and then interleaved, effecting an improvement in resolution by doubling the sampling rate, Dye (1989).

The above methods have applications primarily in recovering data from satellite imagery.

One method which was implemented, is similar in concept to cubic convolution. It involves considering a 3x3 array of input pixels surrounding the output pixel. The grey scale values of the input pixels are weighted by the reciprocal of the distance separating the output pixel with the input pixel under consideration, see Figure 8.4 .

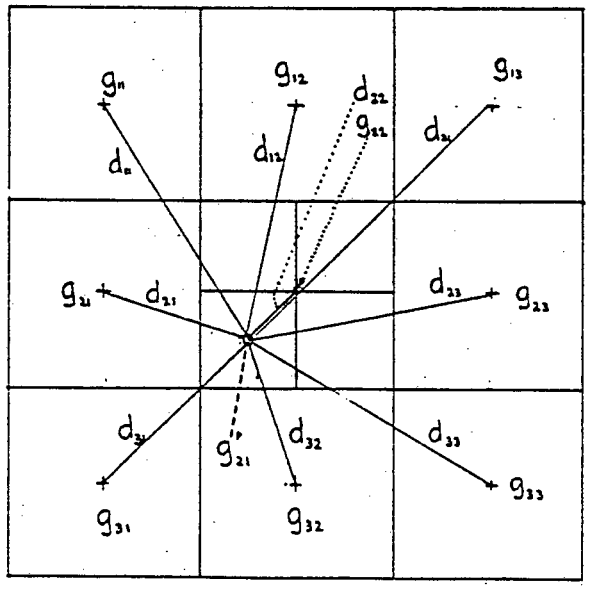

Figure 8.4 Pixel grey value weighting as a function of the distance between pixel and sub-pixel

The resolution enhancing algorithm is:

$$g'_{pq} = \frac{\sum_{i=1}^{3} \sum_{j=1}^{3} g_{ij} \times (1/d_{ij})}{\sum \sum (1/d_{ij})}$$

where - the array of input pixels (g_{ij}) surround the output pixel (g'_{pq})
- d_{ij} is the distance between the output pixel (g'_{pq}) and input pixel (g_{ij})

The implementation of this system failed to improve target centring accuracy. The likely reason for this is that the effect of the algorithm was similar to a low-pass filter, thus blurring the image.

8.2.2 Resolution Enhancement using a Point in the Plane

The method used in this algorithm is to form a plane using the grey scale values of three pixels surrounding the sub-pixel. The sub-pixel grey scale is evaluated by considering the grey scale value of the plane at the sub-pixel location.

Given four points (the sub-pixel and three surrounding pixels), the determinant with the co-ordinates of these points is a measure of the volume formed by them. A zero determinant implies a zero volume between the four points, thus indicating that all the points are in the same plane. (For the following evaluation, a pixel and sub-pixel will be considered to be points in 3-D space where the grey value contributes the third dimension, i.e. the *Z* axis.)

The area occupied by the original pixel (M_1) becomes the area for the four sub-pixels (P_{s1}, P_{s2}, P_{s3} and P_{s4}), see Figure 8.5

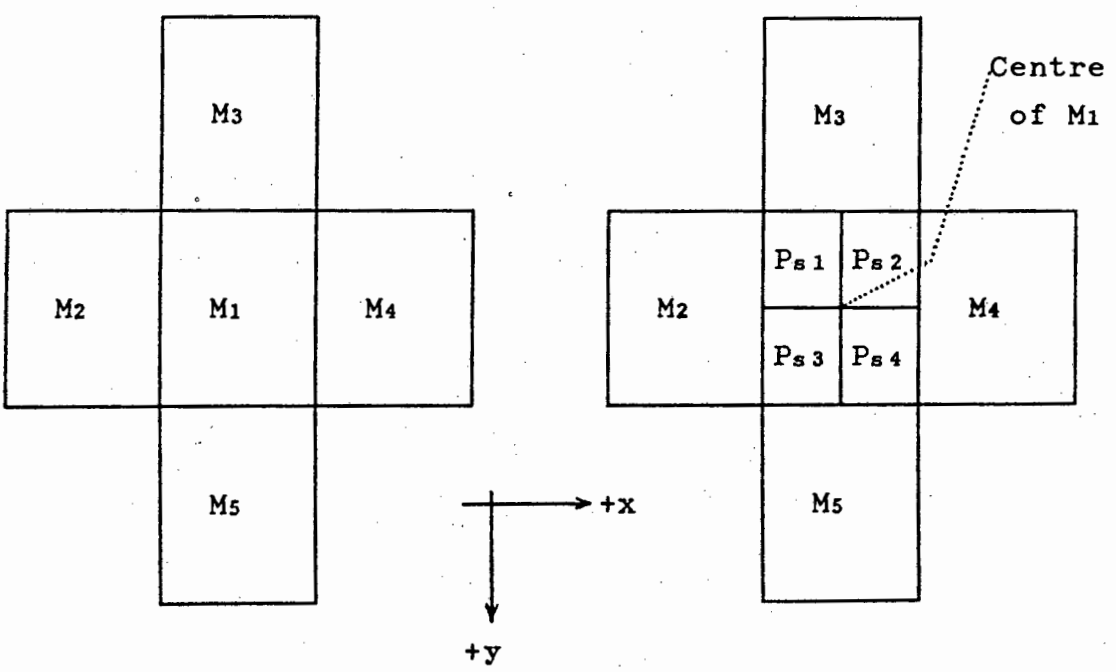

Figure 8.5 Sub-pixel evaluation in relation to the original pixel, with co-ordinate axes

For the original pixel M_1 at location (x_i, y_i, z_i), the sub-pixel # P_{s1} with co-ordinates (- 1/4, - 1/4, z_{i1}) relative to the centre of M_1, falls in the plane formed by points M_1, M_2 and M_3. Similarly :

Sub pixel	at location	falls in plane formed by
#P_{s2}	+ 1/4, - 1/4, z_{i2}	M_1, M_3 and M_4
#P_{s3}	- 1/4, + 1/4, z_{i3}	M_1, M_4 and M_5
#P_{s4}	+ 1/4, + 1/4, z_{i4}	M_1, M_5 and M_2

For all the sub-pixels of pixel M_1, the value of z_{ni} is evaluated for n = 1..4. The results are then stored in an enlarged image window for the sub-pixel grey values. All the sub-pixels grey values for the new image window pixels are similarly evaluated and stored.

The algorithm was developed to evaluate larger sub-pixel arrays, resolving the target window to a higher resolution. As an example, the new array may magnify the original pixel to 4x4 sub-pixels, see Figure 8.6 .

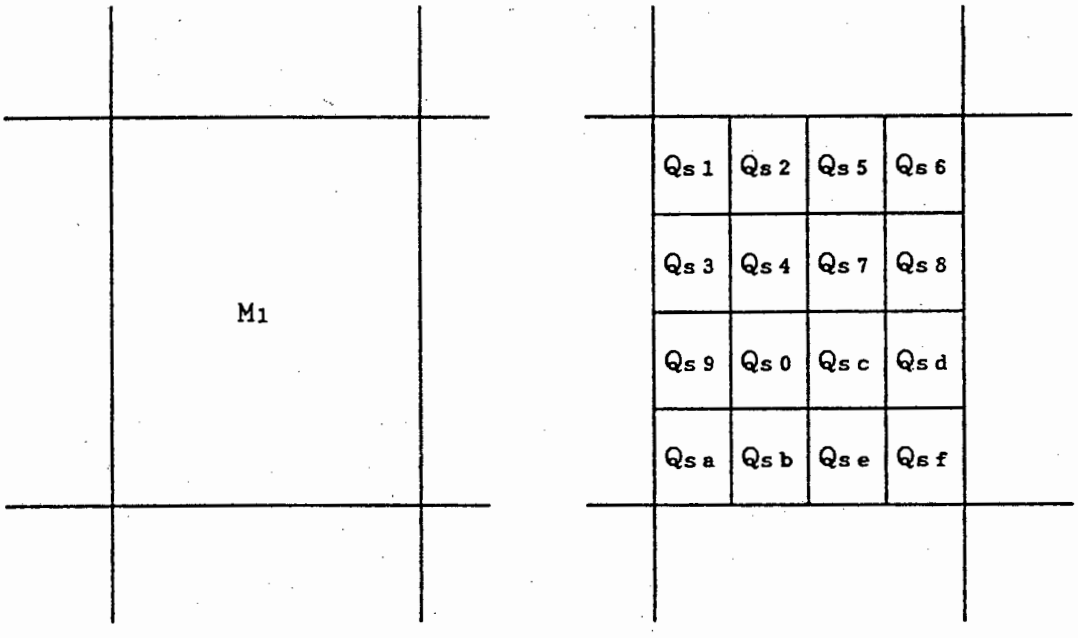

Figure 8.6 Demonstrating a 4x4 sub-pixel in relation to the original pixel

In a similar manner to the 2x2 pixel resolution enhancement, the 4x4 sub-pixel array is evaluated using:

sub-pixel	at location xi	yi	zi	falls in plane formed by
Q_{s1}	$-3/8$	$-3/8$	z_1	M_1 M_2 M_3
Q_{s2}	$-1/8$	$-3/8$	z_2	"
Q_{s3}	$-3/8$	$-1/8$	z_3	"
Q_{s4}	$-1/8$	$-1/8$	z_4	"
Q_{s5}	$1/8$	$-3/8$	z_5	M_1 M_3 M_4
Q_{s6}	$3/8$	$-3/8$	z_6	"
	etc			

The magnified target window is passed to the centring algorithms for further evaluation of the algorithms' centring ability.

8.3 AREA BASED ALGORITHM

THE WEIGHTED CENTRE OF GRAVITY ALGORITHM

The weighted centre of gravity algorithm is an area based method traditionally used to evaluate the centre of a target. As from here, the weighted centre of gravity algorithm will be referenced as the centre of gravity or C.G. algorithm.

The source of the centre of gravity equation is commonly available, e.g. Humphrey (1971). The traditional equation is:

$$M = \sum_i \sum_j (e_{ij})$$

$$x = \frac{1}{M} \sum_i \sum_j (e_{ij}) \times i$$

$$y = \frac{1}{M} \sum_i \sum_j (e_{ij}) \times j$$

where - e_{ij} is the grey scale intensity of a pixel located in row i, column j of the image.

The above formula is successful in determining the centre of a target with a background grey level of 'zero', but fails to give an accurate centre determination for targets in a window with a finite background level. A digital video camera denotes a black background as finite noise signal and thus as a finite grey level.

To avoid the influence of a finite background grey level on non-symmetrically placed targets within a target window, the formula was modified by Wong (1986) to:

$$M = \sum_i \sum_j (f_{ij})$$

$$x = \frac{1}{M} \sum_i \sum_j (f_{ij}) \times i$$

$$y = \frac{1}{M} \sum_i \sum_j (f_{ij}) \times j$$

where - e_{ij} is the pixel grey scale value
- $f_{ij} = 1$ for $e_{ij} <= \text{threshold}$
- $f_{ij} = 0$ for $e_{ij} > \text{threshold}$

The threshold level, determined for the particular target window, was set to threshold = integer ($^1/_2$(mean + minimum)) for a system with targets being black in colour, and the background being white. For all targets, especially those smaller than 20x20 pixels, the perimeter grey scale pixels denoting the falloff from saturation level to the threshold level has a large effect on the accuracy as demonstrated in [7.3]. The falloff pixels are accounted for by Trinder (1989) with the equations:

$$M = \sum_i \sum_j (g_{ij})$$

$$x = \frac{1}{M} \sum_i \sum_j (g_{ij}) * i$$

$$y = \frac{1}{M} \sum_i \sum_j (g_{ij}) * j$$

where - $g_{ij} = e_{ij} - \text{Threshold}$ for $e_{ij} >= \text{Threshold}$
- $g_{ij} = 0$ otherwise.

In this formulation, e_{ij} is the pixel grey value within the target window. This method results in a translation of the threshold level to zero whilst maintaining the profile of

the target. Further assessment of the importance of choosing the correct threshold level is given in [9.2.1].

8.4 PERIMETER BASED ALGORITHMS

In addition to the area based centring algorithm, target centres may be determined using perimeter based algorithms.

The perimeter based algorithms are two stage processes:

- the image window is first sent to one of a number of *edge detection* algorithm
- the resulting edge is then passed to one of the *bestfitting curve* algorithms to find the target centre.

8.4.1 Finding the Edge Around the Target

Chain coding is a simple method to find the edge of an object. It is described in [8.1.2.2] and Appendix E: flowchart 3a. The drawback of this method is that the edge is only found to the closest pixel approximation.

The majority of edge detection algorithms investigated, including those implemented, scanned the target window firstly row by row, then column by column, searching for the edges to the target.

OVERVIEW OF METHODS AVAILABLE FOR EDGE DETECTION

i) In the successive differences method, a secondary curve is formed from the difference between the current and former pixel's grey scale value on a row. The edge of the row is defined to lie at the point of maximum slope

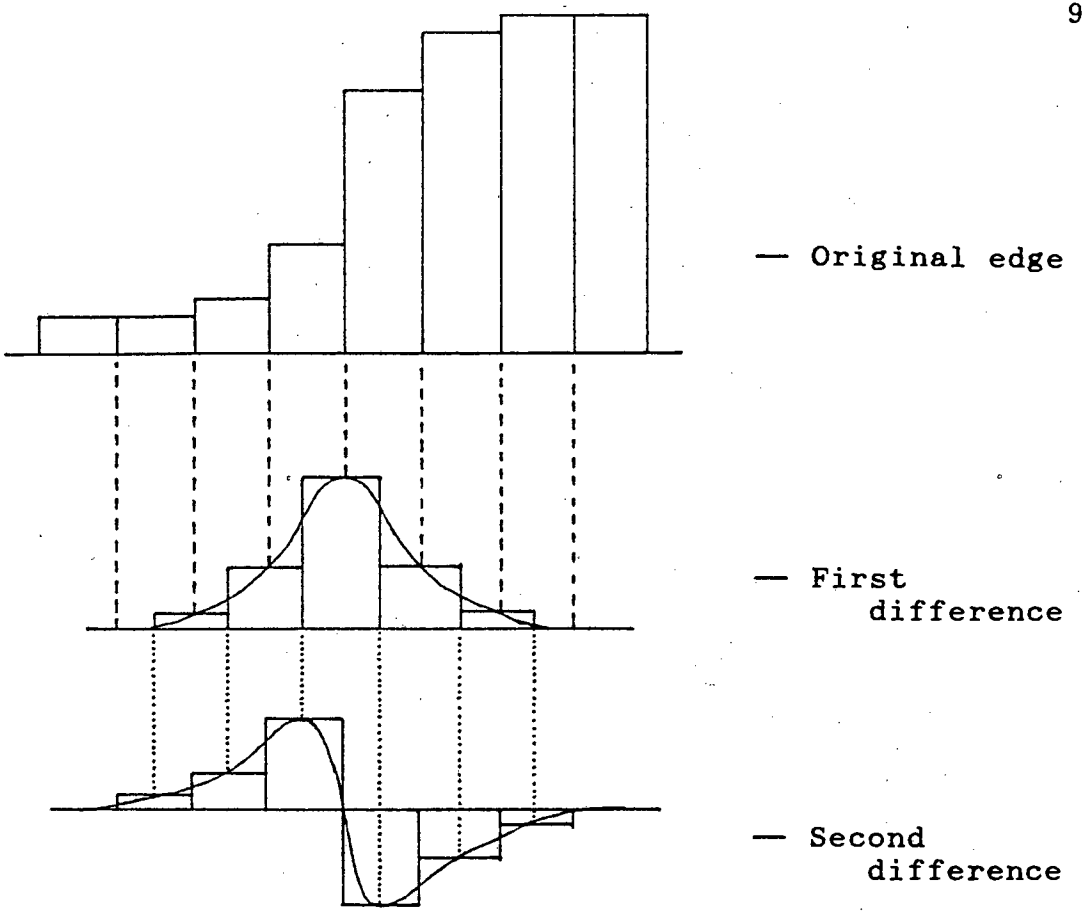

Figure 8.7 Illustrating the First and Second difference edge detection

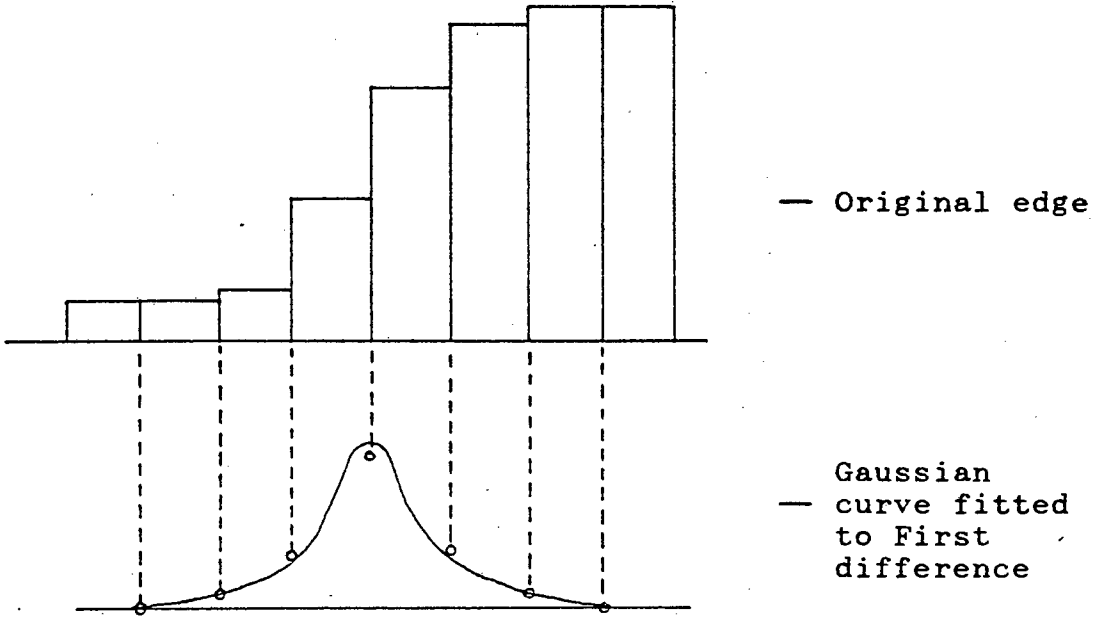

Figure 8.8 Fitting a Gaussian curve to the successive differences of an edge

of the row, which lies at the maximum of the curve of successive differences. Because of the difficulty in defining the sub-pixel maximum to a sampled set of data, the second difference may be evaluated indicating the edge at the zero crossing (which is easier to locate) of the resulting second difference curve. The first and second difference curves are illustrated in Figure 8.7 . The problem of the first and second difference edge detection methods are the sensitivity of the curves to noise, in particular the second difference method which may exhibit multiple zero crossings in the presence of noise.

ii) To overcome the problem of a poorly defined peak in the first differences method, Seitz (1988), a Gaussian curve is fitted to the sampled differences, using a form of hill climbing to find the peak of the curve, see Figure 8.8.

iii) Another method which is used is the convolution of the image with a Laplacian-of-Gaussian, described by Huertus (1986). The edges are defined by zero crossings of the resulting curves. Drawbacks of the approach include the difficulty of chosing an appropriate width for the curve to obtain zero crossings and a heavy demand on computing time. The concept is illustrated in Figure 8.9. A similar form of edge detection has been implemented by El-Hakim (1989).

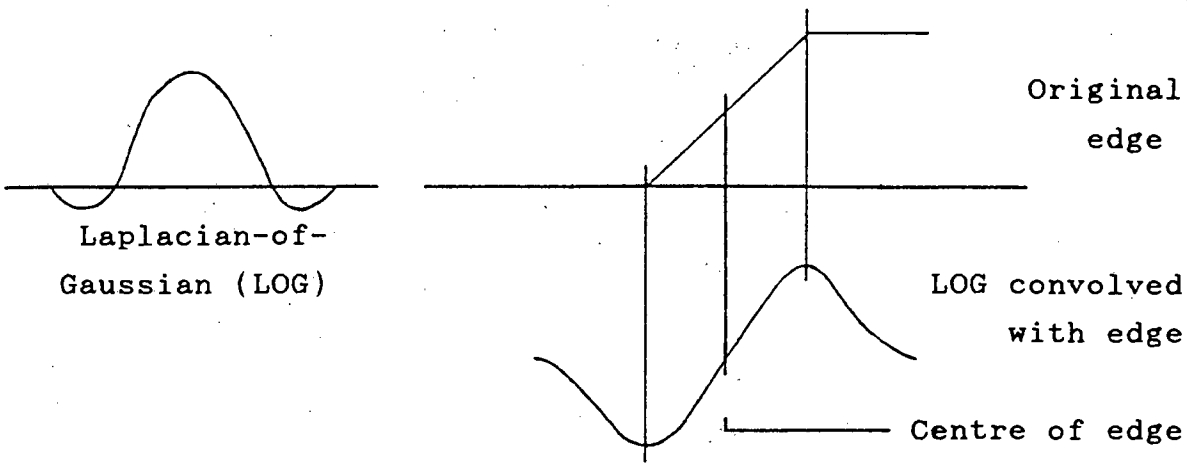

Figure 8.9 The Laplacian-of-Gaussian convolution

THE METHODS IMPLEMENTED

Many other edge detection methods exist. The criteria for the edge detection algorithms chosen include their accuracy, simplicity of implementation and speed of operation.

The methods that were implemented are:

- thresholding
- interpolation
- moment preservation

8.4.1.1 Thresholding the Image to Evaluate the Target Edges

This algorithm is the simplest to implement. The image window is scanned first row by row, with two pointers for each row indicating firstly the pixel before which the one dimensional curve passes up through the threshold level and then indicating the pixel after which the profile passed down through the threshold level. The resulting array is one of the row values in relation to an integer column-up-pixel and integer column-down-pixel as the profile passes up and down through the threshold level respectively. A similar array is obtained for all columns, using a column by column scan of the image. Figure 8.10a and Figure 8.10b illustrates an example of a target window together with the

associated row and column arrays for a threshold level of 45 in the target window.

	1	2	3	4	5
1	5	6	7	4	2
2	10	50	42	40	11
3	9	100	200	40	8
4	7	40	190	50	9
5	6	7	4	9	10

Figure 8.10a An example of a target window with a threshold level = 45

row	column up	column down
1	0	0
2	1	3
3	1	4
4	2	5
5	0	0

column	row up	row down
1	0	0
2	1	4
3	2	5
4	3	5
5	0	0

Figure 8.10b The row and column threshold arrays associated with the target window (in Figure 8.10a)

The thresholding algorithm is a crude approximation to the edge of the target since an integer edge is specified surrounding the target with a possible error of up to one pixel. Nevertheless it is useful as a 'worst case' edge detection algorithm, with which to compare the other edge detection algorithms.

8.4.1.2 Interpolating the Image for Edge Determination

The implementation of the interpolation function is similar to that of the threshold edge detection algorithm.

The image is again scanned row by row, searching for the pixel which passes up through the threshold level. That pixel and the pixel before it are used to evaluate at what point the profile passes through the threshold level, by interpolating between both pixels' grey scales, see Figure 8.11 .

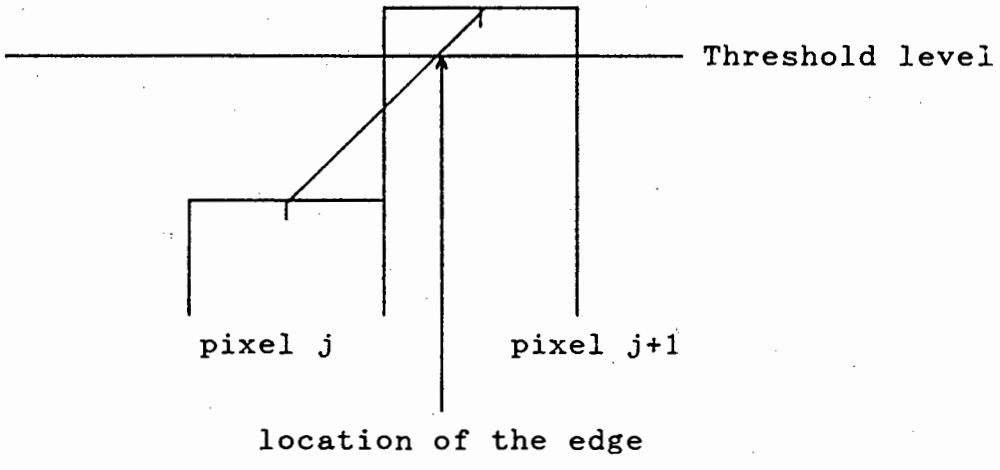

Figure 8.11 Edge determination by interpolation

If the grey scale of column #(j) is given by 'pixel(j)' and that of column #(j + 1) given by 'pixel(j + 1)', the 'column' location at which the threshold passes up through the threshold level is given by:

$$\text{interpolated edge location} = (j) + \frac{\text{Threshold} - \text{pixel}(j)}{\text{pixel}(j+1) - \text{pixel}(j)}$$

Similarly, the pixel before which the grey scale passes down through the threshold level and the following pixel are used to evaluate the second sub-pixel edge location of that column.

Two arrays are obtained in a similar manner to the threshold edge detection algorithm, indicating row by row and column by column, the sub-pixel edge location both before and after the target.

8.4.1.3 Using Moment Preserving to Indicate the Edge on a Target

In order to determine the edge to a set of data points, moment preserving (referred to as the 'Mikhail' method) is used as a criterion of best fit, Mikhail (1984). A simplified system is initially considered, where the data is modelled to an ideal edge, see Figure 8.12 .

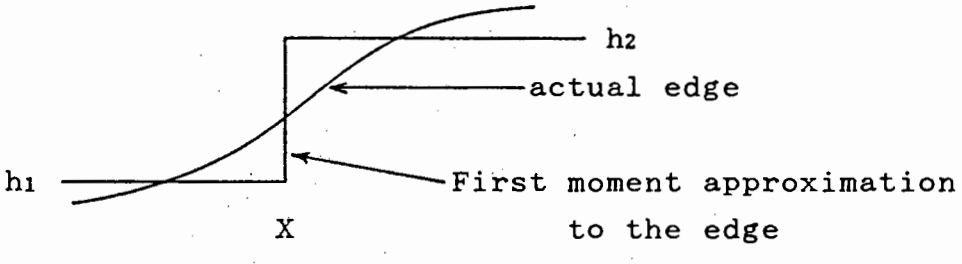

Figure 8.12 Data fitted to an ideal edge

The three unknowns are the base level h_1, the location of the step X, and the level of the step h_2. Rather than solving for the step location X, the edge location is defined as k + 0.5, where k is the number of samples below the edge. The first three moments m_1, m_2 and m_3 are

evaluated to solve for the 3 unknowns (h_1, h_2 and X) with reference to the ideal edge.

The above equations may be solved using:

$$m_j = {}^1/_n \sum_{i=1}^{n} l_i{}^j$$

$$k = \frac{n}{2} \left[1 - \frac{c}{\sqrt{(4+c^2)}} \right]$$

$$c = \frac{3\, m_1\, m_2 - m_3 - 2(m_1)^3}{\sigma^3}$$

where - l_i represents the row of pixel grey values
- c represents the skewness of the data
- $\sigma^2 = m_2 - m_1{}^2$

The algorithm has been extended to cope with rising and falling edges of a row. The new formulation requires the evaluation of four moments (m_1, m_2, m_3 and m_{12}) to find the four unknowns (h_1, h_2, X_1, and X_2), see Figure 8.13 .

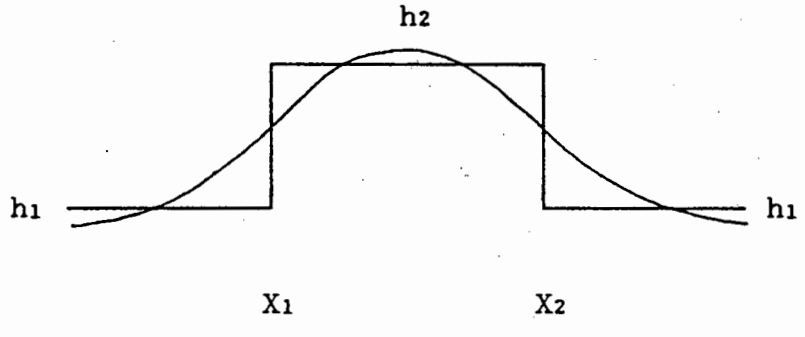

Figure 8.13 Fitting a curve to an ideal rising step and falling step

Regions of poor edge detection are governed by the type and rate of falloff. For most of the edges of targets evaluated

in this thesis, especially the edge to the central rows and columns of a target, the edges rise from background to saturation level within 2 to 3 pixels, see Figure 8.14 and are accurately evaluated by moment preservation methods. The edges on the side of the target are not so well defined and the edge location is consequently not as certain.

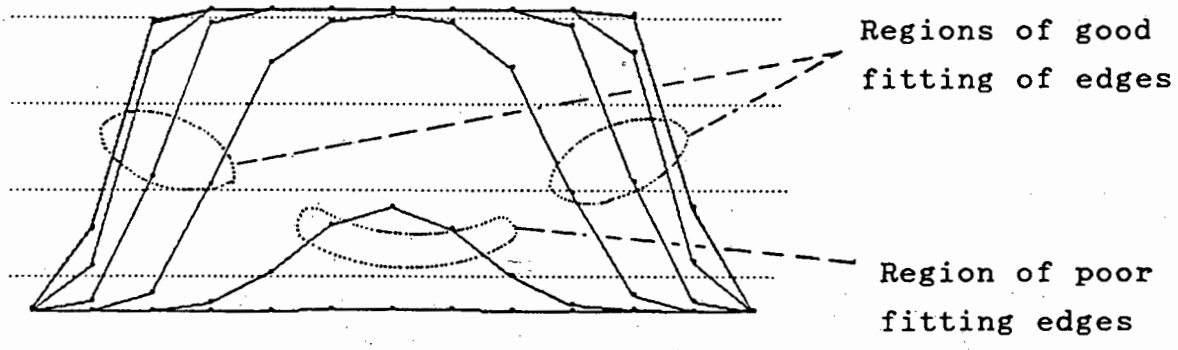

Figure 8.14 Regions of good and bad edge detection

The first and last rows and columns are removed to obtain a more accurate resolution for edge detection around the perimeter of the target. Similar elimination of edge points for interpolation and threshold edge detection is motivated for the same reason.

8.4.2 Fitting Curves to Edge Data for Symmetrical Targets

8.4.2.1 Intersection of Straight Lines

Zhou (1986) proposed an algorithm where, given the edge location of all rows of an ellipsoidal target, the centre point between edge points of all these rows form a line passing through the centre of the target. Similarly the centrepoint between edges of all columns form a line passing through the target centre. The two lines (forming the diameters), intersect at the centre of the target. The principle is illustrated in Figure 8.15 .

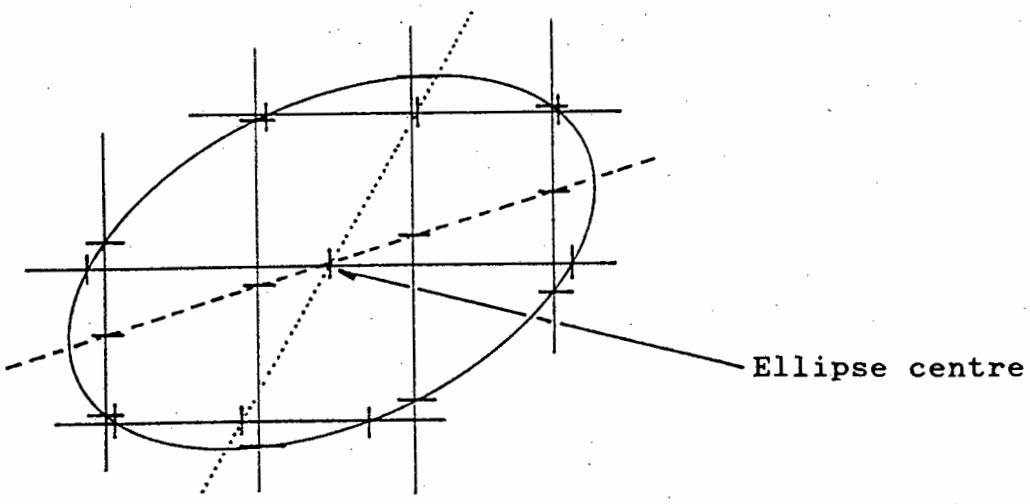

Figure 8.15 Intersection of lines passing through the middle of rows and columns of an ellipse

8.4.2.2 Using Least Squares to Solve for Bestfit Ellipse

The form of the ellipse equation is:

$ax^2 + 2bxy + cy^2 + dx + ey + 1 = 0$,

an equation with five unknown parameters (a,b,c,d,e) and two observables (x,y).

The equation is solved using least squares to evaluate the unknown parameters. The parameters are updated with the residual correction. The least squares adjustment is repeated until all the residual vector corrections are reduced to below a suitable level.

The centre location of the ellipse is given by:

$$y = \frac{\frac{b*d}{2*a} - \frac{e}{2}}{c - b^2/a}$$

$$x = \frac{-e/2 - c*y}{b}$$

8.4.2.3 Using Least Squares to Solve for a Bestfitting Circle

The circle was implemented as a target shape because of the similarity of the circle to an ellipse. Circles are symmetrical and a 'first order approximation' to an ellipse, thus the bestfitting circle on an elliptical target should have the same centre as that of the ellipse, see Figure 8.16

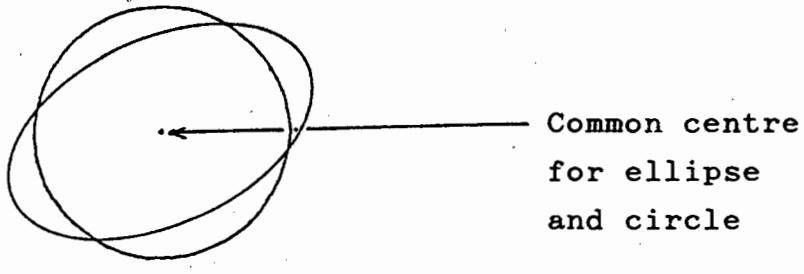

Figure 8.16 Using a circle to solve for ellipse centre

The formulation for the circle is:

$$(x_i - x_o)^2 + (y_i - y_o)^2 - r_o^2 = 0$$

where - x_o, y_o is the circle centre
- r_o is the circle radius
- x_i, y_i are the edge observations.

8.4.3 Fitting Curves to Edge Points to Recognise Partially Occluded Targets

Targets seldom form perfectly symmetric ellipses in the image.

Some of the influences resulting in targets appearing non-symmetrical within the image are:

i) shadows projected by other targets or framework on the target
ii) uneven low intensity lighting
iii) poorly fabricated targets
iv) wires supporting other targets between the target and the camera may obscure the target.

A wire could have the effect of cutting a target in half. The 'two' targets could conceivably be rejected on the basis that they are too close to one another. A more difficult task is to either identify and then reject the partially obscured target, or have an algorithm that determines the target centre, rejecting the effect of those pixels which are distorted from their expected values.

A method whereby an object is found from a conglomeration of parts has been researched by Turney (1985), where the position of best-match between a template of the expected object and the real image is obtained. Use is made of the Hough Transform which has been modified from traditionally identifying collinear subsets of points to this application, where it is used to identify arbitrary sets of points.

A validity check was performed by Wong (1986) on all control points in the image, using the criteria of shape, size and position of the points. Since the control targets are circular in shape, the ratio of the second moments about the two principal axes is expected to be '1'. Shapes with a ratio greater than two were rejected as control points.

Two methods have been implemented to reduce the error on partially occluded targets. The first method uses least squares to fit the ellipse and then uses gross error detection to reduce the effect of those edge points which have the largest associated residuals. Another method implemented is a variation on the Hough Transform where lines are found to pass through the target centre.

An image with synthetic targets was made, where the targets each had a Gaussian chunk taken out of their side to resemble partial occlusion (see Figure 7.14). All the algorithms were run through the image to check their ability to find the correct centres of the partially occluded objects and to determine whether the two algorithms designed to compensate for partial occlusion worked as expected.

8.4.3.1 Gross Error Detection as Used on Least Squares Bestfit Ellipse

In order to remove or reduce the effect of the gross errors in edge determination from the image, a data cleaning process may be applied, since undetected errors will distort the solution. The undetected gross errors would distort the solution vector $\underline{x}$, leading to a misrepresentation of the target location.

The rejection of observation model that has been implemented is the variance *inflation* method. Using this model, the residuals $\underline{v}$ of the adjustment which exceed a given threshold

are used to trigger a reduction in weighting of the observation. The effect of the modified weighting is to reduce the contributions of their associated observations to have less influence on the adjustment result. The Danish method is implemented, Rüther (Surveying Course Notes).

In the Danish method, those residuals y which exceed a given threshold value 'c' have their influence on the adjustment reduced by mutiplying the observation's weight by a reducing factor F.
The reducing factor F_i for each observation is found as

$$F_i = \begin{cases} 1 & \text{if } |V_i| \times P_i/\sigma_o < c \quad \text{i.e. an uncontaminated observation} \\ \exp(-|V_i| \times P_i/(\sigma_o c)) & \text{for all other cases} \end{cases}$$

where - 'c' is a constant chosen to fall between 2 and 3.

The weighting for the observations are then altered by:

$$P_i = P_i \times F_i$$

The least squares adjustment, followed by residual assessment and the adjustment, is repeated until there is no longer any significant change in all the residual values.

8.4.3.2 The Modified Hough Algorithm

The Hough Transform was developed and patented by Hough in 1962 and popularised by Duda (1977). It deals with recognising specific structural relationships between pixels in an image. The Hough Transform solves curve fitting by considering the parameters of the curve in parameter space instead of the traditional use of the x-y plane. The

principle of the Hough Transform, in an application to detect straight lines, is outlined in Appendix F.

Solving the ellipse equation using the Hough transform can be accomplished by using a 5 dimensional parameters space, with an 'accumulator' of the form A(i, j, k, l, m), corresponding to the ellipse centre (x_o, y_o) , major and minor ellipse radii and the ellipse orientation. The procedure is to increment four of the parameter values, solving for fifth parameter and then updating the accumulator corresponding to the 5 parameters $c_1, c_2, c_3, c_4, 0$.

There are two primary drawbacks to the Hough transform method, limiting the usefulness of the method:

i) The accuracy of the transform is limited to the quantization k of the parameter plane. The method is dependent on finding the pixel in the parameter plane of the highest value i.e. that with the majority of lines (in the z parameter plane) thus automatically placing a top limit on the maximum level of quantization, since it is a prerequisite that many of the valid lines must pass through the centre pixel.

ii) The complexity increases with an increasing number of parameters, placing a large demand on computer storage and the time necessary to perform the Hough transform.

Ballard (1981) recommends the additional use of the slope at the point selected on the edge to reduce the number of free parameters and thus computing time, where the slope is the tangent to the curve at the point chosen.

A different approach is used by Muammar (1989), involving a three stage extraction of the ellipse parameters of a partially occluded ellipse. The first stage involves finding the centre of the ellipse. The second stage involves evaluating the ellipse orientation and in the

third stage, the major and minor ellipse radii are found. For our purposes, the first stage of finding the ellipse centre is sufficient. (The second and third stages may however prove useful to evaluate the appropriateness/ validity of the target as a target ellipse.)

To solve the first stage, two points $P_1(x_1, y_1)$ and $P_2(x_2, y_2)$ lying on the perimeter of the ellipse are considered. The tangents to the points P_1 and P_2 intersect at point $T(t_x, t_y)$ and the midpoint of the line joining P_1 and P_2 is $M(m_x, m_y)$. A line passing through the points T and M, passes through the centre of the ellipse, see Figure 8.17 .

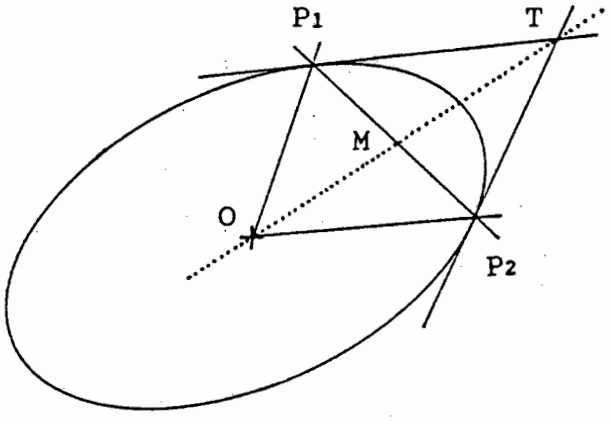

Figure 8.17 An ellipse showing the intersecting tangent points and midpoint m

The equation for the line intersecting with the ellipse centre (TMO) is given by $y = cx + d$,

where $$-\ c = \frac{t_y - m_y}{t_x - m_x}$$

$$-\ d = m_y - cm_x$$

For point T:

$$t_x = \frac{y_1 - y_2 - g_2 x_2}{g_2 - g_1}$$

$$t_y = \frac{y_1 g_2 - y_2 g_1 + g_2 g_1 (x_2 - x_1)}{g_2 - g_1}$$

and for point M:

$$m_x = \frac{x_1 + x_2}{2} \quad , \qquad m_y = \frac{y_1 + y_2}{2}$$

where - g_1 and g_2 are the slopes for points P_1 and P_2 respectively.

Lines formed from all pairs of points on the same ellipse will intersect at the point $O(x_0, y_0)$. Instead of placing the lines going through the ellipse centre into a space array, as originally done by Hough (this time an array in the x-y co-ordinate space), intersections of lines with all other lines are placed in an array and the mean of these intersections relates to the ellipse centre. Once an initial estimate is obtained, the poor intersections are eliminated, and the target centre is re-evaluated. Points P_1 and P_2 are chosen at an angular spread of approximately 90° apart for the angle formed by P_1-O-P_2 and intersections are also obtained from diameter lines perpendicular to one another.

8.5 SUMMARY

The algorithms implemented are listed in table 8.1 .

The program described in this chapter involves reading in three images sequentially. For each image, 32 target centring algorithms are used to find all the target centres within the image. The target centres for each algorithm (and each image) are stored to file.

The image target centres are to be compared with their actual centres in Chapter 9 to evaluate algorithm precision.

			ALGORITHM NUMBER																													
			1	2	3	4	5	6	7	8	9	10	11	12	13	14	15	16	17	18	19	20	21	22	23	24	25	26	27	28	29	30	31	32
Area Based Algorithm	———	C.G.																												o	o	o		
Perimeter Edge Based Algorithm	Find Edge Points	Threshold	o			o			o			o			o			o			o			o			o							
		Interpolation		o			o			o			o			o			o			o			o			o						
		Mikhail			o			o			o			o			o			o			o			o			o				o	o
	Fit Curve to Edge Points	Line Intersect	o	o	o							o	o	o							o	o	o											
		Bestfit Ellipse				o	o	o							o	o	o							o	o	o								
		Bestfit Circle							o	o	o							o	o	o							o	o	o					
		Gross Error																															o	
		Modified Hough																																o
	Magnification of Target Window	x1	o	o	o	o	o	o	o	o	o																			o	o		o	o
		x2										o	o	o	o	o	o	o	o	o												o		
		x3																			o	o	o	o	o	o	o	o	o					

Table 8.1 Summary of Target Centring Algorithms

CHAPTER 9

9.0 RESULTS OF THE PRECISION OF CENTRING ALGORITHMS

9.1 RUNNING THE ALGORITHMS ON THE VARIOUS IMAGES

The target centring algorithms that were implemented were each tested on three images, having targets with known centre co-ordinates:

- IMAGE 1 : An image with nine synthetic targets
- IMAGE 2 : An image with nine synthetic targets - each target having a blemish
- IMAGE 3 : A real image of a control frame snapped with the PHOENICS system.

For each image, the deviation of all the targets of each target centring algorithm from the known centre is used as a measure of the precision of the algorithm. The results of the centre determination for each image are given below, followed by a general assessment of the features of selected algorithms.

9.1.1 Image of Nine 'Perfect' Synthetic Targets

The purpose of the synthetic target images is to test the algorithms on as perfect a digitised ellipse as possible, to evaluate the shortcomings of the algorithms and to determine their maximal possible accuracy. The accuracy of each algorithm together with the time taken by the algorithm are illustrated in Figure 9.1 .

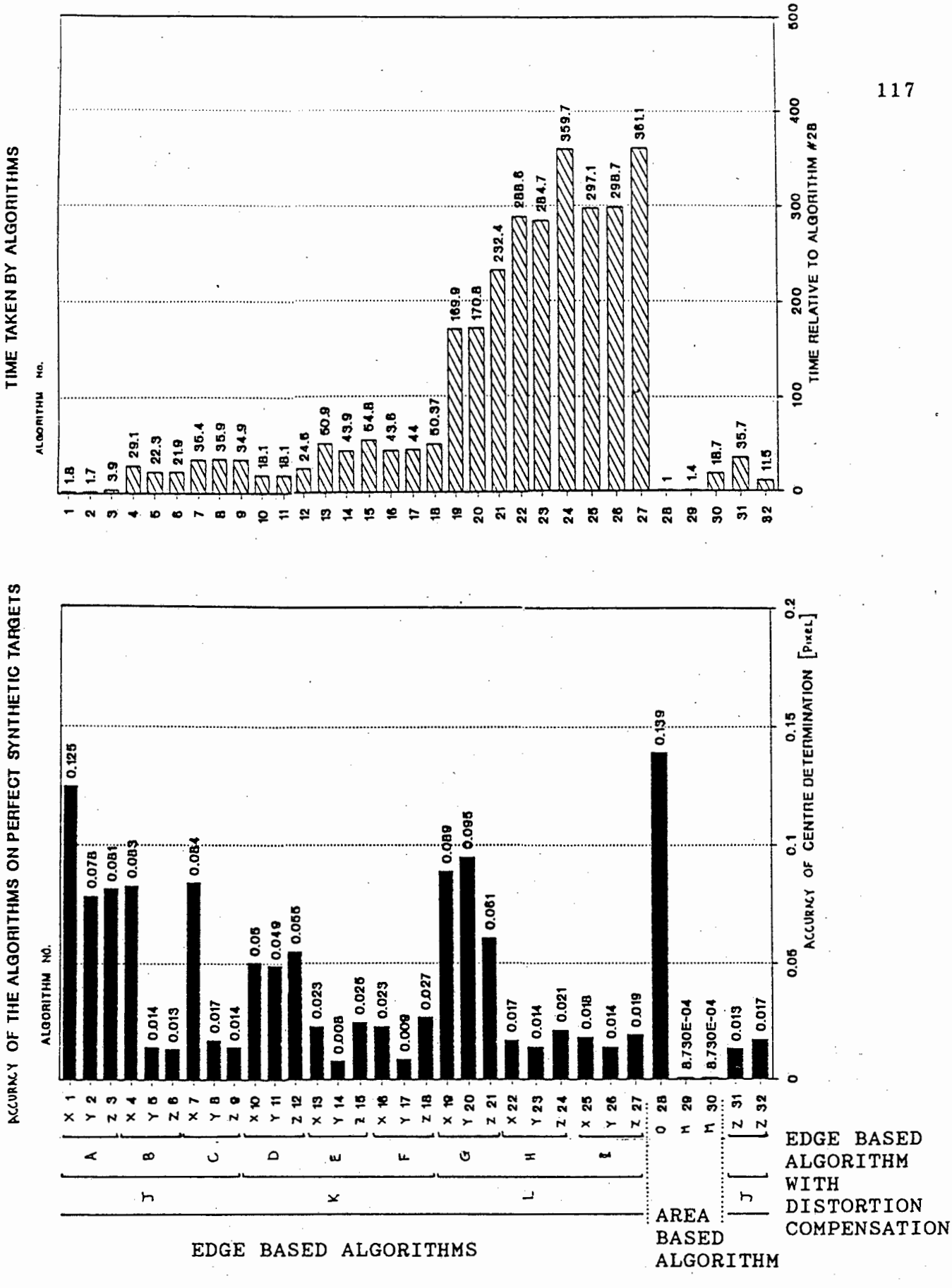

Figure 9.1 Accuracy of and relative time taken by each algorithm on an image containing synthetic targets

From the graph of algorithm accuracy :

9.1.1.1 For ALL Algorithms

i) The most accurate centre determination is achieved using the centre of gravity algorithm, where the threshold level subtracted from pixel grey values is set precisely at the continuous background level, see Figure 9.1: Region M, hereafter referred to as [M].

ii) The least precise algorithm for centre determination is the centre of gravity algorithm, where no threshold level is subtracted from the pixel grey values [O].

iii) (The magnification of the target window has no influence on the precision of the centre of gravity algorithm [M].)

9.1.1.2 For the Edge Based Algorithms Without Distortion Correction (Algorithms #1,..#27)

REGIONS J,K,L refer to magnification of the target window by 'x1', x2, and x4 respectively

REGIONS A,D,G refer to the intersection algorithm (worst method, used as a benchmark)

B,E,H refer to the bestfitting ellipse algorithm

C,F,I refer to the bestfitting circle algorithm

REGIONS X use edge detection by thresholding (worst method, used as a benchmark)

Y use edge detection by interpolation

Z use edge detection by moment preservation (Mikhail)

i) Using the data from Figure 9.1, a comparison of the effect of magnification by 'x1', x2 and x4 can be obtained by overlaying all combinations of edge detection and standard bestfitting algorithms at different magnifications, see Figure 9.2
   - algorithms 1..9 have a magnification of 'x1'
   - algorithms 10..18 are algorithms 1..9 with magnification of x2 respectively
   - algorithms 19..27 are algorithms 1..9 with magnification of x4 respectively

   Figure 9.2 indicates that magnifying the target window by x2 gives the most precise result over all edge based algorithms [Algorithm 14].

   Magnification has an overall effect of enhancing the accuracy of the edge detection algorithms using thresholding [X] and interpolation [Y], and degrading the performance of moment preservation [Z].

   There is little benefit to the implementation of the magnification by x4 algorithm (except for the improvement of centre determination for the threshold edge based algorithm, which has poor centring ability because of its inherent simplicity). In addition, the magnification by x4 algorithm made large demands on computing time and memory.

ii) Figure 9.1 indicates that with a magnification of x1, the best centre results are obtained using the interpolation and Mikhail edge detection algorithms, which both perform with the same degree of accuracy.

Figure 9.2 Effect of Magnification on Edge Based Algorithms

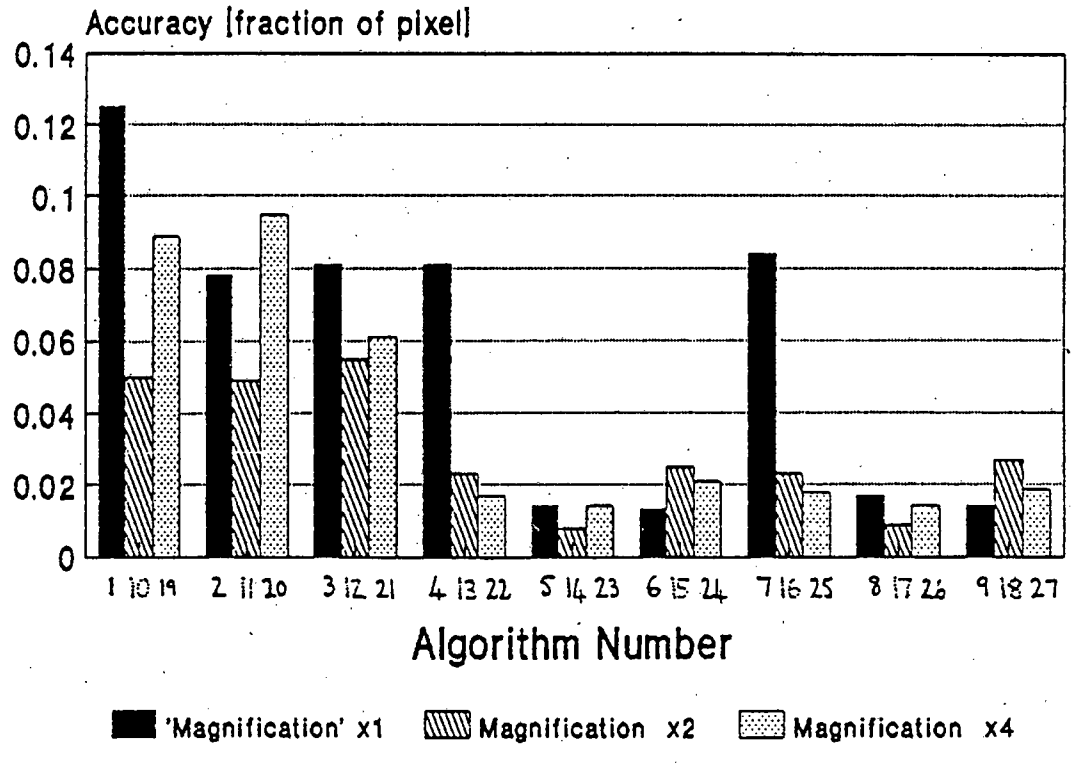

Accuracy measured in fraction of a pixel

When magnified by x2 however, the interpolation [Y] algorithm gives enhanced results and the Mikhail [Z] edge detection algorithm gives worse results.

iii) The most accurate results for bestfitting algorithms are obtained using the bestfitting ellipse and bestfitting circle. These algorithms work well with both interpolation [Y] and Mikhail [Z] at a magnification of 'x1', but at a magnification of x2 only interpolation produces improved results.

iv) Overall, the best centring ability is obtained using the bestfitting ellipse and bestfitting circle algorithms with an interpolation [Y] edge detection function and a magnification of x2.

9.1.1.3 Edge Based Algorithms with Correction for Target Occlusion

These edge based algorithms were implemented only with a magnification of 'x1' window.

Both the Hough and bestfitting ellipse with gross error detection [N] give results approximating those obtained with a bestfitting ellipse and bestfitting circle at a magnification of 'x1'.

9.1.2 Image of 9 Synthetic Ellipses with Blemishes (Shadows)

This image was included in the test to check the robustness of the algorithms to blemishes on the target, in particular, the Hough transform and the bestfitting ellipse with gross error detection, see Figure 9.3 .

Fig 9.3 Accuracy of Algorithms on an Image of Synthetic Targets with a Blemish

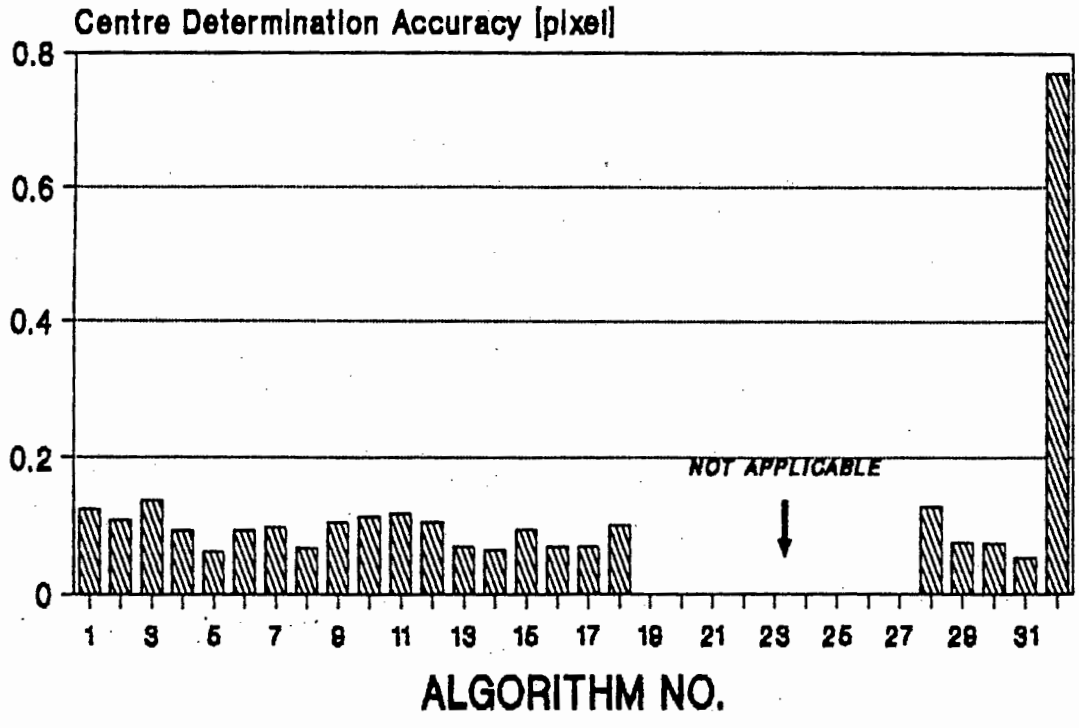

Fig 9.4 Accuracy of Algorithms on an Image of Real Targets

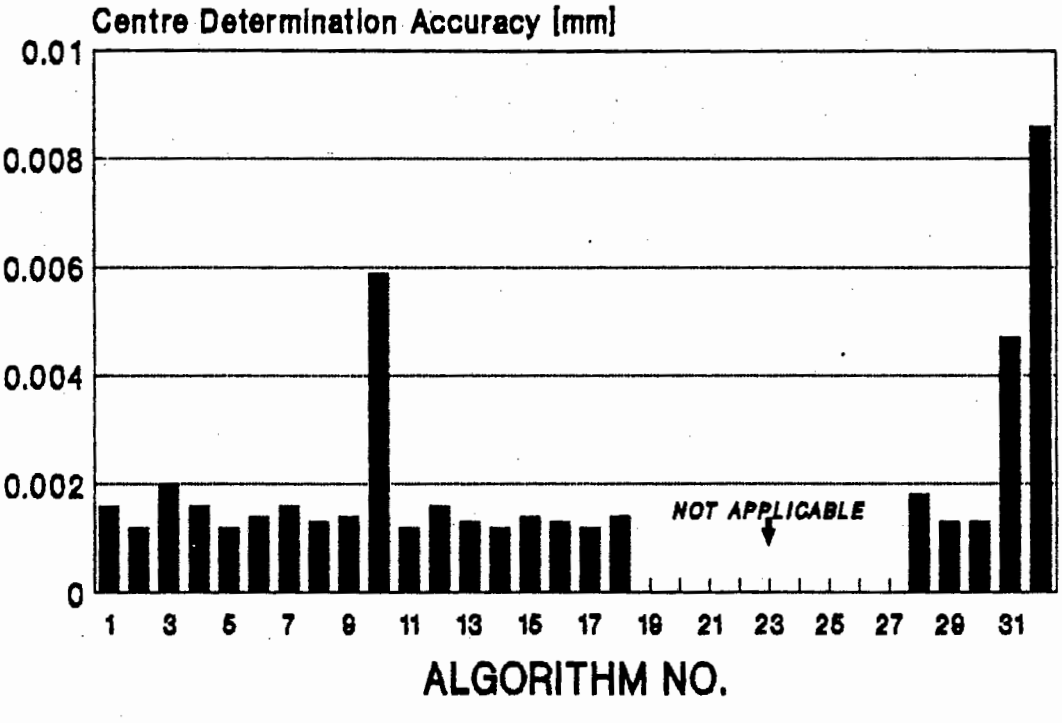

For all algorithms, the results indicate that:

- The best centre determination is achieved using the bestfitting ellipse with gross error detection.

- The worst accuracy is obtained using the Hough transform.

- Magnification of the target window does not improve the results.

- The best edge detection algorithm is interpolation, followed by thresholding.

- The worst edge detection algorithm is Mikhail.

- Of the standard bestfitting algorithms, the bestfitting ellipse gave the most accurate results.

- The majority of algorithms locate target centres to within $^1/_{10}$ of a pixel from the target centre co-ordinate specified by the parameter listing.

9.1.3 Image of Real Targets

An image was taken of real targets. The purpose of measuring the accuracy of the algorithms on these targets is to investigate the accuracy of the centring algorithms in the presence of noise. The results, illustrated in Figure 9.4 , indicate that:

- The best edge detection algorithm is interpolation.

- The least accurate algorithms are the Hough transform and bestfitting ellipse with gross error detection.

- That magnification of the target window does not improve centring accuracy.

- The majority of the algorithms give centre co-ordinates with a common standard deviation of $^{17\mu m}/_{1.7\mu m}$ [pixel width/pixel accuracy] = $^{1}/_{10}$ of a pixel. They are the:

  - o area based algorithm:
    - C.G. with threshold subtracted from grey values
  - o edge based algorithm (using interpolation for edge detection, with a magnification of 'x1' or x2):
    - bestfitting line-intersection
    - bestfitting ellipse
    - bestfitting circle

Note The control frame was surveyed to an equivalent precision of approximately $^{1}/_{10}$ pixel in the image plane, [6.3]. This is the same order of precision with which the target centres are evaluated, using the target centring algorithms. The precision of the target centres in the image (as found by target centring algorithms) is measured by correlating them with the known (surveyed) target 3-D co-ordinates. It is thus not certain whether the precision of the target centring algorithms is limited by noisy targets or the accuracy with which the control frame target co-ordinates were surveyed. In both cases however, there is sufficient difference in the results in Figure 9.4 to allow for comparative assessment of the algorithm components.

The accuracy of the various algorithms are summarised in table 9.1

Table 9.1 Summary of Algorithm accuracy on the three test images

ALGORITHM NUMBER	ACCURACY [pixel] IMAGE 1	ACCURACY [pixel] IMAGE 2	ACCURACY [mm] IMAGE 3	ACCURACY [pixel] IMAGE 3
1	0.12500	0.12500	0.00160	0.09412
2	0.07800	0.11000	0.00120	0.07059
3	0.08100	0.13800	0.00200	0.11765
4	0.08300	0.09400	0.00160	0.09412
5	0.01400	0.06300	0.00120	0.07059
6	0.01300	0.09300	0.00140	0.08235
7	0.08400	0.09900	0.00160	0.09412
8	0.01700	0.06800	0.00130	0.07647
9	0.01400	0.10600	0.00140	0.08235
10	0.05000	0.11400	0.00590	0.34706
11	0.04900	0.11900	0.00120	0.07059
12	0.05500	0.10700	0.00160	0.09412
13	0.02300	0.06900	0.00130	0.07647
14	0.00800	0.06500	0.00120	0.07059
15	0.02500	0.09500	0.00140	0.08235
16	0.02300	0.07000	0.00130	0.07647
17	0.00900	0.06900	0.00120	0.07059
18	0.02700	0.10200	0.00140	0.08235
19	0.08900			
20	0.09500			
21	0.06100			
22	0.01700			
23	0.01400			
24	0.02100			
25	0.01800			
26	0.01400			
27	0.01900			
28	0.13900	0.12800	0.00180	0.10588
29	0.00087	0.07500	0.00130	0.07647
30	0.00087	0.07500	0.00130	0.07647
31	0.01300	0.05300	0.00470	0.27647
32	0.01700	0.07700	0.00860	0.50588

9.2 ASSESSING SELECTED ALGORITHMS

9.2.1 Results of the Centre of Gravity Algorithm

The effects of the variation of the threshold level (subtracted from pixel grey values) detailed above [9.1.1.1], is best illustrated with a curve indicating the accuracy of the centre of gravity algorithm versus the entire range of threshold levels subtracted from the pixel grey scale value of synthetic symmetric targets, see Figure 9.5a . (In the case of the threshold level being greater than the grey level, the new grey level is set to zero.)

From Figure 9.5a, the following observations may be made. The centre determination:

i) is poor (accuracy of $\pm$ $^1/_{10}$ pixel) for threshold levels chosen below the background grey level
ii) is best for the threshold in a band above the background level (accuracy of centre between $^1/_{1000}$ and $^1/_{200}$ of a pixel)
iii) gets progressively worse as the threshold level approaches a grey level of saturation ($^1/_{150}$ to $^1/_{15}$ of a pixel centring accuracy)

Thus the choice of a threshold level of 'just above' the background level in a target window is essential for accurate performance of the centre of gravity algorithm, see Figure 9.5b .

9.2.2 Edge Detection: Interpolation and Mikhail

The interpolation algorithm works better than moment preservation edge detection in most of the test cases. The falloff from saturation to background for most targets in the images considered, occurred within two to three pixels, resulting in a 'smoothed' falloff.

Accuracy of C.G. Algorithm versus Threshold level subtracted

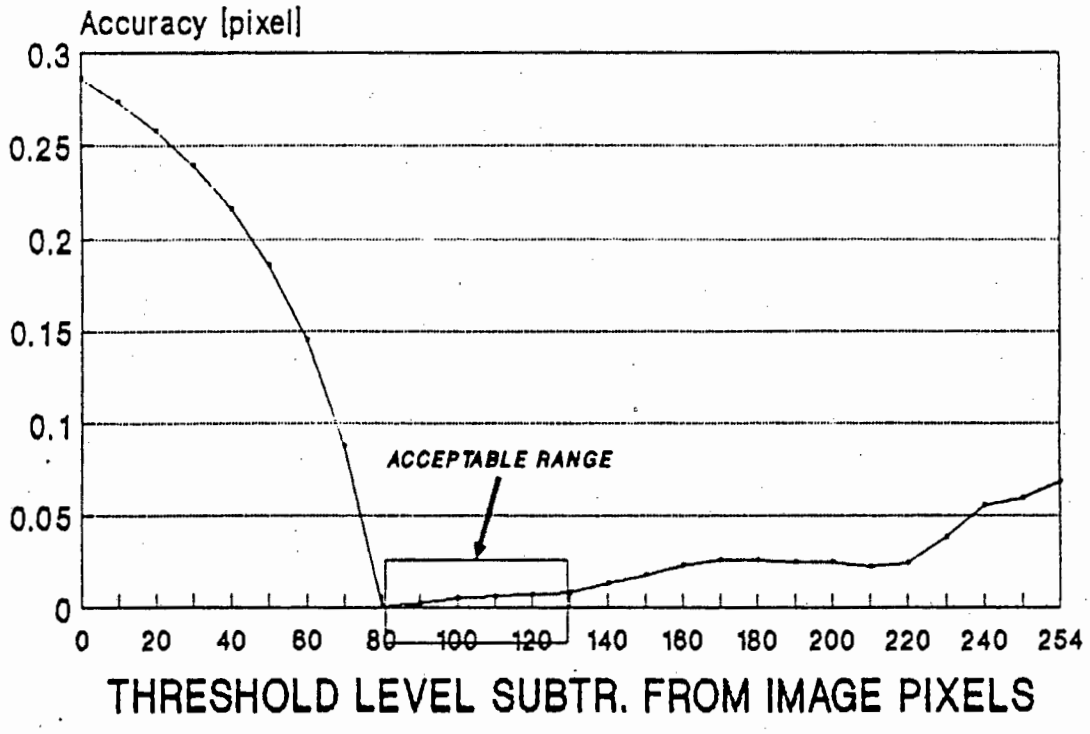

Figure 9.5a Accuracy of centre of gravity versus the threshold level subtracted from the grey scale pixel value

Typical Cross-Section Through a Target Indicating Best Threshold for C.G. Alg.

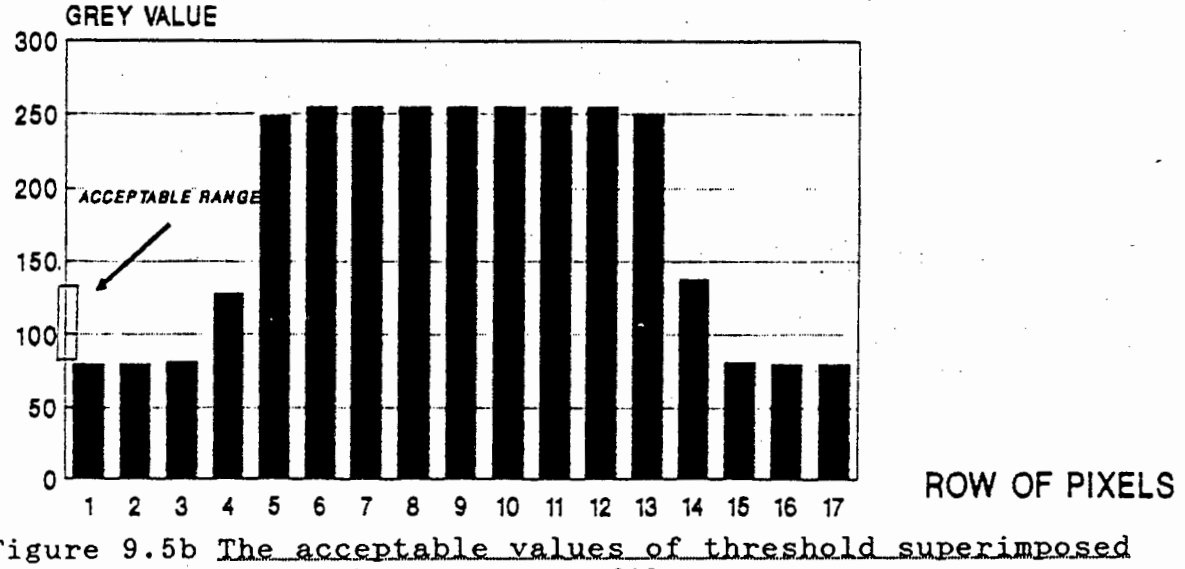

Figure 9.5b The acceptable values of threshold superimposed on the target profile

The interpolation edge detection algorithms work best with images with a gradual falloff, (since it approximates/ follows the slope of the falloff from saturation to background level) and does not work well for targets with a fast falloff, see Figure 9.6 .

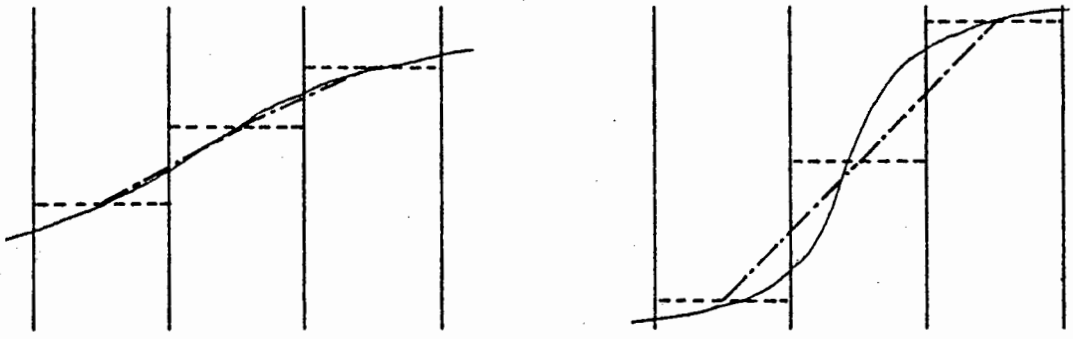

Figure 9.6 Using interpolation to follow curves

In the moment preservation algorithm, the edge is obtained by fitting a step to the curve. Best results are expected for images with a 'sharp' falloff from saturation to background levels, see Figure 9.7 . The moment preservation algorithm is the more robust of the two edge detection algorithms since it does not require choosing a threshold level.

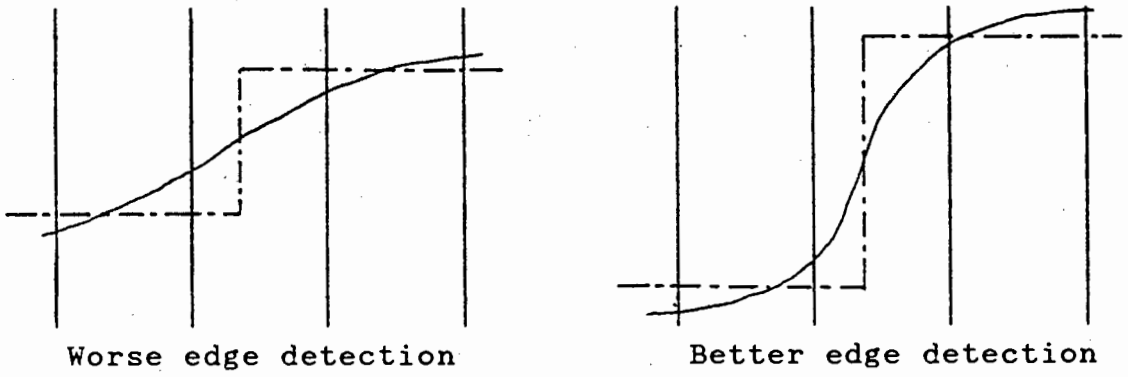

Figure 9.7 Using Moment preservation to follow curves

It is thus best to have a priori knowledge of the imaging system (the expected sharpness of falloff) when selecting the edge detection algorithm to implement.

9.2.3 Accuracy of Intersecting Diameters Algorithm

The method detailed requires the intersection of lines to define the centre of the ellipse. The method works best for circles and ellipses with major and minor axes parallel to the x and y axes, where the intersecting lines are perpendicular to one another.

The intersecting lines become more and more acute as the ellipse is rotated from 0° to 45°, see Figure 9.8 .

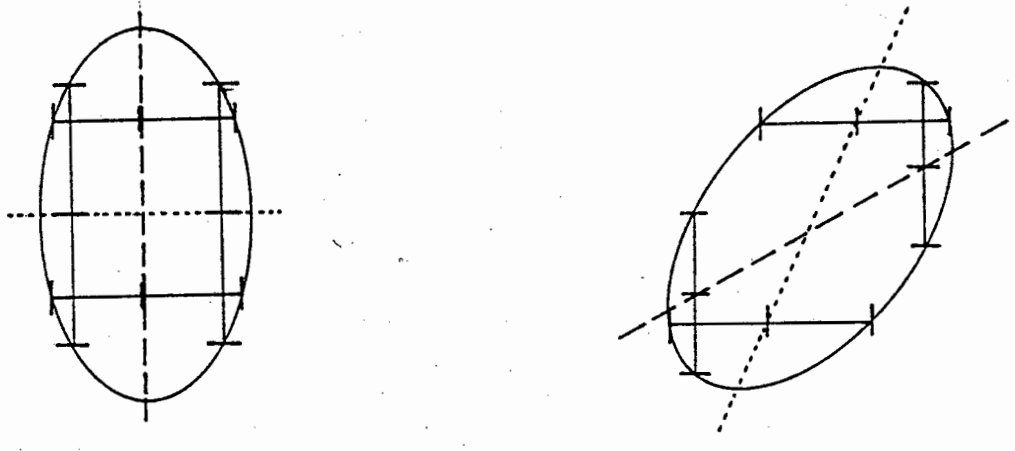

Figure 9.8 Effect of rotation of the ellipse on intersecting lines accuracy

Thus, the ellipses may be seen to have 'more precise' regions of rotation for major and minor radii as indicated in Figure 9.9 below.

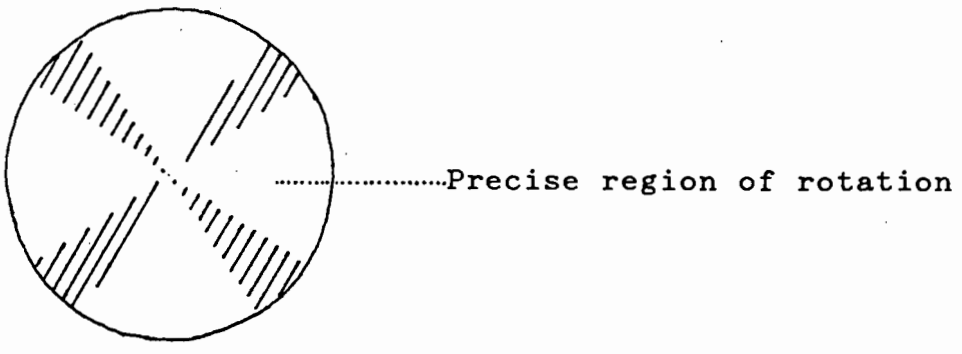

Figure 9.9 *Regions* of rotation for an ellipse for the intersecting centrelines algorithm

The size of the ellipse is also a critical factor to the accuracy of the algorithm, Zhou (1988), where best results are obtained for ellipses in the range of 20x20 to 100x100 pixels, and specifically a minimum of 10x10 pixels. The average size of synthetic and real target is around 10x10 pixels in size, thus corresponding to lowest performance ability of this algorithm .

9.2.4 The Hough Transform

Difficulty experienced with the modified Hough transform lies in the inaccuracy of its centring ability, since the 'diameter' lines generated by the algorithm do not pass through the centre, leading to a cluster/spread of diameter line intersecting points.

Removing the intersecting points furthest from the cluster centre, as (conceptually) recommended by Hough, has the tendency of worsening the results, since the cluster loses its symmetry. One of the reasons attributed to the wide spread of intersections results from a *poor estimation* of

the *slope of the perimeter*. Three methods were investigated to approximate the slope of the perimeter at points along the boundary, see Figure 9.10 . They are:

i) A bestfitting straight line through the point and perimeter points either side of the point under consideration, using least squares. A variety of weightings were used, including: giving the centre point a higher weighting than the two side points; giving the side points higher weighting than the centre point; and giving all three points equal weighting.

ii) A bestfitting circle through the point under consideration and four perimeter points, two on either side of the perimeter point under consideration. The tangent of the circle in line with the perimeter point is chosen as the tangent to the ellipse.

iii) A line passing through points on either side of the point under consideration.

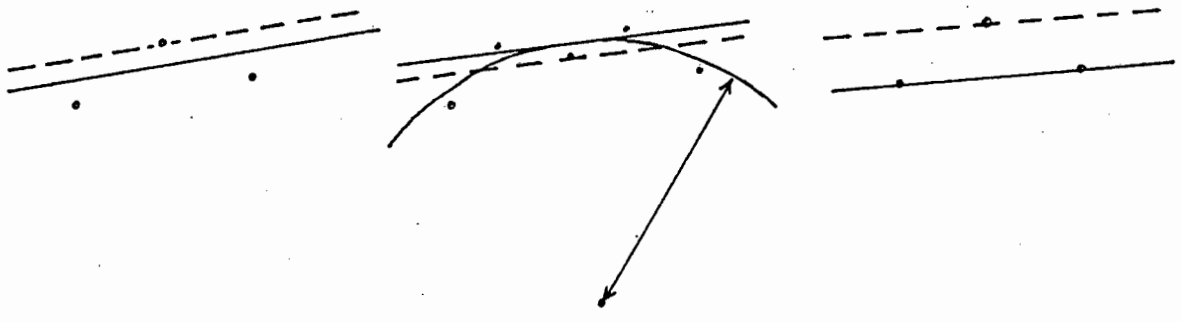

(i) bestfitting straight line (ii) bestfitting circle (iii) line through two neighbouring points

Figure 9.10 Different curves used to determine the tangent to the target perimeter points

For all the above methods, the tangent to the ellipse, associated with the point under consideration was shifted so as to pass through that point. All three methods produce a similar (wide) spread of intersection points (centres).

It was found that using least squares to fit a circle to five consecutive perimeter points, produced (circle) centrepoints to a higher precision than the those centrepoints obtained using the Hough transform. This indicates the inherent shortcoming of the Muammar approach to the Hough transform i.e. that the method is dependent on the precision of placing/locating the tangent on the perimeter, which influences the sensitivity of the resulting solution. The influence of slight variations of perimeter approximations on the 'ability' of the diameter to pass through the target centre is demonstrated in Figure 9.11.

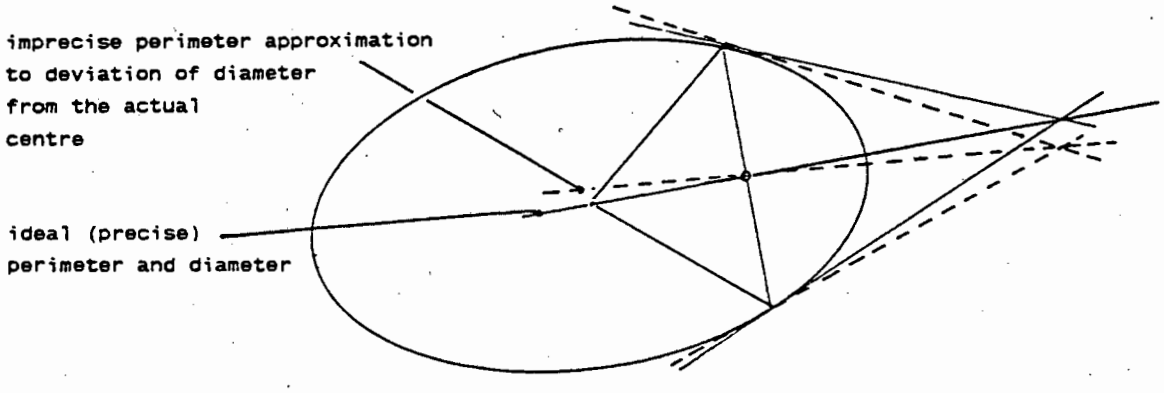

Figure 9.11 Effect of slight variations of the perimeter approximation, on the ability of the Muammar approach to generate a diameter line passing through the centre of a target.

[The third method (which was the simplest to implement) was chosen to evaluate the tangent for the analysis of the Muammar approach to the Hough Transform.]

CHAPTER 10

10.0 CONCLUSIONS AND RECOMMENDATIONS

10.1 CONCLUSIONS

From the test results obtained in the previous chapter, the following conclusions may be drawn:

i) The primary objective of the thesis was to investigate existing target centring algorithms in order to assess their relative accuracies. The comparison of algorithms was successfully accomplished using three types of images to test different aspects of the algorithms. Two target centring algorithms were found to work reliably on all three images.

ii) A program to develop synthetic targets was written to test the target centring algorithms. The program produced synthetic symmetrical targets with a choice of the falloff functions (blurring on the target perimeter). The program to develop synthetic targets, achieved accuracies of up to $^{1}/_{1000}$ of a pixel (as measured using the centre of gravity algorithm) on targets of approximately 10x10 pixels.

iii) Experience was obtained in the design, fabrication and surveying procedures of a precise control frame.

Different target materials were considered with criteria of accurate fabrication and sharp contrast with the background. Target distortion due to the thickness of targets was also considered. The best target was found to be a natural anodised aluminium circular target with a black anodised surround (on the same sheet).

The target centring algorithms were also tested on targets in a real image. The accuracies obtained were generally in the order of $^1/_{10}$ of a pixel. This is comparable to results reported by researchers using NRTP systems.

iv) There is a large difference between accuracies obtained using synthetic and real targets.

v) Because target centres are found to a high accuracy in synthetic targets, it implies that the grey values (obtained by the program to generate synthetic targets in an image) of the pixels are determined precisely. Therefore synthetic targets can be used to model noise interference and blemishes (as found in images of real targets), in a controlled manner, so as to assess the effect of noise on target centring algorithms.

vi) The modified Hough transform was implemented as an approach to compensate for slight imperfections/ blemishes on the digitised target due to the effects of noise, partial occlusion or shadows on the target. This method was found to give accurate centre determination (as good as that obtained using the bestfitting ellipse), on the ideal synthetic targets in IMAGE 1. However, this method produces the poorest centring accuracy on targets with an added blemish (IMAGE 2) and on real targets (IMAGE 3). This must be attributed to the fact that:

- The poor approximations in the cluster of 'centre points', are <u>not</u> removed when averaging to evaluate the cluster centre point since, in this approach, it was found that this reduced the centring accuracy. In the original Hough transform, the precision of partially occluded

targets was obtained by *ignoring* the effect of the poor approximations.

- The Hough transform inherently has a poor centring ability due to the quantisation of the parameter space, limiting the size of the quantisation blocks (see Appendix F) to that through which a number of intersecting diameters are bound to pass. Since the influence of noise (from real targets) degrades the evaluation of the tangent to the perimeter, leading to a deviation of the diameter from passing through the actual target centre, larger quantisation blocks are necessary to ensure that a number of diameters pass through a single quantisation block. This leads to a degradation of the centring ability, since the centring accuracy, when using the quantisation blocks specified by Hough (in the parameter space) and modified by Muammar (to the co-ordinate space), is simply:

  $$1/[\text{the quantisation level}]$$

  For this reason, the approach to find the centre of a cluster of points was adopted to improve on the accuracy obtained using the quantisation blocks.

Thus,

- Although the original Hough transform is good in concept i.e. it ignores the influence of outlying centre points in the parameter space by only considering the quantisation block with the majority of lines passing through it, it is limited by a large parameter space, 5 Dimensional for the practical implementation of finding the ellipse parameters.
- Although the Muammar approach uses the intersecting perimeter points (considering the co-ordinate space as an alternative to the parameter

space, thus quantising the co-ordinate space and considering the quantisation block with the majority of diameter points passing through it), its shortcoming is the inaccuracy to which the tangent can be evaluated.

- In attempting to circumvent the problem of limited precision, due to discrete quantisation as introduced by Hough, a method to consider the centre of a cluster of co-ordinates from the intersection of diameters (representing target centres) was developed to improve on the quantisation approach. However this method failed in that the elimination of poor intersections was found to *degrade* the centring ability of the algorithm.

vii) The target centring algorithms which were implemented consisted of a series of combinations of 'sub'-algorithms.
The best combinations were found to be:

- o The centre of gravity algorithm implemented without magnification (since magnification does not affect precision of the centre of gravity algorithm at all).
- o The bestfitting ellipse (the target is elliptical in shape), using interpolation as an edge detection algorithm (best able to follow a gradual falloff), on target windows magnified by two (improving the target resolution).

- The centre of gravity algorithm is capable of defining the centre accuracies to a high precision in images of ideal targets. However its precision is dependent on choosing an appropriate threshold level for the image.

The use of an arbitrary threshold level can cause a serious degradation of the target centring ability. The level of the threshold was investigated on an image of ideal synthetic targets. The analysis suggests that the threshold level should be set to the background level.

With the introduction of noisy targets (such as images of real targets), the accuracy of the centre of gravity algorithm diminishes drastically.

Another 'fault' with the centre of gravity algorithm is its inability to compensate for or recognise the presence of blemishes (caused by uneven lighting, a shadow or partial obscuring) on the target,

- The bestfitting ellipse has a reasonable target centring potential on images of synthetic targets ($\pm$ $^1/_{150}$ of a pixel accuracy)
  Using the standard formulation of least squares adjustment to evaluate the target centres in an image containing targets with a blemish, it locates targets to a marginally better precision than the centre of gravity algorithm. However, with the addition of gross error detection (where points with a poor fit to the ellipse perimeter are rejected), there is a considerable improvement in target centring ability over the centre of gravity algorithm.

  For an image of real (noisy) targets, the bestfitting ellipse has the same order accuracy as the C.G. algorithm, however, the performance of bestfitting ellipse with gross error detection degrades considerably. This is probably due to the contribution of noise causing random rejection of perimeter points. Thus the bestfitting ellipse with gross error detection cannot be viably implemented in a real image, without

either some form of noise removal, or an improvement of the rejection criteria.

= The use of the centre of gravity algorithm has been shown to have the greatest target centring ability (on ideal synthetic targets) and has the added advantage over all edge based algorithms of being easy to implement and fast in execution (at least twenty times faster than the quickest *viable* best fitting perimeter based algorithms).

= The bestfitting ellipse has been shown to be robust in the presence of noise, with the possibility of compensating for blemishes in an otherwise noise free environment.

10.2 RECOMMENDATIONS

On the basis of the findings and conclusions of this thesis, the following recommendations are made:

i) Further investigation should be undertaken to make use of the advantages of the variations of the Hough transform (outlined in [10.1] section 'v'), to form a robust target centring algorithm which is able to combine the advantages of the various components.

ii) The centre of gravity algorithm with threshold subtraction must be seen as the first choice to be implemented as a target centring algorithm, however the level of the threshold needs to be further investigated using images of real targets to optimise successful implementation.

iii) As an alternative to the centre of gravity algorithm, the best fitting ellipse (using interpolation as edge detection and magnification of two) may be considered. The best fitting ellipse algorithm evaluates target centres to the same order of accuracy as the centre of gravity algorithm in images of real and distorted targets. The running time of this procedure must be drastically reduced to be viable for implementation in NRTP systems (since it is 40x slower than the centre of gravity algorithm in execution).

iv) For further studies, the program to generate accurate synthetic targets could be extended to form synthetic targets with an additional predetermined quantity of noise, so as to resemble real targets. These degraded targets may be used to further investigate the selection of an appropriate threshold level for the centre of gravity algorithm.

10.3 CLOSING REMARKS

PHOENICS is an ongoing project and modules are being developed to enhance the existing system. Some aspects of PHOENICS which are currently being researched and developed include:

- The introduction of parallel processors to speed up the operation of the entire system.
- Developing and improving the photogrammetric software.

In the near future, PHOENICS will be a fully automated PC based, NRTP system with a wide range of applications.

CHAPTER 11

11.0 REFERENCES

Atkinson, P. 1985. Preliminary Results of the Effect of Resampling on Thematic Mapper Imagery. ACSM-ASPRS Fall Convention Technical Papers, September 8/13, Indianapolis, pp 929-936.

Ballard, D.H. 1981. Generalizing the Hough Transform to Detect Arbitrary Shapes. Pattern Recognition, Vol.13, No.2, pp 111-122.

Bayer, G., Krzystek, P. and Mohlenbrink W. 1988. Real Time Positioning of Objects by Dynamic Target Tracking. ISPRS, 16th Congress, Kyoto, Vol.27, Part B5, Commission V, pp 32-43.

Canny, J. 1986. A Computational Approach to Edge Detection. IEEE Transactions on Pattern Analysis and Machine Intelligence, PAMI-8, No.6, November, pp 679-698.

Davis, L.S. 1975. A Survey of Edge Detection Techniques. Computer Graphics and Image Processing, No.4, pp 248-270.

Duda, R.O. and Hart, P.E. 1977. Use of the Hough Transformation to Detect Lines and Curves in Pictures. Communications of the AGM, Vol.15, No.1, January, pp 11-15.

Dye, R. and Wood, L. 1989. Resolution Improvement by Multi-Temporal Data Merging. ISPRS Journal of Photogrammetry and Remote Sensing, Vol.4(1), September, pp 14-20.

El-Hakim, S.F. 1986. Real-Time Image Metrology with CCD Cameras. Photogrammetric Engineering and Remote Sensing, Vol.52, No.11, November, pp 1757-1766.

El-Hakim, S.F. 1989. A Hierarchical Approach to Stereo Vision. Photogrammetric Engineering and Remote Sensing, Vol.55, No.4, April, pp 443-448

Elghazali, M.S. 1986. Performance of Surface Fitting Algorithms Using Fictitious Double Fourier Data, ASPRS-ACSM, Fall Convention, Anchorage, Alaska, September 28 - October 3rd, pp 203-213.

Flory, R.E. 1985. Image Acquisition Technology. Proceedings of the IEEE, Vol.73, No.4, pp 613-636.

Forstner, W. 1986. Digital Image Matching Techniques for Standard Photogrammetric Application. Technical Papers, ACSM-ASPRS Annual Convention Photogrammetry, Vol.4, pp 210-219.

Forstner, W. and Gulch, E. 1987. A Fast Operator for Detection and Precise Location of Distinct Points, Corners and Centres of Circular Features. ISPRS Intercommission Workshop, Interlaken, June, pp 281-305.

Fryer, J.G. and Brown, D.C. 1986. Lens Distortion for Close-Range Photogrammetry. Photogrammetric Engineering and Remote Sensing, Vol.52, No.1, January, pp 51-58.

Gonzalez, R.C. and Wintz, P. 1987. Digital Image Processing, 2nd. ed. Addison Wesley Publishing, pp 130-136.

Gottwald, R. and Berner, W. 1987. The New KERN 'System for Positioning and Automated co-ordinate Evaluation' - Advanced Technology for Automated 3-D Co-ordinate Determination. ASPRS-ACSM Annual Convention Technical Papers, Vol 3, March 24 - April 3, Baltimore, pp 260 - 266.

Gruen, A.W. 1985. Adaptive Least Squares Correlation: A Powerful Image Matching Technique, S.A. Journal of Photogrammetry, Remote Sensing and Cartography 14,(3), pp 175-187.

Gruen, A.W. and Beyer, H.A. 1987. Real-Time Photogrammetry at the Digital Photogrammetric Station (DIPS), of the ETH Zurich, The Canadian Surveyor, Vol.41, No.2, pp 181-199.

Hadem, I. 1988. Derivation of Approximate Values by Recognition of Circular Targets. ISPRS, 16th Congress, Kyoto, Vol.27, Part B5, Commission V, pp 240-252.

Haggren, H. 1986. Real-Time Photogrammetry as used for Machine Vision Applications. Proceedings of Symposium : Real-Time Photogrammetry: A New Challenge, Ottawa, Canada, ISPRS, Vol.26, Part 5, June, pp 374-382.

Huertas, A. and Medioni, G. 1986. Detection of Intensity Changes with Sub-pixel Accuracy Using Laplacian-Gaussian Masks, IEEE Transactions on Pattern Analysis and Machine Intelligence, Vol.PAMI-8, No.5, September, pp 651-664.

Humphrey, D. and Topping, J. A Shorter Intermediate Mechanics, S.I. edition, Longman, London, 1971, pp 590-592.

Hung, S.H.Y. 1985. On the Straightness of Digital Arcs. IEEE Transactions on Pattern Analysis and Machine Intelligence, Vol.PAMI-7, No.2, March, pp 203-215.

Lenz, R. and Fritsch, D. 1983. On the Accuracy of Videometry. ISPRS 16th Congress, Kyoto, Vol.27, Part B5, Commission V, pp 335-345.

Luhmann, T. 1986. Automatic Point Determination in a Reseau-Scanning System. ISPRS, Proceedings of Symposium, June 1986, Ottowa, Vol.26, Part 5, pp 400-408.

Mikhail, E.M., Akey, M.L. and Mitchell, O.R. 1984. Detection and Sub-Pixel Location of Photogrammetric Targets in Digital Images. Photogrammetria, 39, pp 63-83.

Muammar, H.K. and Nixon, M. 1990. A 3-Stage Procedure for Ellipse Extraction. Annual Report, University of Southampton , pp 169-171.

Real, R.R. 1986. Components for Video-based Photogrammetry of Dynamic Processes. International Archives of Photogrammetry and Remote Sensing, Vol.26, No.5, pp 432-443.

Real, R.R. and Fujimoto, Y. 1986. Digital Video Stereoscopy: Real-Time Instrumentation Issues. ISPRS Comm.2, Baltimore, May.

Rüther, H. Network Adjustment and Deformation Analysis. Course Notes : Department of Surveying, University of Cape Town.

Rüther, H. and Adams, L.P. 1984. Two Phase Photogrammetry with Displaced Control. International Archives of Photogrammetry and Remote Sensing, Vol.26, No.5, pp 323-331.

Rüther, H. and Parkyn, N. 1990. Near Real Time Photogrammetry on a Personal Computer. Photogrammetric Record, Vol.13, No.75, April, pp 415-422.

Saleh, R.A.K. and Derenyi, E.E. 1988. Radiometric Fidelity of Satellite Images Resampled by Cubic Convolution, ACSM-ASPRS Fall Convention, Technical Papers, Virginia, September 11-16, pp 106-115.

Seitz, P. 1988. Optical Superresolution Using Solid State Cameras and Digital Signal Processing. Optical Engineering, Vol.27, No.7, July, pp 535-540.

Stefanides, A., Agouris, P. and Schenk, A.F. 1990. Evaluation of the Performance of a Digital Camera. ASCM-ASPRS Annual Convention, Denver, Colorado, Technical Papers, Vol.5, March, pp 109-118.

Tabatai, A. and Mitchell, O. 1984. Edge Location to Sub-pixel Values in Digital Imagery. IEEE Transactions on Pattern Analysis and Machine Intelligence, PAMI-6, No.2, March, pp 188-201.

Thapa, K. 1988. The Use of Zero-Crossings for Cartographic Line Generalization. Technical Papers, ACSM-ASPRS Annual convention, Vol.2, pp 116-128.

Thurgood, J.D. and Mikhail, E.M. 1982. Photogrammetric Aspects of Digital Images, ACSM-ASP Convention, Technical Papers, March 14-20, Denver, Colorado, pp 295-304.

Trinder, J.C. 1987. Measurements on Digitized Hardcopy Images. Photogrammetric Engineering and Remote Sensing, Vol, 53, No.3, March, pp 315-321.

Trinder, J.C. 1989. Precision of Digital Target Location. Photogrammetric Engineering and Remote Sensing, Vol.55, No.6, June, pp 883-886.

Turney, J.L., Mudge T.N. and Volz R.A. 1985. Recognizing Partially Occluded Parts, IEEE Transactions on Pattern Analyses and Machine Intelligence, Vol.PAMI-7, No.4, July, pp 410-421.

Wildschek, R. 1989. Surface Capture Using Near Real Time Photogrammetry for a Computer Numerically Controlled Milling System. A Masters Thesis.

Wong, K.W. 1986. Close-Range Mapping with a Solid State Camera. Photogrammetric Engineering and Remote Sensing, Vol.52, No.1, January, pp 67-74.

Wong, K.W. 1987. Real-Time Machine Vision Systems. The Canadian Surveyor, Vol.41, No.2, Summer, pp 173-180.

Wong, K.W., Lew, M. and Wiley, A.G. 1988. 3-D Metric Vision for Engineering Construction. ISPRS, 16th Congress, Kyoto, Vol.27, Part B5, Commission V, pp 647-656.

Zhou, G. 1986. Accurate Determination of Ellipse Centres in Digital Imagery. Awad Convention , Washington DC, March 16-21, ACSM-ASPRS Technical Papers, Vol.4, pp 254-264.

Zhou, G. and Roberts, T. 1988. Potential Applications of Kern Space to Measuring Targets at a Large Range of Distances, ACSM-ASPRS Technical Papers, Annual Convention Vol.1, pp 154-163.

APPENDIX A

THE COLLINEARITY CONDITION IN PHOTOGRAMMETRY

The mathematical formulation of the collinearity condition takes into account the following physical characteristics: that the object point, perspective centre and image point all lie in a straight line. A description of the components involved in the system is given below, together with a mathematical model expressing the relationships between them, see Figure A1.

The image vector is defined by:

$$\underline{a} = \begin{bmatrix} x_i - x_p \\ y_i - y_p \\ f \end{bmatrix} \qquad \ldots 1$$

Where
- x_p, y_p are the principal point co-ordinates in the image plane
- f is the principal distance of the lens
- x_i, y_i are the co-ordinates of image point P_i

The vector from the point in object space to the perspective centre is defined by:

$$\underline{A} = \begin{bmatrix} X_i - X_c \\ Y_i - Y_c \\ Z_i - Z_c \end{bmatrix} \qquad \ldots 2$$

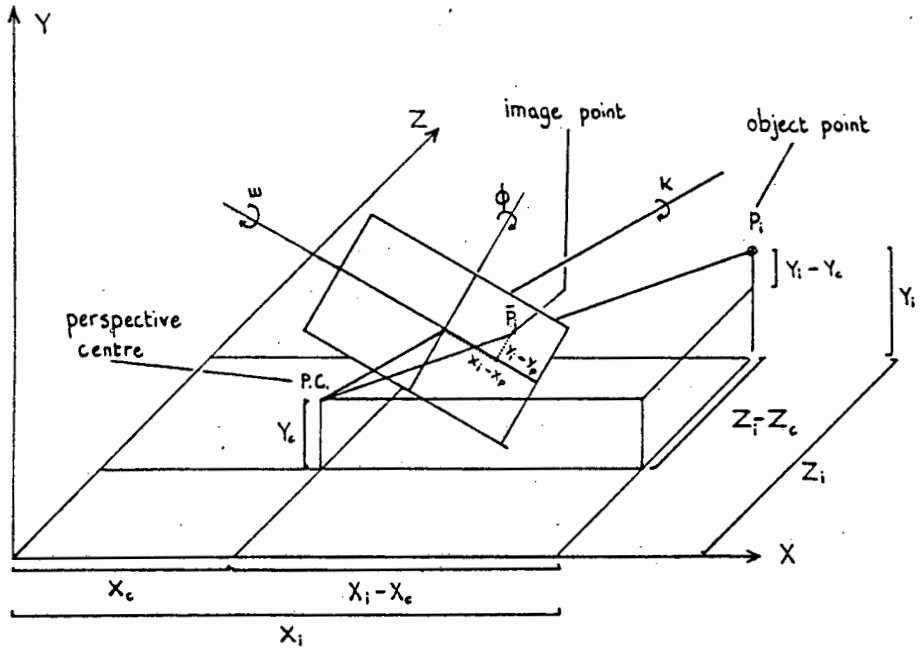

FIGURE A1 DEMONSTRATING COLLINEARITY BETWEEN AN IMAGE POINT, THE PERSPECTIVE CENTRE AND THE OBJECT POINT.

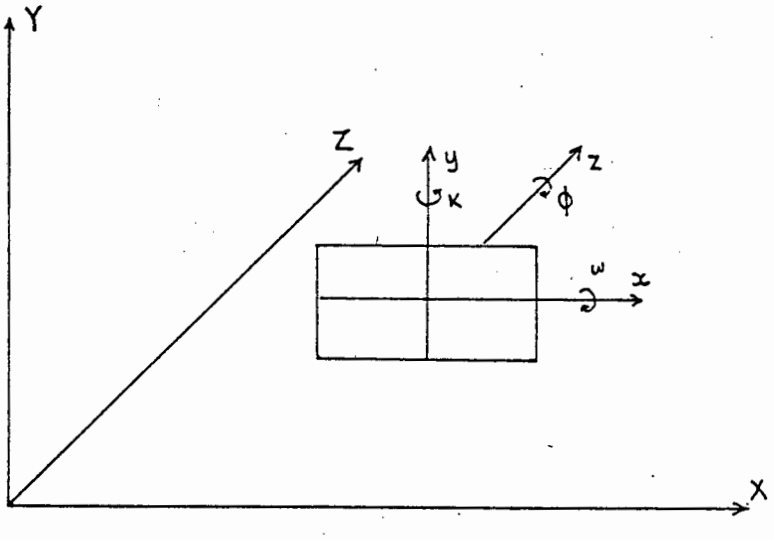

FIGURE A2 ROTATIONS OF THE IMAGE PLANE TO ALIGN WITH THE OBJECT SPACE

where - X_i, Y_i, Z_i are the co-ordinates of the object point P_i

- X_c, Y_c, Z_c are the co-ordinates of the perspective centre

The angular relationship between image and object space is described by a 3x3 orthogonal rotation matrix. One of the common methods to determine the rotation matrix is to sequentially rotate about:

the x axis with rotation 'w' Omega,
y axis with rotation 'Φ' Phi,
and z axis with rotation 'K' Kappa, see Figure A2.

The rotation about the x axis is defined by the rotation angle 'w', which is taken as positive, when the +y axis rotates towards the +z axis, giving:

$$\underline{M}_x = \begin{bmatrix} 1 & 0 & 0 \\ 0 & \cos w & \sin w \\ 0 & -\sin w & \cos w \end{bmatrix}$$

Similarly the rotation about the y and z axis are given as

$$\underline{M}_y = \begin{bmatrix} \cos \Phi & 0 & -\sin \Phi \\ 0 & 1 & 0 \\ \sin \Phi & 0 & \cos \Phi \end{bmatrix} \quad \text{and}$$

$$\underline{M}_z = \begin{bmatrix} \cos K & \sin K & 0 \\ -\sin K & \cos K & 0 \\ 0 & 0 & 1 \end{bmatrix}$$

The net rotation matrix between the object and image co-ordinate system is given by:

$$\underline{M} = \underline{M}_x \, \underline{M}_y \, \underline{M}_z$$

The collinearity condition requires that the vectors of $\underline{a}$ and $\underline{A}$, when converted to a common co-ordinate system, are equal, with the exception of scale factor 'k', thus

$$\begin{bmatrix} x_i - x_p \\ y_i - y_p \\ f \end{bmatrix} = k \, \underline{M} \begin{bmatrix} X_i - X_c \\ Y_i - Y_c \\ Z_i - Z_c \end{bmatrix} \qquad \ldots 3$$

or

$$\begin{bmatrix} x_i - x_p \\ y_i - y_p \\ f \end{bmatrix} = k \begin{bmatrix} m_{11} & m_{12} & m_{13} \\ m_{21} & m_{22} & m_{23} \\ m_{31} & m_{32} & m_{33} \end{bmatrix} \begin{bmatrix} X_i - X_c \\ Y_i - Y_c \\ Z_i - Z_c \end{bmatrix}$$

expanding by multiplying out the matrix :

$$x_i - x_p = k \, [m_{11} (X_i - X_c) + m_{12} (Y_i - Y_c) + m_{13} (Z_i - Z_c)] \qquad \ldots 4$$

$$y_i - y_p = k \, [m_{21} (X_i - X_c) + m_{22} (Y_i - Y_c) + m_{23} (Z_i - Z_c)] \qquad \ldots 5$$

$$f = k \, [m_{31} (X_i - X_c) + m_{32} (Y_i - Y_c) + m_{33} (Z_i - Z_c)] \qquad \ldots 6$$

and dividing eqn. [4] by eqn. [6], and similarly eqn. [5] by eqn. [6] :

$$x_i - x_p = f^* \frac{[m_{11}(X_i - X_c) + m_{12}(Y_i - Y_c) + m_{13}(Z_i - Z_c)]}{[m_{31}(X_i - X_c) + m_{32}(Y_i - Y_c) + m_{33}(Z_i - Z_c)]} \quad \ldots 7$$

$$y_i - y_p = f^* \frac{[m_{21}(X_i - X_c) + m_{22}(Y_i - Y_c) + m_{23}(Z_i - Z_c)]}{[m_{31}(X_i - X_c) + m_{32}(Y_i - Y_c) + m_{33}(Z_i - Z_c)]} \quad \ldots 8$$

which define the image points x_i, y_i in terms of the object points X_i, Y_i, Z_i.

The least squares formulation may be used to evaluate the parameters of equations [7] and [8], requiring as inputs, a list of target co-ordinates for the image and the corresponding object points.

APPENDIX B

THE TARGET CO-ORDINATES OF THE SURVEYED CONTROL FRAME

A template indicating the distribution of targets on a control frame, together with their associated target number, is given in Figure B1.

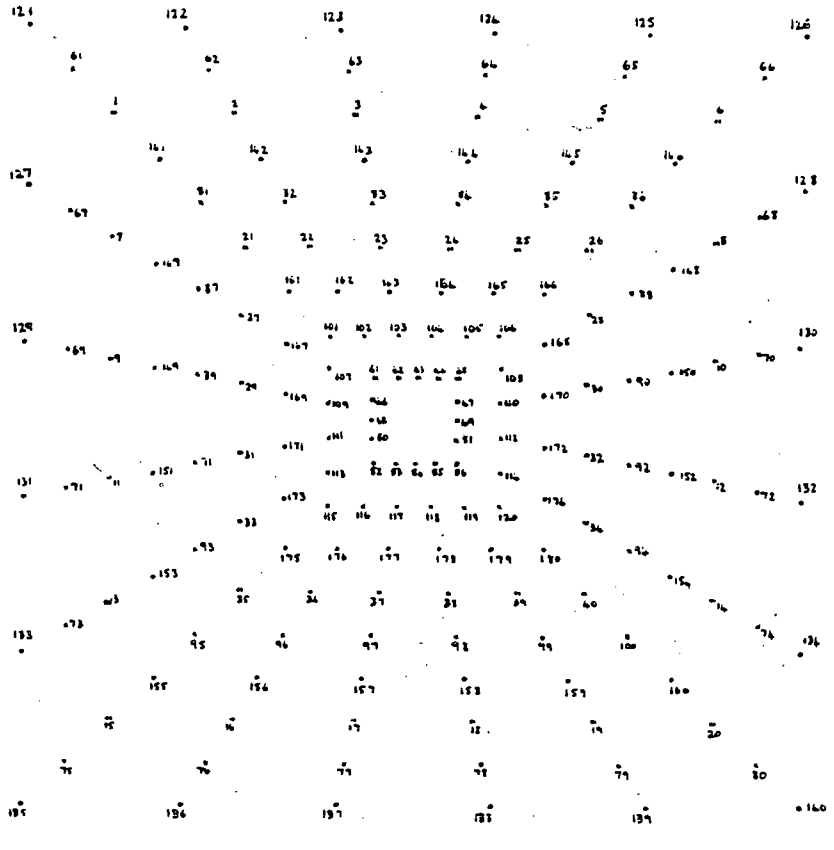

Figure B1 Target locations as seen from the camera position

A complete listing of the target X,Y,Z co-ordinates within the control frame follows. The majority of the targets were surveyed to a positional accuracy of .1mm . Those targets with a poor fixing (± .3mm) are indicated with a '*'

Target locations:

	Target no	X [mm]	Y [mm]	Z [mm]
	1	2160.93	1800.32	2766.78
	2	2272.18	1800.08	2759.22
	3	2378.52	1800.01	2751.83
	4	2488.04	1799.54	2744.26
*	5	2595.73	1799.02	2736.55
	6	2705.55	1796.98	2729.87
	7	2159.78	1687.91	2769.76
	8	2706.62	1689.02	2733.79
	9	2160	1581.6	2771.64
	10	2705.87	1580.05	2737.52
	11	2159.78	1472.9	2774.88
	12	2705.27	1477.13	2740.83
	13	2159.04	1363.51	2778.22
	14	2705.77	1362.91	2744.56
	15	2160.59	1258.46	2781.08
	16	2269.91	1256.61	2774.23
	17	2379.14	1256.08	2767.63
	18	2485.85	1255.88	2760.91
	19	2594.56	1255.1	2754.5
	20	2703.86	1254.55	2747.93
	21	2278.82	1680.07	2762.11
	22	2336.73	1680.24	2757.92
	23	2400.51	1681.28	2753.19
	24	2462.6	1681.31	2748.65
	25	2526.13	1681.65	2744.15
	26	2589.81	1679.3	2739.82
	27	2278.43	1614.64	2763.74
*	28	2589.78	1618.19	2742.49
	29	2278.3	1552.5	2765.31
	30	2589.44	1554.74	2745.16
	31	2277.45	1489.26	2766.83
	32	2588.68	1492.97	2747.67
	33	2278.39	1427.16	2768.42
	34	2588.69	1429.3	2750.21
	35	2276.86	1364.55	2770.06
	36	2337.85	1363.13	2766.06
	37	2401.61	1364.61	2762.25
	38	2462.75	1365.43	2758.81
	39	2527.66	1364.76	2755.26
*	40	2587.47	1365.28	2752.58
*	41	2388.82	1567.7	2776.33
*	42	2408.95	1567.85	2775.35
*	43	2428.63	1567.43	2773.81
*	44	2448.34	1567.76	2772.33
*	45	2469.07	1567.34	2770.86
*	46	2388.2	1546.97	2777.19
*	47	2468.61	1546.35	2771.7
*	48	2387.49	1527.02	2778

*	49	2469.13	1526.66	2772.32
*	50	2387.56	1506.91	2778.91
*	51	2468.46	1505.27	2773.29
*	52	2387.84	1486.18	2779.5
*	53	2408.49	1487.07	2778.3
*	54	2428.34	1486.18	2776.89
*	55	2448.78	1485.7	2775.58
*	56	2468.8	1485.59	2774.05

There are no targets in the range 57..60

61	2063.42	1907.34	2917.25
62	2214.12	1907.66	2907.09
63	2365.8	1906.82	2896.58
64	2515.68	1906.65	2886.52
65	2666.09	1906.15	2876.32
66	2818.5	1906.49	2865.84
67	2061.99	1755.26	2920.79
68	2820.81	1757.42	2869.62
69	2061.25	1604.52	2924.29
70	2821.41	1605.3	2873.77
71	2062.05	1453.2	2927.92
72	2821.65	1454.96	2878.17
73	2062.47	1301.24	2932.69
74	2821.97	1304.07	2882.99
75	2065.65	1152.43	2936.67
76	2221.03	1150.6	2927.25
77	2370.85	1151.27	2917.14
78	2522.14	1151.03	2906.73
79	2671.87	1151.47	2896.59
80	2822.23	1152.09	2886.69
81	2204.2	1765.11	2913.18
82	2297.05	1766.35	2906.82
83	2392.1	1765.98	2900.27
84	2485.39	1766.44	2893.52
85	2579.22	1767.15	2886.96
86	2671.24	1767.51	2880.72
* 87	2203.36	1667.25	2915.59
88	2672.32	1671.13	2883.25
89	2203.19	1574.68	2918.05
90	2672.11	1576.07	2886.02
91	2203.02	1479.31	2920.41
92	2672.15	1481.84	2888.84
93	2203.21	1386.56	2922.63
94	2671.92	1387.93	2891.94
95	2205.63	1291.96	2923.97
96	2298.81	1290.24	2918
97	2392.68	1291.15	2912.17
98	2485.41	1291.56	2906.21
99	2581.45	1291.3	2900.15
100	2673.61	1293.58	2894.78
101	2344.24	1624.41	2909.21
102	2382.24	1625.75	2906.16

	103	2420.03	1625.45	2903.16
	104	2461.4	1625.52	2899.91
	105	2499.69	1625.32	2896.89
	106	2536.83	1624.11	2894.47
	107	2344.9	1586.19	2909.67
	108	2537.53	1585.02	2895.5
	109	2343.68	1546.71	2910.23
	110	2537.85	1545.13	2896.45
	111	2343.75	1507.84	2910.6
	112	2538.3	1505.72	2897.39
	113	2344.27	1469.45	2910.83
	114	2539.1	1466.79	2898.8
	115	2345.1	1429.27	2911.13
*	116	2382.29	1429.06	2909.27
	117	2422.47	1428.83	2906.74
	118	2460.69	1429.04	2904.42
	119	2499.52	1429.41	2901.84
	120	2538.65	1429.61	2899.26
	121	1952.47	2028.11	3064.68
	122	2154.79	2028.81	3051.67
	123	2355.28	2028.56	3038.29
	124	2553.14	2027.6	3025.11
	125	2753.08	2026.92	3011.44
	126	2954.93	2026.82	2996.82
	127	1953.56	1826.34	3071.19
	128	2955.92	1828.53	3003.21
*	129	1953.9	1625.64	3077.59
	130	2956.22	1629.04	3009
	131	1953.52	1425.28	3084.98
	132	2956.27	1429.31	3015.12
*	133	1953.36	1226.39	3092.39
	134	2956.09	1229.82	3021.98
	135	1953.87	1027.86	3099.36
	136	2158.4	1029.75	3085.68
	137	2357.17	1029.79	3072.2
	138	2556.66	1030.52	3058.69
*	139	2755.27	1030.03	3045.28
	140	2955.63	1029.43	3028.36
	141	2119.63	1864.21	3061.09
	142	2252.95	1863.96	3051.91
	143	2386.55	1865.16	3042.49
	144	2520.41	1865.58	3033.41
*	145	2654.86	1865.89	3023.36
	146	2787.22	1866.87	3014.86
	147	2117.86	1729.76	3065.9
	148	2785.5	1735.78	3019.48
	149	2117.16	1596.92	3070.44
	150	2784.08	1602.35	3023.84
	152	2782.97	1468.5	3028.13
	153	2114.39	1328.52	3078.9
	154	2782.56	1334.17	3032.25
	155	2113.6	1199.31	3082.26
	156	2247.57	1198.68	3073.4
*	157	2382.27	1198.82	3063.26

158	2514.45	1199.95	3054.52
159	2648.58	1199.69	3044.94
160	2781.51	1202.3	3035.41
161	2282.58	1694.97	3057.65
162	2351.29	1695.64	3052.93
163	2417.6	1695.82	3048.05
164	2482.79	1695.97	3043.08
165	2548.45	1696.16	3038.2
166	2616.83	1696.05	3032.72
167	2283.34	1629.11	3060.01
168	2616.55	1632.3	3035.06
169	2282.63	1563.18	3061.78
170	2616.18	1563.56	3038.32
171	2281.74	1497.47	3063.63
172	2615.84	1497.32	3041.04
173	2282.77	1431.01	3065.67
174	2615.28	1431.8	3043.6
175	2282.36	1365.86	3068.23
176	2347.83	1366.16	3063.59
177	[This target was not surveyed]		
178	2478.61	1366.44	3054.64
179	2544.61	1366.68	3049.89
180	2614.7	1366.81	3045.04

APPENDIX C

THE PROCEDURE WHICH WAS USED TO CORRELATE IMAGE TARGET CO-ORDINATES WITH THE SURVEYED THREE DIMENSIONAL (OBJECT) TARGET CO-ORDINATES

Target centres on a control frame were located on an image using the PHOENICS program SEARCH. The targets found by the program are displayed in listing 1 below, in the order that they were located by the program. A co-ordinate of 0,0 indicates a target was located but the centre was not found. An image containing the targets, together with a number corresponding to the order in which each target was located, is illustrated in Figure C1.

Thereafter, the image (Figure C1) was compared to the control frame to correlate the number code of the targets located on the image with the numbering scheme of the control frame, see Figure C2. The renumbered image target listing is displayed in listing 2.

The renumbered target co-ordinates were correlated with the control frame co-ordinate list using the PHOENICS program : PREP, to determine the accuracy of the target centring algorithm. In order to determine the accuracy of the target centring procedure compensating for the effects of lens distortion, an option in the program to invoke a lens distortion correction was applied. The results of the targeting *accuracy* are listed in listing 3.

Listing 1: Targets located by the centring program

target #	X [pixels]	Y [pixels]
1	0	0
2	243.98	22.48
3	314.56	21.14

4	383.98	22.95
5	175	23.85
6	306.74	60.91
7	364.33	60.82
8	247.7	61.29
9	423.8	61.88
10	191.36	62.41
11	30.05	63.13
12	30.01	64.99
13	191.39	67.72
14	247.79	66.7
15	307.57	66.15
16	364.31	66.24
17	423.8	67.08
18	134.92	70.12
19	509.72	76.05
20	53.87	87.54
21	480.32	105.77
22	82.04	107.45
23	250.02	109.1
24	297.44	109.01
25	343.75	108.97
26	393.55	109.33
27	157.34	110.33
28	203.39	111.1
29	108.33	123
30	454.86	123.67
31	261.82	143.4
32	296.84	144.1
33	331.85	143.81
34	226.79	145.07
35	426.57	144.43
36	366.87	144.73
37	133.46	149.04
38	393.85	171.07
39	156.49	174.59
40	266.62	184.97
41	290.51	185.07
42	242.56	185.39
43	314.93	185.33
44	338.96	185.61
45	217.55	187.06
46	367.21	191.27
47	191.3	192.63
48	192.42	196.26
49	367.94	197.18
50	27.83	204.46
51	509.39	205.37
52	53.32	213.02
53	481.88	215.88
54	80.86	219.51
55	340.47	219.47
56	107.77	220.54
57	456.27	221.82

58	216.53	220.88
59	426.31	228.05
60	134.02	230.01
61	247.52	230.88
62	262.99	231.06
63	278.71	230.45
64	293.61	230.81
65	308.98	232.08
66	395.4	238.97
67	157.29	241.46
68	193.53	241.47
69	367.75	244.94
70	339.94	251.92
71	247.9	252.89
72	308.78	253.48
73	216.67	254.23
74	216.88	259.83
75	247.41	273.71
76	308.98	275.13
77	260.9	280.13
78	216.46	289.19
79	339.75	289.04
80	193.2	290.89
81	367.64	293.89
82	246.74	295.83
83	308.76	296.19
84	159.03	306.11
85	395.33	305.46
86	134.26	310
87	426.83	310.1
88	261.9	316.83
89	292.88	317.52
90	109.51	317.54
91	246.69	318.32
92	277.83	317.89
93	309	318.03
94	457.02	319.65
95	218.03	320.18
96	339.78	320.13
97	217.1	326.48
98	339.83	326.35
99	456.12	325.81
100	81.94	329
101	481.3	331.5
102	509.58	335.49
103	193.83	340.02
104	54.28	340.5
105	368.47	344.22
106	30.06	345.99
107	290.05	355.8
108	314.23	355.9
109	240.79	357
110	264.69	357.18
111	338.47	356.46

112	219.01	357.44
113	395.39	372.88
114	158.72	373.51
115	195.04	392.03
116	426.21	391.5
117	135.31	392.66
118	228.44	392.27
119	334.5	394.56
120	262.98	394.75
121	297.95	395.24
122	367.9	395.02
123	110.26	414.64
124	455.32	421.62
125	160.29	434.51
126	206.12	437.74
127	253.15	437.93
128	83.95	438.27
129	299.87	439.52
130	347.29	440.03
131	392.91	439.36
132	479.39	442.31
133	507.54	462.29
134	57.98	463.85
135	139.01	469.65
136	194.42	470.03
137	426.1	469.34
138	251.52	471.44
139	367.46	471.32
140	309.62	472.69
141	0	0
142	0	0

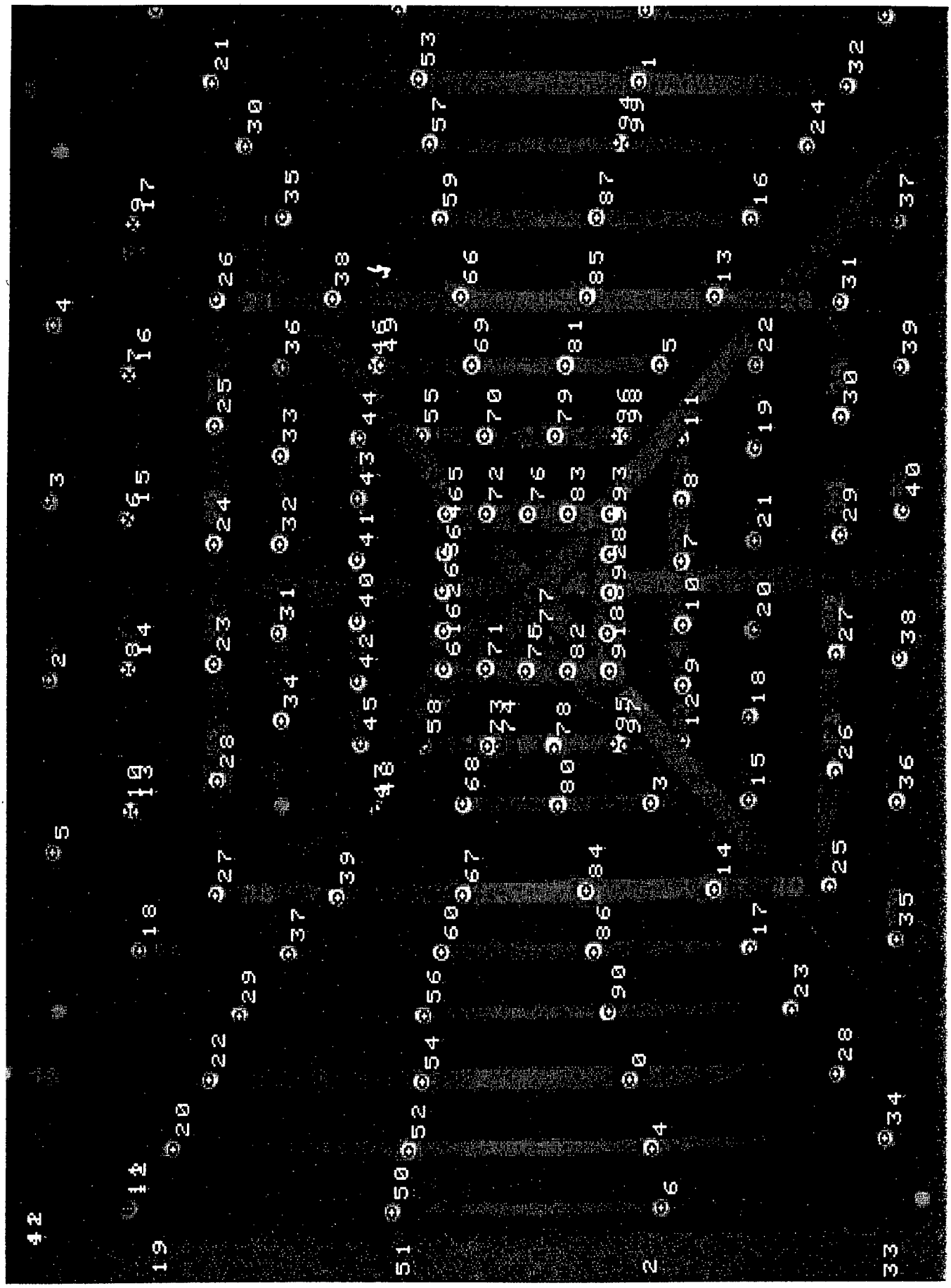

Figure C1 Targets together with their initial associated numbers

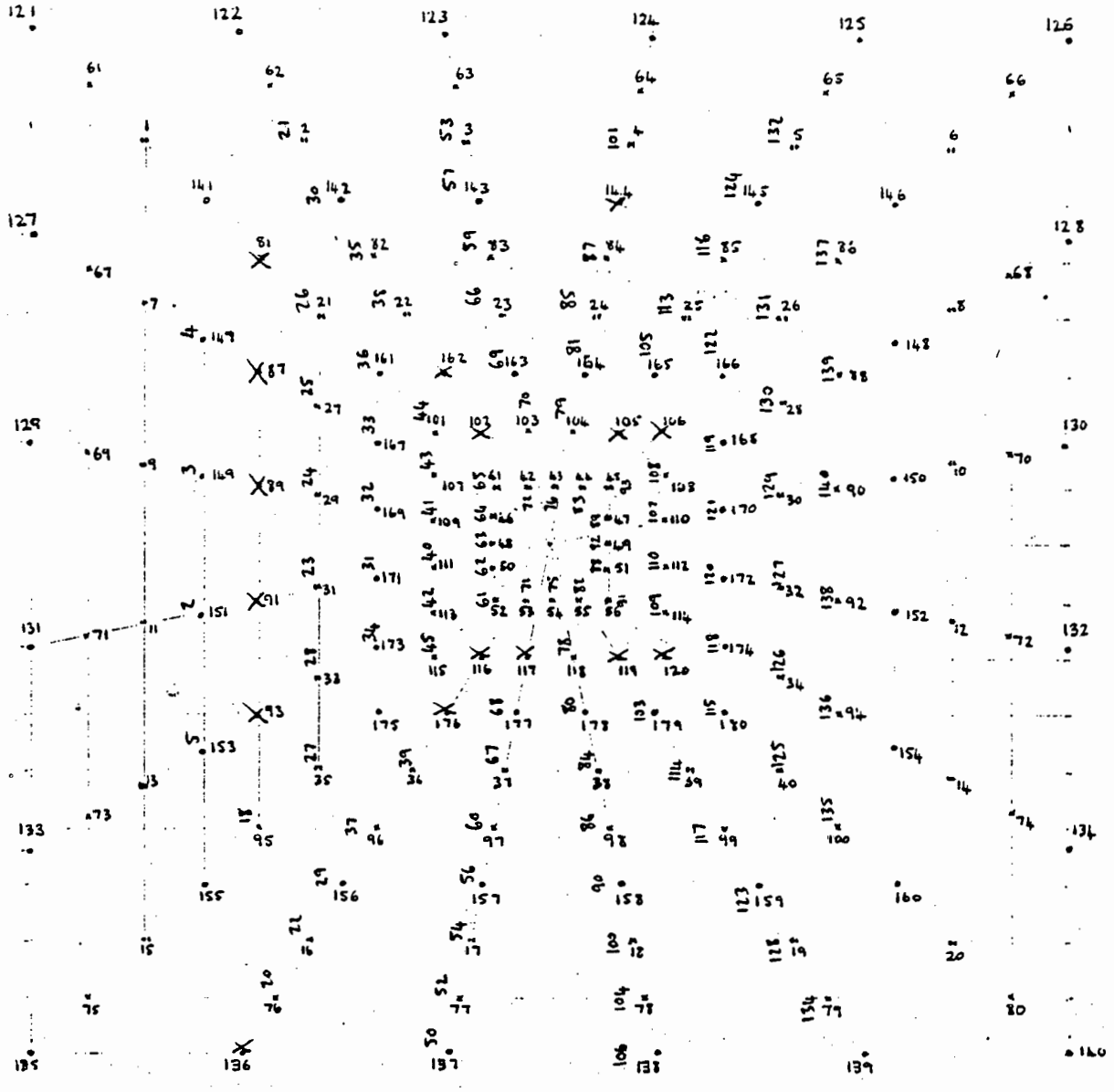

Figure C2 Manual comparison of the image target numbers with a template of the control frame

Listing 2 : The renumbered image target listing

target #	X [pixels]	Y [pixels]
149	314.56	21.14
147	383.98	22.95
153	175	23.85
95	134.92	70.12
76	53.87	87.54
2	480.32	105.77
16	82.04	107.45
31	250.02	109.1
29	297.44	109.01
27	343.75	108.97
21	393.55	109.33
35	157.34	110.33
33	203.39	111.1
156	108.33	123
142	454.86	123.67
171	261.82	143.4
169	296.84	144.1
167	331.85	143.81
173	226.79	145.07
82	426.57	144.43
161	366.87	144.73
96	133.46	149.04
22	393.85	171.07
36	156.49	174.59
111	266.62	184.97
109	290.51	185.07
113	242.56	185.39
107	314.93	185.33
101	338.96	185.61
115	217.55	187.06
137	27.83	204.46
77	53.32	213.02
3	481.88	215.88
17	80.86	219.51
157	107.77	220.54
143	456.27	221.82
83	426.31	228.05
97	134.02	230.01
52	247.52	230.88
50	262.99	231.06
48	278.71	230.45
46	293.61	230.81
41	308.98	232.08
23	395.4	238.97
37	157.29	241.46
163	367.75	244.94
103	339.94	251.92
53	247.9	252.89
42	308.78	253.48

54	247.41	273.71
43	308.98	275.13
118	216.46	289.19
104	339.75	289.04
178	193.2	290.89
164	367.64	293.89
55	246.74	295.83
44	308.76	296.19
38	159.03	306.11
24	395.33	305.46
98	134.26	310
84	426.83	310.1
51	261.9	316.83
47	292.88	317.52
158	109.51	317.54
56	246.69	318.32
49	277.83	317.89
45	309	318.03
18	81.94	329
4	481.3	331.5
179	193.83	340.02
78	54.28	340.5
165	368.47	344.22
138	30.06	345.99
110	290.05	355.8
108	314.23	355.9
114	240.79	357
112	264.69	357.18
25	395.39	372.88
39	158.72	373.51
180	195.04	392.03
85	426.21	391.5
99	135.31	392.66
174	228.44	392.27
168	334.5	394.56
172	262.98	394.75
170	297.95	395.24
166	367.9	395.02
159	110.26	414.64
145	455.32	421.62
40	160.29	434.51
34	206.12	437.74
32	253.15	437.93
19	83.95	438.27
30	299.87	439.52
28	347.29	440.03
26	392.91	439.36
5	479.39	442.31
79	57.98	463.85
100	139.01	469.65
94	194.42	470.03

86	426.1	469.34
92	251.52	471.44
88	367.46	471.32
90	309.62	472.69

Listing 3: The results of correlating the image with the control frame

```
PHOTOGRAMMTRIC POINT DETERMINATION
copyright : H. Ruther - 1988

Final Results
=============

Project :  hdrreduc.rec

CASE 1 : Separate PDx and PDy evaluation with uniform scale

I M A G E  1
------------

RESULT FOR IMAGE  1 AFTER 12 ITERATIONS
---------------------------------------

Transformation parameters (and lens dist. coeff.)
with their standard deviations

      B11          B12          B13          B14
  -0.000028    -0.003767    -0.000146     6.110235
   0.000001     0.000011     0.000002     0.018311

      B21          B22          B23          B24
   0.003697    -0.000015    -0.000197    -8.366897
   0.000011     0.000001     0.000002     0.024439

      B31          B32          B33
  -0.000042     0.000002    -0.000439
   0.000001     0.000000     0.000001

Lens distortion : D.Brown Model

     K1           K2           K3           P1           P2
-.27749e-02

Standard Deviation of Weight Unit =    .005 mm

Principal Distance X =    8.540 mm
                   Y =    8.385 mm  Mean =    8.463 mm
               Ratio =  1.01851

Principal Point Position : X =   0.301 mm  Y =  -0.346 mm
```

Perspective Centre Position

X = 2379.051 mm Y = 1524.501 mm Z = 2057.965 mm

Omega = -5.4105 Phi = -89.7572 Kappa = 0.2086

Observed control point image coords, corrections & lens distortion

Observations a posteriori :Xap = X+vx-dx and Yap = Y+vy-dy

No	X mm	vx mm	Y mm	vy mm	dx mm	dy mm
2	3.612	-0.007	1.683	-0.013	-0.139	-0.085
3	3.637	-0.003	0.449	-0.003	-0.109	-0.026
4	3.627	-0.009	-0.846	-0.005	-0.104	0.016
5	3.597	-0.002	-2.087	0.007	-0.127	0.067
16	-2.801	0.006	1.664	-0.002	0.118	-0.076
17	-2.820	0.003	0.409	0.005	0.089	-0.022
18	-2.802	-0.005	-0.818	-0.000	0.085	0.013
19	-2.770	-0.004	-2.041	0.007	0.105	0.058
21	2.215	0.000	1.643	0.002	-0.040	-0.042
22	2.219	0.010	0.951	0.000	-0.029	-0.019
23	2.244	-0.005	0.191	-0.007	-0.022	-0.006
24	2.243	0.003	-0.554	-0.004	-0.021	0.002
25	2.244	0.000	-1.309	0.006	-0.025	0.013
26	2.204	0.000	-2.054	0.000	-0.035	0.031
27	1.413	0.001	1.647	0.006	-0.016	-0.029
28	1.470	0.004	-2.061	-0.000	-0.014	0.020
29	0.667	0.002	1.646	0.004	-0.004	-0.023
30	0.706	0.003	-2.055	-0.004	-0.003	0.015
31	-0.096	0.003	1.645	0.003	0.005	-0.023
32	-0.046	-0.006	-2.038	-0.003	0.003	0.014
33	-0.847	0.002	1.623	0.011	0.017	-0.028
34	-0.803	-0.005	-2.035	0.003	0.012	0.019
35	-1.588	0.004	1.632	0.000	0.039	-0.041
36	-1.602	-0.004	0.912	0.004	0.027	-0.018
37	-1.589	-0.008	0.163	-0.001	0.020	-0.005
38	-1.561	-0.001	-0.561	0.002	0.018	0.002
39	-1.566	-0.006	-1.316	-0.004	0.023	0.012
40	-1.541	0.003	-1.999	-0.006	0.031	0.028
76	-3.254	-0.000	1.887	0.004	0.174	-0.109
77	-3.263	-0.006	0.481	0.003	0.132	-0.031
78	-3.248	0.004	-0.946	-0.008	0.128	0.022
79	-3.188	0.004	-2.328	0.000	0.156	0.089
82	2.746	-0.002	1.250	-0.007	-0.058	-0.038
83	2.742	0.001	0.313	0.003	-0.043	-0.012

84	2.750	0.002	-0.606	-0.004	-0.041	0.004
85	2.740	0.005	-1.518	-0.005	-0.050	0.024
86	2.739	0.006	-2.389	0.002	-0.068	0.057
88	1.795	-0.006	-2.412	0.002	-0.027	0.037
90	0.863	-0.003	-2.427	-0.002	-0.007	0.027
92	-0.072	0.003	-2.413	0.001	0.005	0.025
94	-0.991	0.004	-2.397	-0.002	0.021	0.033
95	-1.949	-0.001	2.082	-0.004	0.068	-0.074
96	-1.973	0.016	1.198	0.007	0.048	-0.032
97	-1.964	0.004	0.291	0.002	0.035	-0.010
98	-1.960	0.006	-0.605	-0.004	0.032	0.004
99	-1.943	0.008	-1.531	-0.004	0.040	0.021
100	-1.884	-0.008	-2.393	0.005	0.054	0.051
101	1.336	-0.000	0.788	-0.001	-0.007	-0.007
103	1.351	0.003	0.046	-0.001	-0.004	-0.001
104	1.348	0.002	-0.370	0.003	-0.003	0.000
107	0.949	-0.007	0.792	-0.001	-0.003	-0.005
108	0.938	-0.002	-1.119	-0.001	-0.002	0.002
109	0.556	-0.002	0.794	-0.002	-0.001	-0.004
110	0.548	0.003	-1.118	-0.003	-0.000	0.001
111	0.171	0.004	0.796	-0.002	0.000	-0.004
112	0.140	-0.005	-1.133	0.007	0.000	0.001
113	-0.216	-0.007	0.791	-0.007	0.002	-0.005
114	-0.245	-0.003	-1.131	-0.006	0.001	0.002
115	-0.619	0.008	0.772	-0.002	0.005	-0.007
118	-0.637	0.006	-0.372	-0.003	0.002	0.000
137	-3.674	0.010	0.577	0.005	0.184	-0.043
138	-3.638	-0.003	-1.008	-0.001	0.174	0.029
142	3.202	0.004	1.482	0.002	-0.095	-0.060
143	3.224	-0.007	0.383	0.002	-0.074	-0.018
145	3.209	0.008	-1.855	0.000	-0.087	0.045
147	2.060	0.003	2.610	0.004	-0.058	-0.097
149	0.943	-0.001	2.630	-0.005	-0.017	-0.077
153	-1.304	-0.005	2.600	0.000	0.050	-0.092
156	-2.377	-0.004	1.490	0.014	0.078	-0.054
157	-2.387	-0.003	0.397	0.013	0.058	-0.016
158	-2.358	-0.000	-0.689	0.005	0.053	0.007
159	-2.346	0.005	-1.777	-0.001	0.067	0.036
161	1.785	0.004	1.246	0.003	-0.020	-0.021
163	1.799	0.004	0.124	0.001	-0.010	-0.003
164	1.797	0.011	-0.424	0.008	-0.009	0.000
165	1.811	0.010	-0.988	-0.001	-0.011	0.005
166	1.802	-0.002	-1.557	-0.006	-0.015	0.012
167	1.221	-0.001	1.257	0.002	-0.009	-0.015
168	1.264	-0.000	-1.552	0.002	-0.006	0.008
169	0.658	-0.003	1.253	-0.003	-0.003	-0.012
170	0.675	-0.007	-1.559	-0.011	-0.002	0.005
171	0.094	0.000	1.261	-0.006	0.002	-0.012
172	0.112	-0.007	-1.554	0.003	0.001	0.005
173	-0.470	-0.003	1.242	-0.001	0.007	-0.014
174	-0.444	-0.009	-1.526	-0.005	0.004	0.006
178	-1.011	-0.006	-0.391	-0.003	0.006	0.000
179	-1.001	-0.002	-0.941	-0.008	0.007	0.003
180	-0.981	-0.010	-1.524	0.006	0.011	0.010

APPENDIX D

CONVOLUTION

1) The Convolution Principle

Convolution is a mathematical tool to evaluate the effect of one item/equation/image on another. In the case of image processing, convolution masks are often used to :

- identify features represented by the mask
- further process the image.

Some common convolution masks are:

- Low-pass filters : for smoothing sharp edges [7.2.3]
- High-pass filters : to locate edges on an image [8.1]
- 'Feature detection' masks : to identify features on the image in common with the mask [8.1]

In the description that follows, a convolution mask which has the effect of 'low-pass filtering' of the image is described. Low-pass filtering may be achieved using the Gaussian noise function, otherwise known as the point spread function (PSF) with an equation in one dimension of

$$H(x) = ke^{-(\sigma/x)^2},$$

where the curve is bell shaped and σ refers to the 'spread' of the bell, see Figure D1.

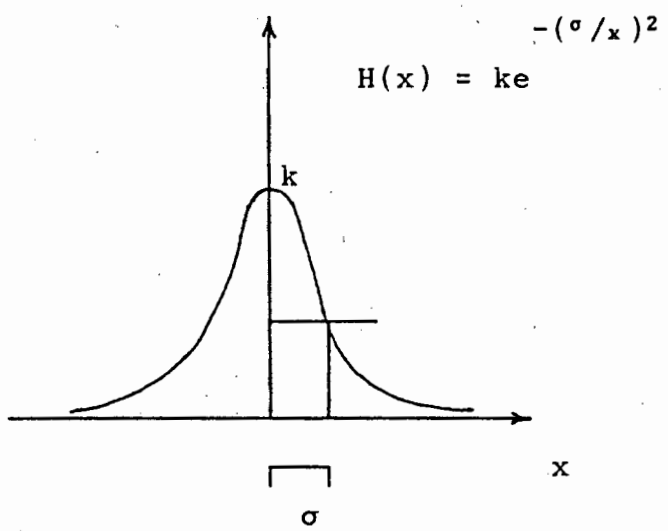

Figure D1 The Gaussian Noise Function

The result of convolving the image with the PSF is to smooth out the sharp edges on an image (acting like a low-pass filter). Convolution of an image with a PSF is a two dimensional application. The method of convolution is illustrated in a 1 dimensional application in Figure D2, where a PSF is convolved with a wall (edge).

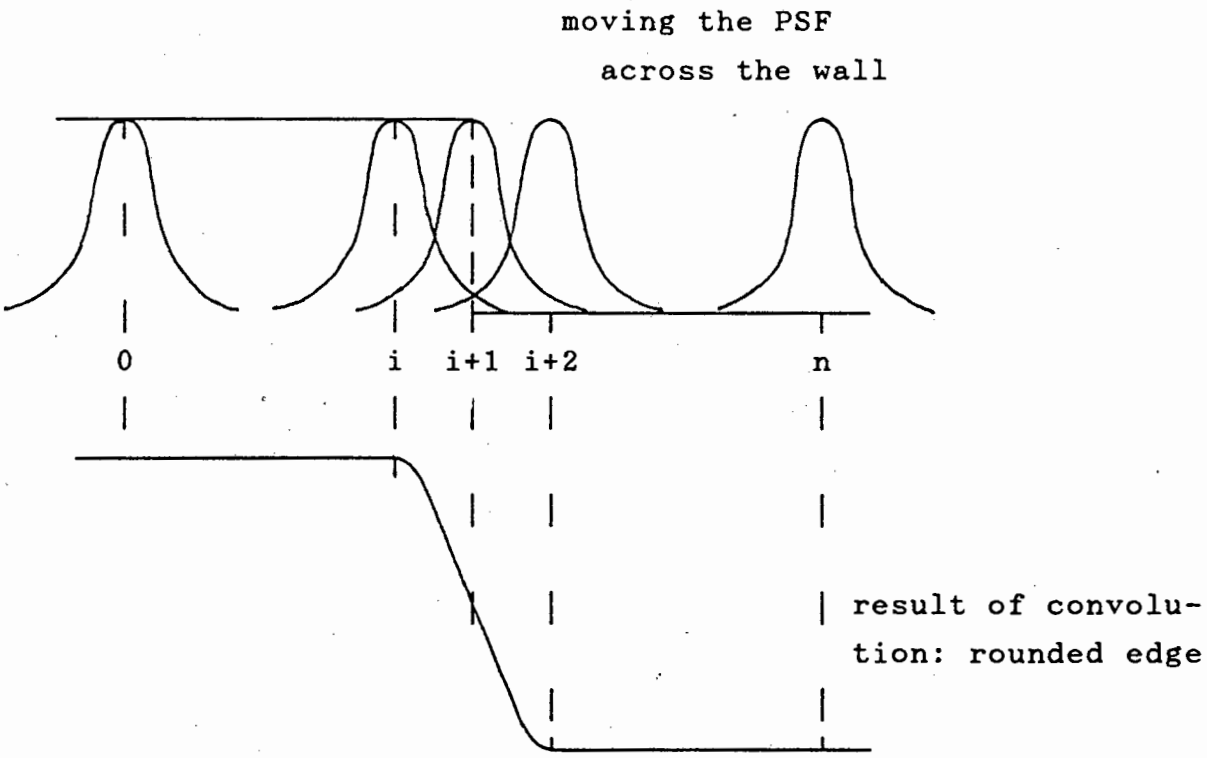

Figure D2 Illustrating the concept of convolution

With reference to Figure D2, the steps involved in the convolution are:

i) set the line position-counter L to 0 i.e. to the beginning of the line
ii) position the PSF at location L of the wall
iii) multiply the entire bell shaped curve with the wall
iv) store the result at position L of the resulting curve/array
v) increment L by the amount appropriate to the fineness/closeness of the resolution required
vi) repeat steps (ii) to (v) until the PSF reaches the end of the line

The resulting curve is also illustrated in Figure D2. Note that:

i) the width of the falloff function is slightly less wide than the PSF

ii) the edge on the resulting image occurs at half the original height of the wall and at the point of maximum slope of the resulting convolved image

iii) the resulting curve is symmetrical

Extending the convolution to two dimensions:
Convolving Ellipseo (an ideal ellipse with direct falloff) with a two dimensional PSF results in a curve illustrated in Figure D3.

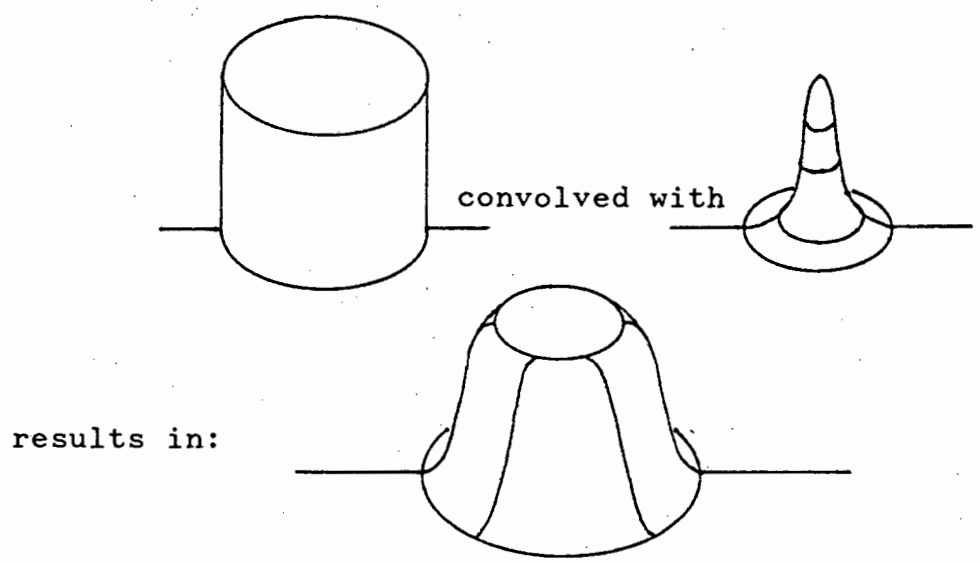

Figure D3 A two dimensional convolution of Ellipseo with a PSF

2) Convolution of a digital image

Convolution of targets in digital images with a PSF results in a discrete approximation to the continuous convolution of the ellipse. An example of a discrete convolution in one dimension is given in Figure D4. Again, the effect of convolution using a gross approximation to the PSF can be

seen to have the effect of a 'smoothing function', removing sharp edges.

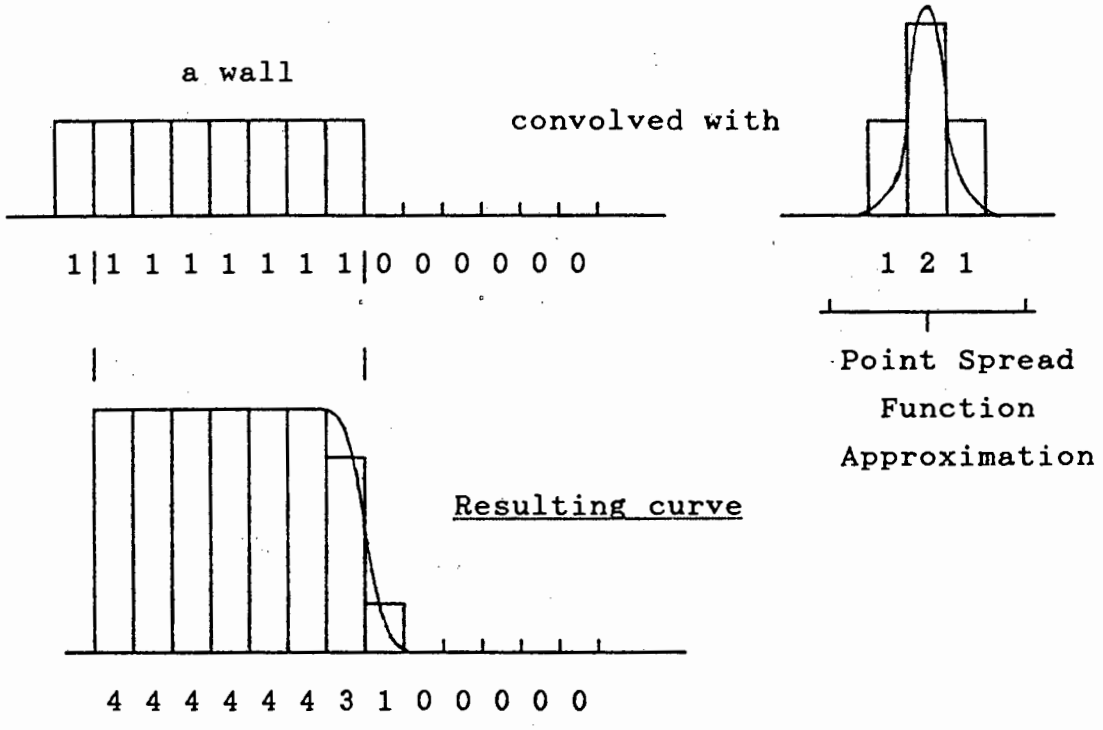

Figure D4 Convolution of a discrete wall with an approximation to a PSF

Problems with convolution using a digitised signal include:

i) The centring accuracy of the originally fabricated ellipse-with-direct-falloff cannot be improved.

ii) For an ellipse with a falloff from saturation to background level within three pixels, the point spread function cannot exceed three pixels, i.e. it would look like the case illustrated in Figure D4, which is a poor depiction/approximation to the point spread function.

One method of obviating the problem of poor PSF definition would be to :

i) fabricate the ellipse with direct falloff at, for example, twice the intended size

ii) convolve it with a point spread function of also twice the original size

iii) reduce the resulting ellipse to half of the expanded size.

APPENDIX E

FLOWCHARTS OF THE TARGET DETECTION PROCEDURE

The 'target detection' aspect of the ***Target detection and centring algorithm***, which is briefly described in Chapter 8.1 , is explained in this Appendix using a series of flow charts:

Flowchart (1) gives an overview of the entire target detection and centring program

Flowchart (2) illustrates locating targets on the image

Flowchart (3) describes finding target extents on an image:
- (3a) the Freeman chain code is described
- (3b) the flow chart to find target extents

GENERAL OVERVIEW OF THE PROGRAM

Flowchart (1)

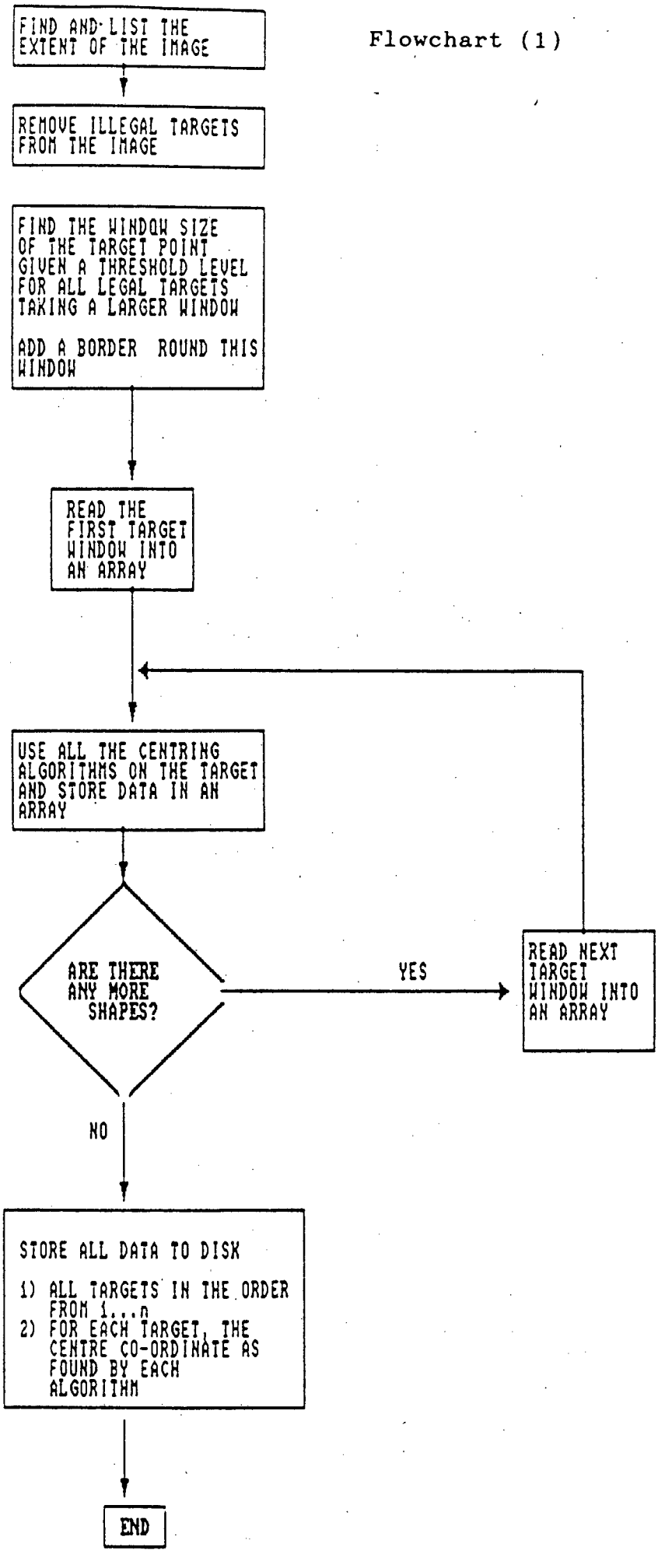

Flowchart (2)

FINDING THE TARGETS OF AN IMAGE

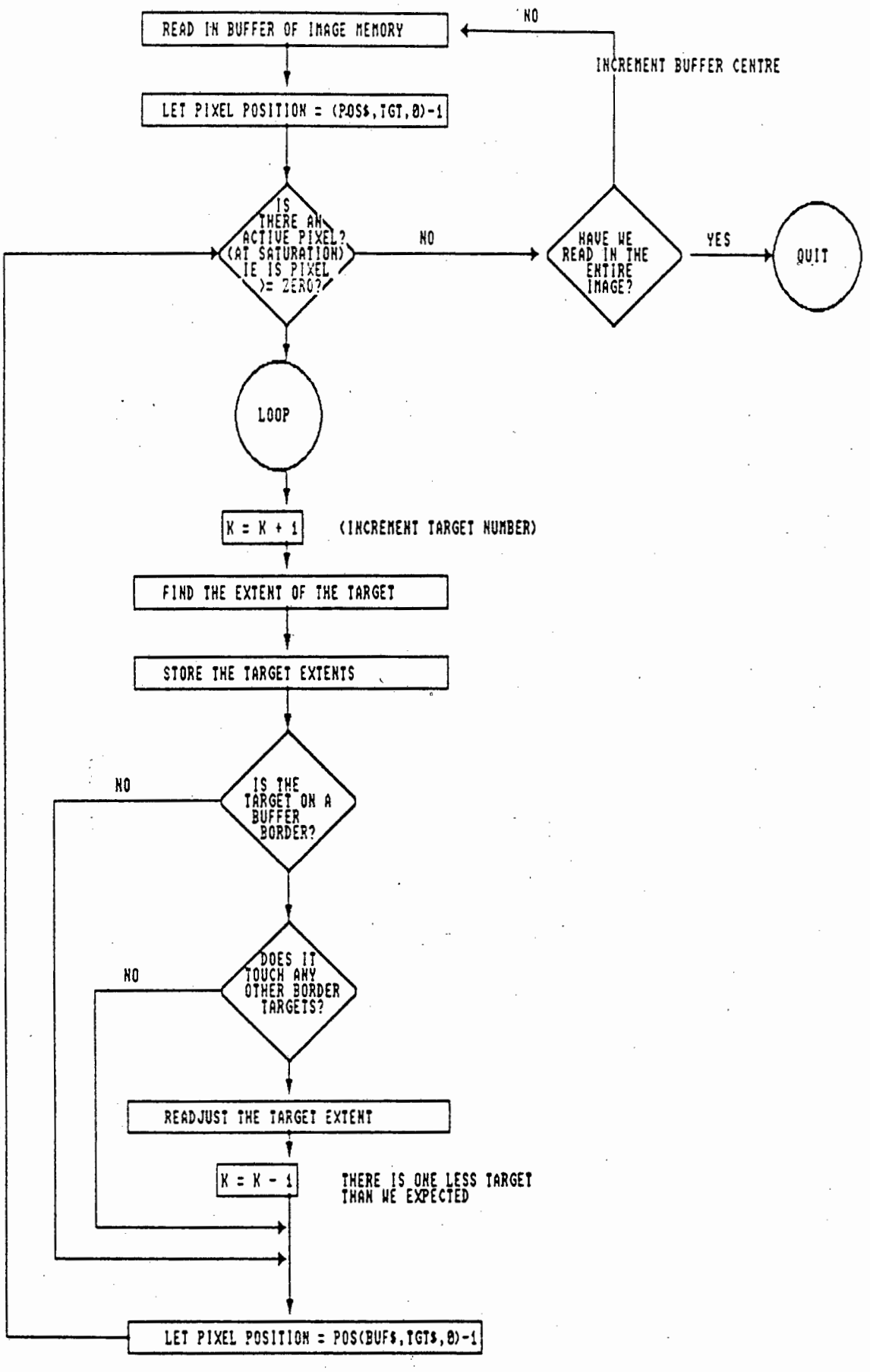

Flowchart (3a)

FIND THE TARGET EXTENTS

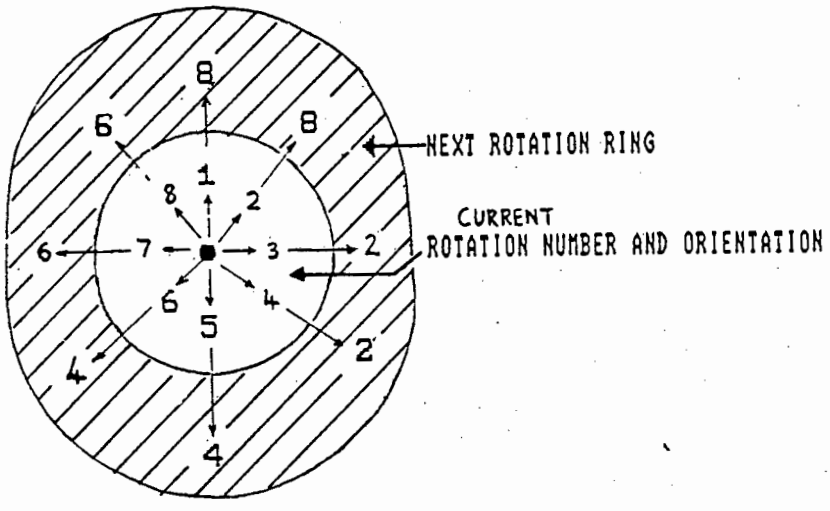

ROTATION RING

EXPLANATION OF THE ROTATION RING: IT GIVES

1. THE DIRECTION ASSOCIATED WITH A ROTATION NUMBER
2. THE DIRECTION OF THE NEXT PIXEL TO SEARCH IF THE CURRENT ONE POINTED TO IS NOT A VALID PERIMETER POINT.
   (THIS IS FOUND BY INCREMENTING 'ROTATION' BY 1
3. THE DIRECTION TO START LOOKING IN, IF THE PIXEL LAST POINTED TO BY ' ROTATION' WAS A VALID PERIMETER PIXEL. (THE NEW VALUE OF ROTATION GIVEN BY 'NEXT ROTATION RING')

FOR EXAMPLE:

IF THE PIXEL POINTED TO WITH A ROTATION AT 1 WAS A PERIMETER PIXEL, THEN THE FIRST DIRECTION TO LOOK WHEN VIEWING FROM THE NEW PERIMETER POINT IS WITH A ROTATION OF 8.

Flowchart (3b)

FIND THE TARGET EXTENTS

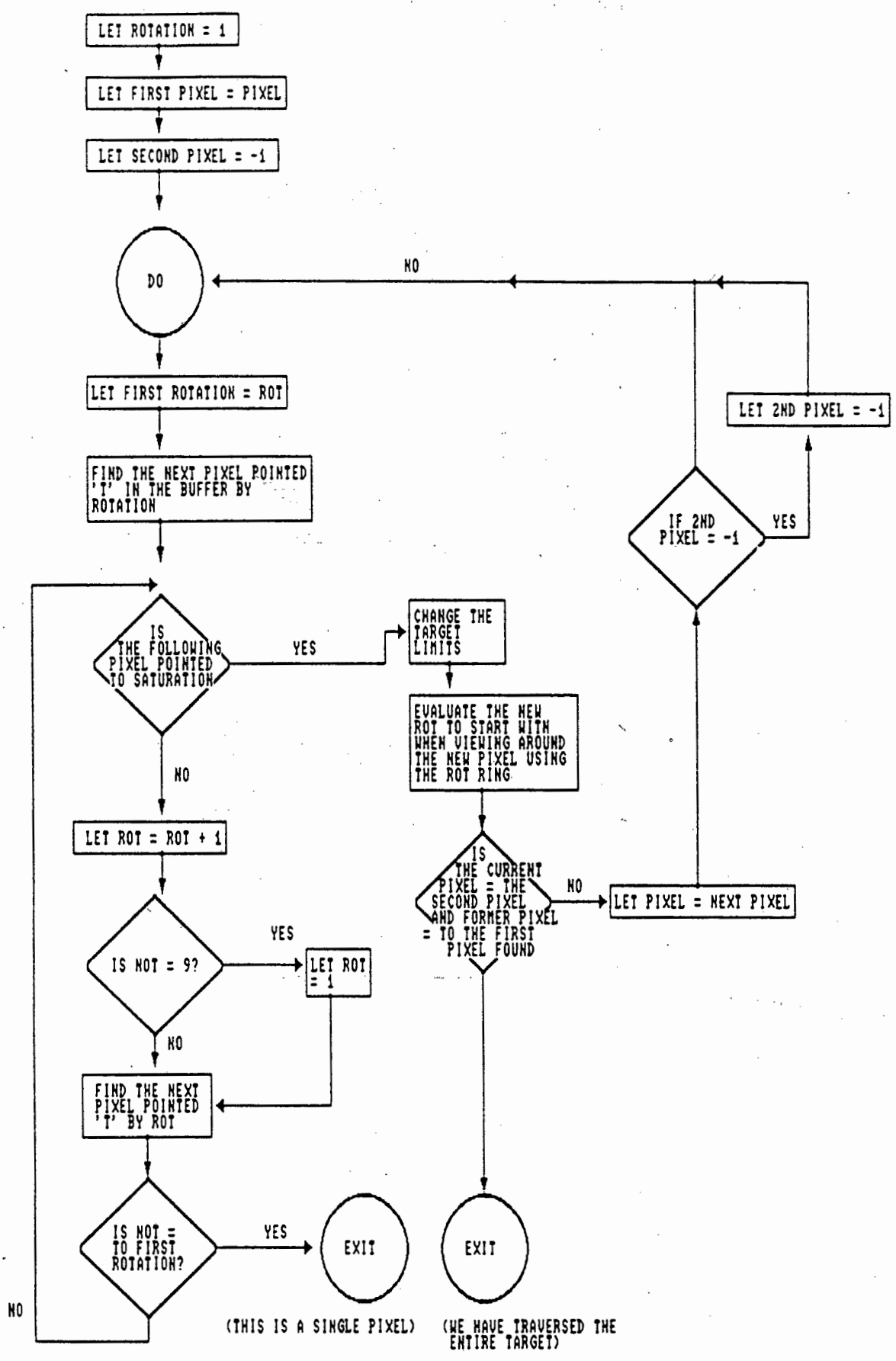

APPENDIX F

WORKED EXAMPLE ILLUSTRATING THE HOUGH TRANSFORM

The principle of the Hough transform can be explained using the following example:
Given n points on an image, find the subset of those points that lie on a straight line. One method to achieve this would be to find all lines determined by every pair of points and then to find all points which are close to the line. The method outlined above is computationally prohibitive in all except the simplest of images since it involves finding $n(n-1)/2 \sim n^2$ lines and then performing $n(n(n-1))/2 \sim n^3$ comparisons of each point to each line.

The problem may be viewed in a different way using the Hough transform, Gonzalez (1987).

Given a point (x_1, y_1) and the equation of the slope intercept form: $y_1 = ax_1 + b$, there are an infinite number of lines passing through $y_1 = ax_1 + b$, for different values of a and b. When the formulation is changed about, giving: $b = -ax_1 + y_1$, considering the a-b plane (parameter space) there is only a single line for the co-ordinates (x_1, y_1). The co-ordinates (x_2, y_2) similarly form a second line intersecting with the first line at (a',b') giving the parameters of the line passing through the points (x_1, y_1) and (x_2, y_2). The concept is illustrated in Figure F1 below.

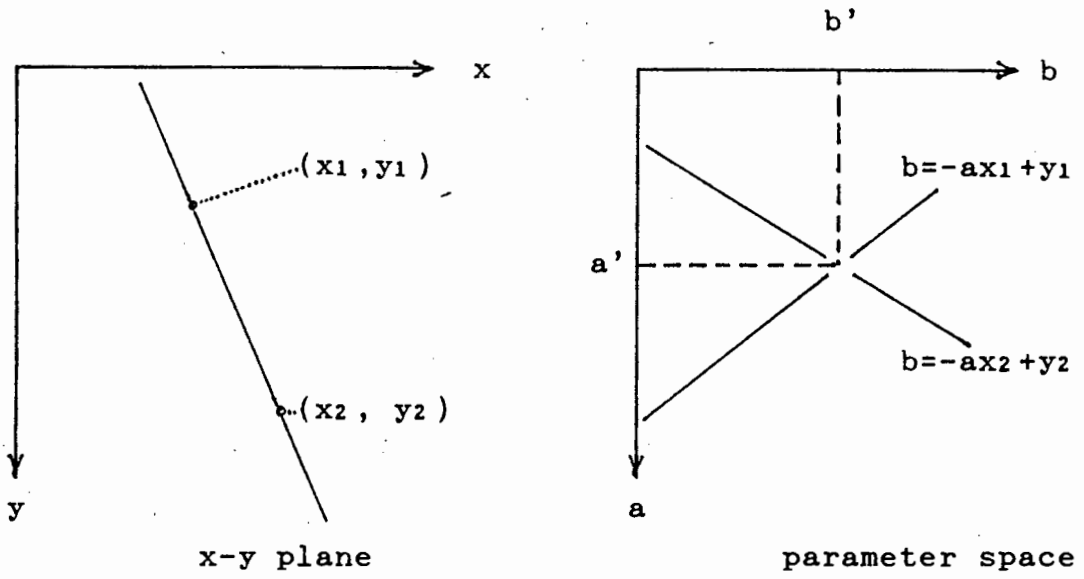

Figure F1 The x-y plane and parameter space

The parameter space is quantized into a matrix, called the accumulator matrix, sub-dividing the parameters a and b each by k increments, between limits (a_{min}, a_{max}) and (b_{min}, b_{max}). For each point (x_h, y_h) the line intersecting the relevant pixels in the parameter space matrix increments the particular matrix location by (say) 1, so for k increments in the matrix, given one point (x_h, y_h), there will be k parameter matrix locations incremented, see Figure F2.

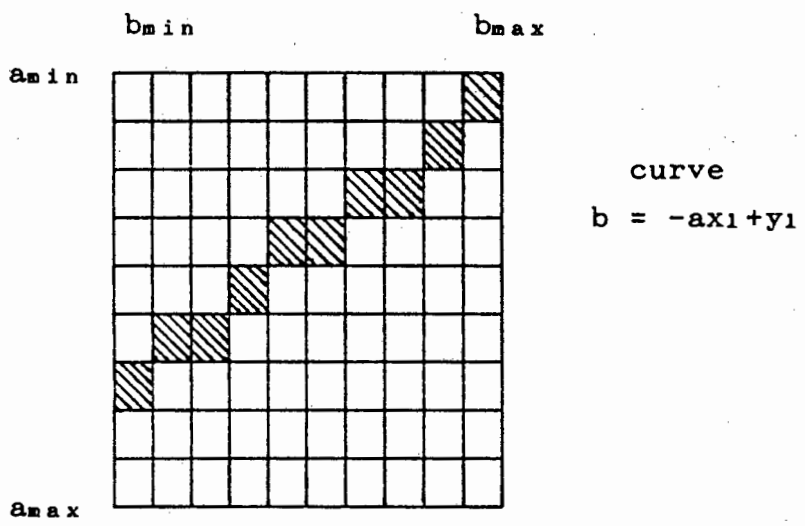

Figure F2 Quantization of the parameter plane

Subdividing the a axis into k segments: for every point (x_i, y_i), k values of 'b' are obtained, relating to the k possible values of 'a'. Given n image points, there are nk computations to fill the parameter space. The process is therefore linear in n.

Although the description relates only to straight lines, the Hough Transform applies to any curve f(x,a) = 0 with parameter vector 'a' and co-ordinate vector 'x'.
Thus for the ellipse

$$\frac{x - c_1^2}{c_2} + \frac{y - c_3^2}{c_4} = 1$$

with the ellipse being rotated by an angle c_5, graphically illustrated in Figure F3, there is a 5 dimensional parameter space, with an accumulator of the form A(i,j,k,l,m).

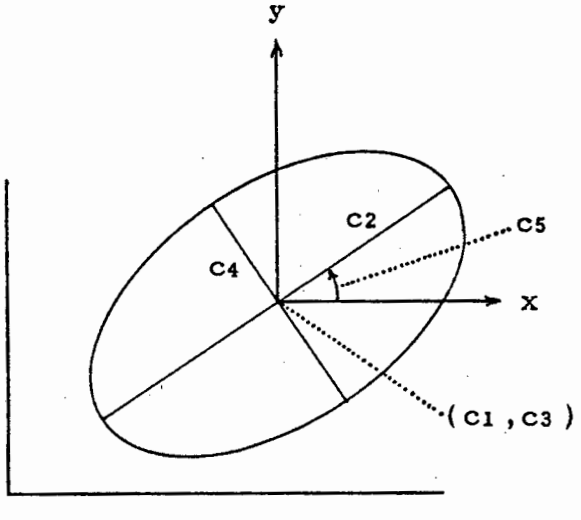

Figure F3 Parameters of an ellipse

The procedure is to increment four of the parameter values, solving for the fifth parameter and then update the accumulator corresponding to the 5 parameters $c_1, c_2, c_3, c_4, 0$.

The traditional implementation of the Hough Transform to solve for five dimensional parameter space is expensive with respect to CPU usage and storage space. Therefore, variations of this approach have been developed.

APPENDIX G

i) STEPS USED TO ASSESS THE *ACCURACY* OF THE *SEARCH* TARGET CENTRING ALGORITHM (i.e. only the C.G. algorithm built into the PHOENICS system) AND THE *EFFECT OF LENS DISTORTION* ON A REAL IMAGE

1. Set up lighting of the objects, camera aperture and focusing.

2. Use Matrox cards and PIP software to read the image into the computer.

3. Store the image to disk.

4. Use 'scaling' on the Matrox card to select a suitable threshold value for the particular image, to view the targets without the object.

5. Store the thresholded image to disk.

6. Use Target Centring Program SEARCH to scan the image:
   - Eliminates bad, partially obscured and incorrect targets from the target list.
   - Automatically numbers the targets in the order they are found (from left to right, top to bottom) , providing an initial estimate for the target centres.
   - The targets and associated numbers are superimposed on the image and displayed on the video screen.
   - The list of target numbers and appropriate target centres are stored to disk.

7. (Convert the record file of the SEARCH target numbers and centres, to a text file.)

8. Refer to the image of target centres with associated target numbers. Compare the image to the surveyed control frame. Renumber the SEARCH numbering of target centres with the numbers given to the targets in the original surveyed control frame analysis and store to a (text) file.

9. (Convert the text file of target centres with modified associated target numbers, renumbered in [i.8] above, to a record file.)

10. Run data of the image target centres through the PREP program to determine the accuracy and standard deviation from the mean of:
    - the targets as viewed by the imaging system in relation to the target locations obtained from the surveyed control frame
    - the target centres obtained by the imaging system, connected by one of a number of lens distortion models, compared to the target locations obtained from the surveyed control frame
    - the options available are:
        - choose the correlation process:
          least squares fit or bundle adjustment
        - number of iterations
        - lens distortion model chosen including:
            - o no lens distortion
            - o Brown model
            - o El-Hakim's model.

    The output of the PREP program is a measure of the accuracy of the C.G. algorithm as used within the PHOENICS system.

A by-product of the least squares adjustment giving the accuracy of targets in relation to the surveyed control frame, is the availability of the ratio of pixel width to pixel height.

(Initially, an estimate of the ratio is input to the program and one of the output parameters to the adjustment is a correction to the pixel ratio. When the pixel ratio approximation is multiplied by its correction, a more accurate approximation to the pixel height-to-width ratio is obtained. The pixel ratio is of great importance when obtaining/using information directly off the imaging system, so as to correctly scale the object viewed.)

Steps 7 to 9 are necessary for the implementation of this system because of the addition of the human interface to renumber the target sequence.

ii) ON ASSESSING THE COMPARATIVE ACCURACY OF *ALL THE TARGET CENTRING ALGORITHMS AS DEVELOPED IN THIS THESIS* ON *REAL* IMAGES

In evaluating the effectiveness of the various target centring algorithms, the steps outlined in the previous section were used and the target centring routine was slotted in.

The sequence of steps used to compare the various target centring algorithms are:

1. Set up lighting of the objects, camera aperture and focusing.

2. Use the Matrox card and PIP software to read the image into the computer.

3. Store the image to disk.

4. Use 'scaling' on the Matrox card to select a suitable threshold value for the particular image, to view the targets without the object.

5. Store the thresholded image to disk.

6. Use the SEARCH Program to scan the image
   - Eliminate bad, partially obscured and incorrect targets from the target list.
   - The program automatically numbers the targets in the order they are found (from left to right, top to bottom) and provides an initial estimate for the target centres.
   - The targets and associated numbers are superimposed on the image and displayed on the video screen. The list of target numbers and appropriate target centres are stored to disk.

7. (Convert the Record file of the SEARCH target numbers and centres, to a text file.)

8. Refer to the image of target centres with associated target numbers. Compare the image to the surveyed control frame. Renumber the SEARCH numbering of target centres with the numbers given to the targets in the original surveyed control frame analysis and store to a (text) file.

9a. Run the program to evaluate the different target centring algorithms:

(- Choose a threshold level for the Edge Detection and Centre of Gravity algorithm.)

The program output is ordered in terms of the targets found. The ordering is from left to right, top to bottom. For each target, the centres as determined by each algorithm is sequentially stored.

9b. Use the *conversion program* to convert the target number associated with each target location (as found using each of the target centring algorithms in [ii.9a]), to the target numbering scheme as defined by the control frame numbering scheme. This is achieved by finding the 'best fit' between target centres found in [ii.9a] with those found in [ii.8] and swapping the corresponding associated target numbers of [ii.9a] for those of [ii.8].

A unique/ separate (record) file is used to store all the target centres together with their associated target numbers (now corresponding to the control frame numbering scheme), for each target centring algorithm.

10. All the target centres for each target centring algorithm are passed through the PREP program to assess the precision of each algorithm with respect to the surveyed control frame. (In order to determine centring accuracy of the algorithms alone, ignoring lens distortion, a lens distortion model is used to compensate for video imaging errors.) The precision of each target centring algorithm is stored.

11. The accuracy of each algorithm is compared, to determine which algorithm has the best centring capability on real targets.

iii) STEPS USED TO ASSESS COMPARATIVE ACCURACY OF *ALL THE TARGET CENTRING ALGORITHMS DEVELOPED IN THIS THESIS*, ON *SYNTHETIC* TARGETS

1. Synthetic elliptical images are fabricated:
   - the number of targets is selected
   - the orientation, size, shape and centre location within the image for each target is defined/ entered
   - the type of falloff function and the steepness of the falloff from saturation to background level is chosen for all ellipses

2. The program to evaluate the centring ability of various algorithms is run on the synthetic image. The output is ordered in the order of the targets located (starting in the top left hand corner, searching the image row by row). For each target, the centres as determined by each algorithm, are placed sequentially.

3. A program then compares (all) the target centres for each algorithm to a list of ellipse centres as specified by the synthetic target manufacturing algorithm [iii.1], outputting the accuracy of each algorithm.

4. The accuracy of each algorithm is compared, to determine which algorithm has the best potential target centring capability.